Unione Europea

UNIVERSITÀ DEGLI
STUDI DI SALERNO

FONDO SOCIALE EUROPEO

Programma Operativo Nazionale 2007-2013

"Ricerca Scientifica, Sviluppo Tecnologico, Alta Formazione"
Regioni dell'Obiettivo 1 – Misura III.4

"Formazione superiore ed universitaria"

Dipartimento di Ingegneria Industriale

Tesi di Dottorato in "Scienza e Tecnologie
per l'Industria Chimica, Farmaceutica e Alimentare"
Ingegneria Chimica (XI Ciclo-Nuova Serie)

In silico and *in vitro* models in pharmacokinetic studies

Supervisor

Prof. Giuseppe Titomanlio

Prof. Gaetano Lamberti

Ph.D. student

Sara Cascone

Scientific Referees

Prof. Werner Weitschies

Prof. Iztok Grabnar

Ph.D. Course Coordinator

Prof. Paolo Ciambelli

La cornacchia e la brocca

Una cornacchia, mezza morta di sete, trovò una brocca che una volta era stata piena d'acqua. Ma quando infilò il becco nella brocca si accorse che vi era rimasto soltanto un pò d'acqua sul fondo. Provò e riprovò, ma inutilmente, e alla fine fu presa da disperazione. Le venne un'idea e, preso un sasso, lo gettò nella brocca.

Poi prese un altro sasso e lo gettò nella brocca.

Poi prese un altro sasso e lo gettò nella brocca.

Ne prese un altro e gettò anche questo nella brocca.

Piano piano vide l'acqua salire verso di sé, e dopo aver gettati altri sassi riuscì a bere e a salvare la sua vita.

"A poco a poco si arriva a tutto."

Esopo

Table of contents

Table of contents ..... **I**

Figures Index ..... **V**

Tables Index ..... **XIII**

Abstract ..... **XV**

Publication List ..... **XIX**

Introduction **1**

1.1 Anatomy of the gastrointestinal tract _____ 2

1.1.1 The stomach 2

1.1.2 The small intestine 5

1.1.3 The colon 7

1.2 Dissolution and absorption _____ 8

1.3 Pharmacokinetic modeling _____ 11

State of the art – *in vitro* and *in silico* models **15**

2.1 USP apparatuses _____ 16

2.2 Non USP apparatuses _____ 21

2.2.1 The Sartorius absorption model 21

2.2.2 In vitro simulation of gastric digestion 22

2.2.3 A multicompartmental model simulating the stomach and small intestine 23

2.2.4 Simulated biological dissolution and absorption system 26

2.2.5 Three staged gastrointestinal model 28

2.2.6 Use of hollow fiber to simulate the intestinal absorption 30

2.2.7 Dissolution test apparatus by Garbacz et al. 31
2.2.8 Stirring device for dissolution testing 33
2.3 Gastric motility 34
2.4 Pharmacokinetic models 40
2.4.1 The first whole body physiologically based pharmacokinetic model 40
2.4.2 The simplified model inspired by Jain et al. 42
2.4.3 Compartment Absorption and Transit model 43
2.4.4 Advanced Compartmental Absorption and Transit model 43
2.4.5 The Advanced Dissolution, Absorption and Metabolism model 44
2.4.6 Physiologically Based PharmacoKinetic model 46
2.4.7 Other physiologically based models 47

State of the art – Absorption models 49
3.1 Absorption models 50
3.1.1 Absorption prediction from theory 50
3.1.2 In vitro methods for absorption predictions 52
3.1.3 Animal perfusion studies 68
3.2.4 Human perfusion studies 75

Aims 79
4.1 Aims of the thesis 80

Materials and methods 81
5.1 Materials 82
5.1.1 Active molecules 82
5.1.2 Polymers 88
5.1.3 Dissolution media 89
5.1.4 Membranes 90
5.2 Methods 90
5.2.1 Tablet preparation 90
5.2.2 Dissolution methods 90
5.2.3 Transport phenomena studies 92

5.2.4 Analytical methods 95

***In vitro* models: chemical history 101**

6.1 pH and temperature control _____ 102

6.2 Results and discussions _____ 105

6.2.1 Conventional release patterns 105

6.2.2 Novel release patterns 107

***In vitro* models: mass transport.....115**

7.1 Permeability studies _____ 116

7.2 Design of an exchange system_____ 127

7.3 Realization of the *in vitro* device _____ 134

7.4 Results and discussions _____ 135

7.4.1 Experimental setup and transport parameters evaluation 135

7.4.2 Conventional release pattern 138

7.4.3 Effect of the flow direction 139

7.4.4 Effect of the reciprocal flow direction 141

7.4.5 Effect of pH history 142

7.4.6 Release profile of an enteric fast release tablet 143

***In vitro* models: mechanical history.....145**

8.1 Design of the gastric motility_____ 146

8.2 Realization of the *in vitro* device _____ 146

8.3 Results and discussions _____ 148

8.3.1 Release pattern in the artificial stomach 148

8.3.2 Effect of the frequency of the contractions 152

***In silico* pharmacokinetics.....155**

9.1 Physiologically based pharmacokinetic model_____ 156

9.2 Influence of dissolution method_____ 159

9.2.1 Influence of pH history 159

9.2.2 Influence of mass transport 163

9.3 Influence of inter-individual parameters _____ 164
9.3.1 Model simulations 168
9.3.2 Model parameters 174

Conclusions 179
10.1 Conclusions _____ 180
10.2 Future perspectives_____ 182

References..... 185

Short curriculum..... 195

Figures Index

Figure 1. Stomach physiology. 3
Figure 2. Gastrointestinal tract physiology. 5
Figure 3. BCS substances classification in term of solubility and permeability. 10
Figure 4. USP apparatus 1 (basket apparatus). 16
Figure 5. USP apparatus 2 (paddle method). 17
Figure 6. USP apparatus 3 (reciprocating cylinder). 18
Figure 7. USP apparatus 4 (flow – through cell) 19
Figure 8. USP apparatuses 5 and 6 (paddle over disc and rotating cylinder, respectively). 20
Figure 9. USP apparatus 7 (reciprocating disk). 20
Figure 10. Schematization of the sartorius Absorption Model. 21
Figure 11. Sartorius dissolution model. a) plastic syringe, b) timer, c) safety lock, d) cable connector, e) silicon tubes, f) silicon O-rings, g) metal filter, h) polyacril reaction vessel. 22
Figure 12. pH decrease during *in vitro* gastric digestion of milk. n = number of experiments. A) 143 mM HCl, 1.5 mL/min, constant shaking; B) 143 mM HCl, 2.0 mL/min, constant shaking; C) 143 mM HCl, 2.0 mL/min, irregular stirring; D) 286 mM HCl, 3.0 mL/min, regular stirring. 23
Figure 13. *In vitro* model developed by Minekus et al. a) gastric compartment; b) duodenal compartment; c) jejuna compartment; d) ileal compartment; e) basic unit; f) glass jacket; g) flexible wall; h) rotary pump; i) water bath; j) peristaltic valve pump; k) peristaltic pump; l, m) pH electrodes; n, o) syringe pumps; p) hollow fibre device. 24
Figure 14. Simulation of the peristaltic waves in the Minekus model. 1) unit 2, 3) pressure chamber; 4) intermediate piece; 5) flexible wall; 6) space between rigid and flexible wall; 8, 9, 10, 11) connectors [20]. 25
Figure 15. Simulated biological dissolution and absorption system by Tam and Anderson. 27
Figure 16. First stage (the *fundus*) of the Wickham and Faulks model. 29

Figure 17. Second stage (the *antrum*) of the Wickham and Faulks model. The movement of the piston simulates the high shear stress of the stomach bottom part. 30

Figure 18. Elevation view of the Rozga and Demetriou artificial gut....31

Figure 19. Schematic representation of dissolution stress test device developed by Gabacz et al. 32

Figure 20. Front view of the vessel with stirrer bar and beads when no stirring is applied. 33

Figure 21. The stomach geometry reconstructed by the use of MRIs [33]. 35

Figure 22. (a) Predicted gastric flow velocity vectors at one time instant, (b) Instantaneous streamlines, (c) Flow velocity along the z-axis shown in (a), plotted at 1 s intervals. The filled curve on the right is the maximum retropulsive flow velocity through the contractions as a function of time. The dotted line follows the propagation of the distal contraction in space–time [33]....36

Figure 23. Effect of viscosity on the formation of the retropulsive-jet like motion and eddy structures [35]....37

Figure 24. Streamlines of the fluid flow within the stomach's middle plane. b) Newtonian fluid with viscosity of 1 Pa·s; c) Shear thinning fluid (k = 0.233 Pa·s, n = 0.59) [36]....38

Figure 25. Predicted versus experimental velocity profiles along a horizontal line [35]....40

Figure 26. Schematization of the Jain absorption model. 41

Figure 27. Algorithm employed for whole body PBPK model reduction....42

Figure 28. ACAT model schematic. 44

Figure 29. Kinetic processes within each intestinal segmento f the ADAM model. 45

Figure 30. Schematic reproduction of the model proposed by Di Muria et al. 46

Figure 31. Physicochemical properties affecting intestinal absorption [10]. 50

Figure 32. Correlation of oral availabilities in humans and measured uptake *in vitro* in everted intestinal rings [10]....53

Figure 33. The Sweetana-Grass diffusion cell. The tissue is mounted between two acrylic half-cells. Buffer is circulated by gas lift. 54

Figure 34. Original Ussing chamber. The half cells with thermostated water jacket, gas lift, and potential diffedrence and current electoredes are shown. 55

Figure 35. Caco-2 cell monolayer cultured on polycarbonate filter [10]. 56

Figure 36. Transepithelial electrical resistance (■) and mannitol flux (○) as indices of monolayer integrity [10]. 57

Figure 37. Relation of solute permeability of several substances across Caco-2 monolayer and human large intestinal tissue. 58

Figure 38. Comparison between percent absorbed in humans and permeability across Caco-2 cell monolayer for several molecules. 59

Figure 39. Correlation between apparent permeability of Caco-2 e MDCK for actively transported compounds (□), passively transported compounds (♦), and efflux substrates (○) [54]. 60

Figure 40. Total Amount of Pgp (Human + Canine) in several subpopulation of MDCK cells (RRCK, MDCKII-WT and MDCKII-MDR1Cells)[55]....61

Figure 41. Relationships between FA and permeability coefficients (□) obtained in 2/4/A1 (A) and Caco-2 (B). Data from the human jejunum in vivo (■). The squares represent sparingly absorbed (FA 0–20%), intermediately absorbed (FA 20–80%) and completely absorbed (80–100%) drugs after oral administration to humans [56]. 62

Figure 42. Permeability versus moleculare weight of PEG oligomers for different cell lines. (□) 2/4/A1 cells, (■) Caco-2 cells, (Δ) MDCKII cells, (▲) human intestine [57]....64

Figure 43. Porosities constituted by large pores (grey) and small pores (black) in MDCKII, Caco-2, 2/4/A1 cell lines and human intestine [57]....65

Figure 44. Cross section of PAMPA sandwich assembly [59]. 66

Figure 45. Absorption in humans versus PAMPA flux at pH 6.5 (a) and 7.4 (b) [58]. 66

Figure 46. (A) GI-tract absorption of 32 drugs versus hexadecane membrane (HDM) log P_e at pH 6.8. (B) GI-tract absorption of 32 drugs versus hexadecane membrane log P_e at pH range 4-8 [60]. 67

Figure 47. Plot of permeability vs. dose number (Do) obtained by PAMPA and HTSA, respectively [61]. 68

Figure 48. Schematic of the membrane transport barriers across the intestinal epithelium during a perfusion of the intestinal lumen [10]. 69

Figure 49. Schematic of an *in situ* perfusion technique [52], R = reservoir, P = pump. 69

Figure 50. Different perfusion flow patterns: (a) oscillating perfusion, (b) recirculating perfusion, (c) single pass perfusion, (d) ligated intestinal loop....70

Figure 51. Correlation between oral absorption in humans and the permeability coefficients in vascularly perfused rat intestine [63]. 71

Figure 52. Schematic illustration of the vascularly perfused rat intestinal preparation and the perfusion apparatus. A pair of mesenteric vessels supplying an intestinal segment (or the superior mesenteric artery and portal vein) were cannulated [52]. 72

Figure 53. Schematic diagram of intestinal vascular perfusion without obstruction of mesenteric or portal blood flow [52]. 73

Figure 54. Schematic illustration of the vascularly perfused rat intestinal-liver preparation and the perfusion apparatus [52]. 74

Figure 55. The multichannel tube system with double balloons enabling segmental jejunal perfusion in man [64]. 76

Figure 56. Schematic of the Loc-I-Gut perfusion technique [64]. 77

Figure 57. The effective permeability of various drugs evaluated using CaCO-2 monolayer, rat jejunal segment in Ussing chamber, the perfused rat jejunum, and the human jejunum [10]. 78

Figure 58. Theophylline structure. 82

Figure 59. Diclofenac structure. 83

Figure 60. Propranolol structure. 84

Figure 61. Vitamin B12 structure. 86

Figure 62. Bovine Serum Albumin structure. 87

Figure 63. HPMC chemical structure. 88

Figure 64. Schematic of a Franz cell. 92

Figure 65. Schematic of the exchange system: A=Acceptor compartment, D=Donor compartment, F=Filter. 94

Figure 66. Example of spectra collected and subtracted. 96

Figure 67. Typical chromatogram of a theophylline solution in pH 6.8 phosphate buffer. The dotted curve is the baseline of the peak. 97

Figure 68. Relation between the concentration and the integral values for a theophylline solution in pH 6.8 phosphate buffer. 98

Figure 69. Relation between the concentration and the integral values for a diclofenac solution in pH 6.8 phosphate buffer. 99

Figure 70. pH history in the gastrointestinal tract. During the first two hours the pH decreases from a value of 4.8 to 1.0, then the environment was neutralized. 103

Figure 71. pH set point evolution in the gastrointestinal tract and pH reproduced with the new device. 104

Figure 72. Release pattern of HPMC/theophylline tablet obtained following the conventional method. The dashed vertical line represents the time of neutralization (120 min). 105

Figure 73. Release pattern of a commercial diclofenac tablet (EG). The dashed vertical line represents the time of neutralization (120 min). 106

Figure 74. Comparison between the release patterns of diclofenac in a matrix of an enteric co-polymer synthetized in our labs (triangles) and in a commercial

tablet (squares). The dashed vertical line represents the time of neutralization (120 min).....107

Figure 75. Release pattern of a HPMC/theophylline tablet following the real pH history. The dashed vertical line represents the time of neutralization (120 min)...108

Figure 76. Release patterns of HPMC/theophylline tablets using conventional (■) and new (□) dissolution method.....108

Figure 77. Release patterns of HPMC/theophylline tablets using conventional (■) and new (□) dissolution methods, first stage of dissolution. The dashed vertical line represents the time of neutralization (120 min).....109

Figure 78. Release pattern of a commercial diclofenac tablet (EG) submitted to a pH history. 110

Figure 79. Release pattern of a commercial diclofenac tablet (EG) according with the conventional dissolution method (USP) and with the new device. 110

Figure 80. Comparison between the release patterns of diclofenac in a matrix of an enteric co-polymer synthetized in our labs obtained with the conventional dissolution method (▲) and with the pH history (Δ).....112

Figure 81. Release pattern of an enteric coated, fast release commercial tablet of diclofenac following the conventional USP method (black squares) or the modified release patter (empty circles). The vertical line represent the time at which the medium is neutralized.....113

Figure 82. Thophylline concentrations profile in the donor (c_D) and in the acceptor (c_A) compartments.....116

Figure 83. Logarithm of the concentration differences versus time for theophylline. The dotted line represent the linear fitting of the experimental data. 118

Figure 84. Predicted concentration profiles compared with the experimental value. 119

Figure 85. Logarithm of the concentration differences versus time for diclofenac. The dotted line represent the linear fitting of the experimental data. 120

Figure 86. Diclofenac concentrations profile in the donor (c_D) and in the acceptor (c_A) compartments. The lines in figure are the model curve. 120

Figure 87. Logarithm of the concentration differences versus time for propranolol. The dotted line represent the linear fitting of the experimental data...121

Figure 88. Propranolol concentrations profile in the donor (c_D) and in the acceptor (c_A) compartments. The lines in figure are the model curve. 122

Figure 89. Logarithm of the concentration differences versus time for vitamin B12. The dotted line represent the linear fitting of the experimental data. 123

Figure 90. Vitamin B12 concentrations profile in the donor (c_D) and in the acceptor (c_A) compartments. The lines in figure are the model curve. 123

Figure 91. Logarithm of the concentration differences versus time for BSA. The dotted line represent the linear fitting of the experimental data. 124

Figure 92. BSA concentrations profile in the donor (c_D) and in the acceptor (c_A) compartments. The lines in figure are the model curve. 125

Figure 93. Comparison between *in vivo* and measured permeability (the upper graph) and dependence of *in vitro* permeability from the stokes radius of the molecules. a = -0.067; b = 0.378; R2 = 0.891..... 126

Figure 94. The two parts of the mass exchanger in which the artificial membrane is inserted. 128

Figure 95. The assembled mass exchanger and the flow pattern..... 129

Figure 96. Geometry of the mass exchanger implemented in Comsol..... 130

Figure 97. Mesh used for the fluid dynamic simulation..... 130

Figure 98. Velocity field into the mass exchanger (blood side). 132

Figure 99. Velocity field into the mass exchanger (intestinal side). 133

Figure 100. Sketch of the model: the donor, acceptor and membrane compartments are shown with their fluxes..... 135

Figure 101. Theophylline concentration evolutions in donor and acceptor compartments varying the flow rate. Donor: full squares; Acceptor: open circles; Mass entrapped in the membrane: full triangles. The lines are the model simulations (continuous = donor, dashed = acceptor, dotted = mass in the membrane)..... 138

Figure 102. Evolutions of theophylline masses for conventional dissolution test (full stars), in the donor vessel (full squares) and in the acceptor vessel (open circles). Flow rate = 20 mL/min. 139

Figure 103. Release patterns of a theophylline tablet in the case in which the acceptor solution has a straight flow (closed symbols) or a lateral flow (open symbols) through the filter. The reference curve is the release pattern without the exchange system. In this graph also line guides are reported (grey = lateral direction of the fluid rich in drug content; black = straight direction of the fluid rich in drug content). On the right the two different layouts are shown. 140

Figure 104. Comparison between the release patterns of a diclofenac commercial tablet (DOC) using a co-current or a counter-current flow following the conventional USP method. On the right the two different layouts are shown... 141

Figure 105. Diclofenac release profile (DOC) in the donor and acceptor compartment following the conventional dissolution method and the pH evolution modified. The reference is the release profile using the conventional method without mass exchange. On the right the layout of the experimental device is shown. 142

Figure 106. Release patterns for enteric fast release diclofenac (co-current flow). On the right the layout of the experimental device is shown. 143

Figure 107. Lattice bag used for the simulation of the stomach on the left, the guide with the contraction elements on the right. 147

Figure 108. Schematic of the apparatus which simulates the peristaltic waves in the stomach. 147

Figure 109. Release pattern of a commercial extended release tablet of diclofenac in the *in vitro* device simulating the mechanics of the stomach. The % release is evaluated on the basis on the drug content in the tablet. 149

Figure 110. Release pattern of a commercial extended release tablet of diclofenac in the *in vitro* device simulating the mechanics of the stomach and the intestinal environment. The % release is evaluated on the basis on the drug content in the tablet. 150

Figure 111. Comparison between the release pattern of a commercial extended release tablet of diclofenac in the *in vitro* device simulating the mechanics of the stomach and the intestinal environment and in the conventional apparatus. The % release is evaluated on the basis on the drug content in the tablet. 151

Figure 112. Release at the bottom of the artificial stomach varying the frequency of the contractions. The % release is evaluated on the basis on the drug content in the tablet. 152

Figure 113. Complete release pattern varying the frequency of the contractions compared with the conventional release. The % release is evaluated on the basis on the drug content in the tablet. 153

Figure 114. Schematic of the *in silico* model. 156

Figure 115. Fitting of the release patterns of a diclofenac tablet obtained with the conventional dissolution method (■ experimental data; continuous curve: fitting) and with the pH history (□ experimental data; dotted line: fitting). 160

Figure 116. Plasma profile of diclofenac after oral administration of a 50 mg dose [91]. Symbols are experimental data, line is the model prediction after parameter optimization. 161

Figure 117. The plasma profiles obtainable: if the real *in vitro* release kinetics would be the one observed using the conventional dissolution method (the continuous line), and if the real *in vitro* release kinetics would be the one observed using the novel apparatus (the dotted line). The horizontal dashed lines represent the minimum effective concentration (the lower one, [92]) and the minimum toxic concentration (the higher one, [93]), therefore they identify the therapeutic window. 162

Figure 118. Comparison between the gastrointestinal concentration profile reproduced *in vitro* (on the left) and simulated *in silico* (on the right). 164

Figure 119. *In vitro* release kinetic of verapamil [95]. 165

Figure 120. Plasma concentration of S-verapamil (left) and S-norverapamil (right) for elderly females (EF). 168

Figure 121. Plasma concentration of S-verapamil (left) and S-norverapamil (right) for elderly males (EM). 168

Figure 122. Plasma concentration of S-verapamil (left) and S-norverapamil (right) for young females (YF). 169

Figure 123. Plasma concentration of S-verapamil (left) and S-norverapamil (right) for young males (YM). 169

Figure 124. Plasma concentration of R-verapamil (left) and R-norverapamil (right) for elderly females (EF). 170

Figure 125. Plasma concentration of R-verapamil (left) and R-norverapamil (right) for elderly males (EM). 170

Figure 126. Plasma concentration of R-verapamil (left) and R-norverapamil (right) for young females (YF). 171

Figure 127. Plasma concentration of R-verapamil (left) and R-norverapamil (right) for young males (YM). 171

Figure 128. Hepatic clearance of verapamil and norverapamil for all the groups of subjects. 174

Figure 129. Absorption kinetic constant in the large intestine of verapamil and norverapamil for all the groups of subjects. 175

Figure 130. Absorption kinetic constant in the large intestine of verapamil and norverapamil for all the groups of subjects. 175

Figure 131. Elimination kinetic constant in the large intestine of verapamil and norverapamil for all the groups of subjects. 176

Figure 132. Elimination kinetic constant in the plasma of verapamil and norverapamil for all the groups of subjects. 176

Figure 133. Elimination kinetic constant in the small intestine of verapamil and norverapamil for all the groups of subjects 177

Figure 134. Plasma volume for R-isomer (left) and S-isomer (right). 177

Tables Index

Table 1. Factors influencing bioavailability [10]. 9
Table 2. Chemical, physical and pharmacokinetic data of theophylline. 83
Table 3. Chemical, physical and pharmacokinetic data of diclofenac sodium. 84
Table 4. Chemical, physical and pharmacokinetic data of propranolol 85
Table 5. Chemical, physical and pharmacokinetic data of vitamin B12. 87
Table 6. Chemical and physical data of BSA. 88
Table 7. Characteristics of the hollow fiber filter. 90
Table 8. Franz cell dimensions. 92
Table 9. Active molecules and their wavelengths studied with the Franz cell 93
Table 10. HPLC method to detect theophylline. 97
Table 11. HPLC method to detect diclofenac. 98
Table 12. Theophylline concentrations versus time. 117
Table 13. Diclofenac concentrations versus time. 119
Table 14. Propranolol concentrations versus time. 121
Table 15. Vitamin B12 concentrations versus time. 122
Table 16. BSA concentrations versus time. 124
Table 17. *In vitro* and *in vivo* permeability of several molecules. 125
Table 18. Physical characteristic of the blood in the portal vein. 131
Table 19. Physical and fluid dynamic characteristics of the portal vein [87], [88]. 131
Table 20. Physical characteristics of the intestinal content. 132
Table 21. Physical and fluid dynamic characteristics of the small intestine. 133
Table 22. Description of the symbols reported in the mass balances. 158

Table 23. Function parameters for the equation fitting the release kinetic both for the conventional dissolution method ($r_{conv}(t)$) and for the novel dissolution method ($r_{mod}(t)$). 160

Table 24. The model parameters used to describe the diclofenac pharmacokinetics obtained. 162

Table 25. Michaelis-Menten kinetics parameters. 167

Table 26. Area under curve of the experimental data and of the model for verapamil and norverapamil (S-isomer). The error is reported. 172

Table 27. Pharmacokinetic parameters of the experimental data and of the model for verapamil and norverapamil (S-isomer). The error is reported. 172

Table 28. Area under curve of the experimental data and of the model for verapamil and norverapamil (R-isomer). The error is reported. 173

Table 29. Pharmacokinetic parameters of the experimental data and of the model for verapamil and norverapamil (R-isomer). The error is reported. 173

Abstract

One of the aims of the thesis was to design and realize an *in vitro* device able to reproduce the gastrointestinal behavior.

To reproduce the temperature and pH history an USP apparatus II coupled with a control system was used. The temperature was kept constant using the USP apparatus, a pH probe was inserted in the dissolution medium to measure the pH. The measured pH was compared (by a software) with a set point. Proportionally at the mean error, a quantity of an acidic or basic solution was inserted, by pumps, in the dissolution medium adjusting the pH at the desired value. Using the real pH history of the gastrointestinal tract, which provide a decrease in the pH value from 4.8 to about 2.0 during the first two hours of dissolution, and then an increase to 6.8, the release pattern from tablets was evaluated. The release patterns of these tablets obtained with the new device were compared with those obtained using the conventional method (which provides a pH 1 during the first two hours of dissolution, and then the neutralization at pH 6.8) and it was found that the drug released during the first two hours was higher in the case in which the real pH history was reproduced. This is due to the fact that the higher pH in the first stage damages the coating of the tablet.

Once the chemical and thermal conditions were reproduced, the reproduction of the transport across the intestinal membrane was faced. An high throughput device which is able to reproduce continuously the exchange between the compartments has been necessary. The USP apparatus was equipped with a device composed by an hollow filter (which simulate the intestinal wall) and two pumps for the fluids simulating the intestinal content and the circulatory system surrounding the gastrointestinal tract content. The fluids enter in contact in the filter and the fluid rich in drug content (that simulates

the intestinal content) gives the drug to the fluid poor in drug (simulating the blood content). The release patterns obtained by the use of this device were studied and compared with those obtained following the conventional dissolution method. Moreover these release patterns obtained using the real pH evolution were coupled with the effect of mass exchange and compared with those obtained using the conventional methods. The results showed that the effect of the real history of pH is higher in the first stage of dissolution, than the effect of the mass exchange is dominant.

The reproduction of the mechanical history of the stomach is than faced. The peristaltic waves were reproduced using a lattice bag (elastic and compressible) connected to a camshaft which, with its rotation ensured the contraction of the bag. The bag was shrunk by connectors and the right position was ensured by guides. Changing the rotation speed of the shaft, the frequency of the contractions could be adjusted. The release pattern of a commercial tablet in the new device was evaluated and compared with the conventional one. The results showed that the non-perfect mixing of the stomach was satisfactory reproduced and this lead to a release pattern completely different. Moreover, the effect of the frequency of the contractions on the release pattern was evaluated.

Second, but not secondary, aim of the thesis was to develop an *in silico* model (physiologically based) which is able to simulate the plasma concentration of drugs.

The model is composed by seven compartments, which simulate the human organ, tissue, or a group of them. The compartments are interconnected between them and seven differential equations (with their initial conditions) describe their behavior. Once the parameter are obtained (by fitting or in literature), using an *in vitro* release pattern, the model is able to simulate the concentrations in all the compartments, including the plasma compartment.

The plasma concentration are simulated both in the case in which the new release pattern (with the real pH history) is used as input, and the case in which the conventional one is used. The results show that in the real case the plasma concentration is very different both in value and in shape than the expected.

The model then was used to simulate the fate of several molecules simultaneously in the human body (i.e. if a racemic mixture is

administered or if the drug is metabolized to another molecule). The system of differential equations is expanded to describe the fate of each molecule. Then, the physiological parameters, such as gender and age, were integrated in the model; in this way, the dependence of the model parameter on the physiological parameter was evaluated.

Finally, the gastrointestinal concentration simulated with the *in silico* model was successfully compared with the drug concentration measured with the *in vitro* model. It could be concluded that the combined approach which uses the *in vitro* and the *in silico* models is a powerful tool in the pharmacokinetic studies.

Publication List

Publication concerning this activities:

1. G. Lamberti, **S. Cascone**, M. Iannaccone, G. Titomanlio, "In-vitro simulation of drugs intestinal absorption", *International Journal of Pharmaceutics*, 439(1-2) 165-168 (2012).
2. G. Lamberti, **S. Cascone**, G. Titomanlio, "An engineering approach to biomedical sciences: advanced testing methods and pharmacokinetic modeling", *Translational Medicine @ UniSa*, 4 (4) 34-38 (2012).
3. **S. Cascone**, F. De Santis, G. Lamberti, G. Titomanlio, "The influence of dissolution conditions on the drug ADME phenomena", *European Journal of Pharmaceutics and Biopharmaceutics*, 79 382-391 (2011).
4. M. Grassi, G. Lamberti, **S. Cascone**, G. Grassi, "Mathematical modeling of simultaneous drug release and in vivo absorption", *International Journal of Pharmaceutics*, 418 (1) 130-141 (2011).
5. **S. Cascone**, G. Lamberti, G. Titomanlio, "A rule of thumb in designing in-vitro systems to simulate the intestinal absorption", submitted to *Heat and Mass Transfer*.

Conference proceedings concerning this activities:

1. **Cascone S.,** Lamberti G., Titomanlio G.,"Modelli in silico ed in vitro per analisi farmacocinetiche" Proceedings of *GRICU 2012* Montesilvano (PE), Italy, 16-19 settembre 2012

2. **Cascone S.**, Dalmoro A., Lamberti G., Barba A.A. "Metodi innovativi di preparazione e testing per sistemi farmaceutici", Proceedings of *GRICU 2012* Montesilvano (PE) Italy, 16-19 settembre 2012

3. **Cascone, S.**; De Santis, F.; Lamberti, G.; Titomanlio, G.; Barba, A.A.; "Alternatives to Laboratory Animals: In Vitro and In Silico Approaches", Proceedings of *8th CESPT*, Graz, Austria, September 16th-18th 2010.

4. **Cascone S**.; Lamberti G.; Paolucci F.; Lamberti G.; Titomanlio G.; "In vitro and in silico approaches to reproduce pharmacokinetic relevant phenomena", Proceedings of *8th World Meeting on Pharmaceutics, Biopharmaceutics and Pharmaceutical Technology*, Istanbul, Turkey 19-22 March, 2012

Chapter One

Introduction

In this chapter the anatomy of the gastrointestinal tract is described. The main concepts of dissolution and absorption are briefly illustrated. Moreover the pharmacokinetic modeling is depicted.

Pharmaceutical industry uses several hundred thousand of animals for in vivo pharmacokinetic studies. Furthermore, during clinical trials, a large number of humans are used to test novel drugs and formulations. However, the basic principle in all in vivo studies is that no unnecessary human or animal-based research should be done. The reduction of tests involving animals or humans can be achieved by developing of in vitro and/or of in silico models. To do this, the biology, the chemistry and the physics of the in vivo test have to be reproduced with the highest accuracy.

1.1 Anatomy of the gastrointestinal tract

The knowledge of the physicochemical features and the motility characteristic of the gastrointestinal tract is necessary to develop an *in vitro* and/or an *in silico* model.

The motor function of the digestive system helps to achieve three main objectives: mechanical shredding and digestion of the dietary nutrients (in conjunction with the secretory function), maximal exposure of the products of digestion to the absorptive surface of the small bowel, and clearance of residues and bacteria from the gut. Thus the stomach largely liquefies the meal (digestive function) and delivers it into the intestine at the rate that matches the processing capability of the intestine (reservoir function). The motility of the small bowel spreads out chime, rapidly expanding the absorptive area, and it subjects the luminar contents to a movement which facilitates mixing and absorption. During the interdigestive periods, cyclic episodes of intense motor activity clear residues from the stomach and the small intestine.

1.1.1 The stomach

Anatomically, the stomach can be divided into three major regions: *fundus* (the most proximal), *corpus* and *antrum*. The region close to the *esophagus* and *duodenum* are called *cardias* and pylorus, respectively.

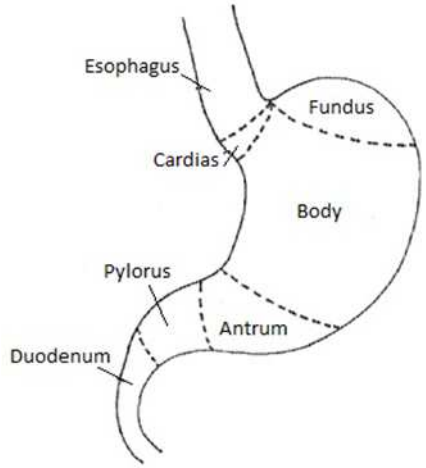

Figure 1. Stomach physiology.

The main function of the stomach is to process and to transport foods. After feeding, the contractile activity of the stomach helps to mix, grind, and eventually evacuate small portions of chime into the small bowel, while the rest of the chime is mixed and ground. Four major types of secretory epithelial cells cover the surface of the stomach and extend down into gastric pits and glands: mucous cells which secrete an alkaline mucus, parietal cells which secrete hydrochloric acid, chief cells which secrete pepsinogen, and G cells which secrete the hormone gastrin. The stomach absorbs very few substances, although small amounts of lipid soluble compounds can be taken up, including aspirin, other nonsteroidal anti-infiammatory drugs, and ethanol.

Concerning the physiological aspect, the stomach may be divided into two regions: the proximal reservoir which consists in the fundus and the upper portion of the body, and the distal active region which includes the distal part of the body, the antrum, and the pylorus.

The proximal stomach sustained contractions that are responsible for generating a basal pressure. These contractions also generate a pressure gradient from the stomach to the small intestine which is responsible for gastric emptying. In fact, a narrow zone of raised pressure has been found at the gastroduodenal junction by experiments carried out on fasted dogs [1]. Swallowing of food and consequent gastric distention inhibit contraction in this region of the stomach, allowing it to balloon out and to form a large reservoir without a significant increase in pressure, this phenomenon is called

"adaptive relaxation". Thus, increased volume of food do not result in a rapid rise in intragastric pressure due to the ability of the *fundus* to relax.

The distal stomach develops strong peristaltic waves of contraction that increase in amplitude as they propagate toward the pylorus. These powerful contractions constitute a very effective gastric grinder; they occur about 3 times per minute. Liquids readily pass through the pylorus in spurts and the rate of emptying of liquids depends on the gradient between the stomach and the *duodenum*. Conversely, the solids must be reduced to a diameter of less than 1-2 mm before passing the pyloric gatekeeper. Larger solids are propelled by peristalsis toward the pylorus, but then they are refluxed backwards when they fail to pass through the pylorus, this continues until they are reduced in size sufficiently to flow through the pylorus. Thus, the main role of the distal stomach is not to affect emptying of digestible solid, but to provide continence for, and trituration of, these solids. The time required for trituration would be avoided if solids were homogenized before ingestion [2]. The distal stomach has a minor role in gastric emptying of liquids.

When the stomach is filled, peristaltic waves are decrease. The presence of fat in a meal can completely stop these movements for a short period until it is diluted with gastric juice or removed from the stomach. Peristaltic waves start as weak contractions at the beginning of the stomach and progressively become stronger as they near the distal stomach regions. The waves help to mix the stomach contents and propel food to the small intestine.

In spite of the large amount of studies about the stomach movements and physiology, a study of the literature revealed such a diversity of opinions on the subject that further investigations appeared advisable. A detailed description of the peristaltic movements and their implications could be found in MCrea et al. [3].

The rate of stomach emptying is influenced by the pH, by the osmolarity, by the hormones, and by the volume of ingested foods. When an indigestible solid is ingested with a digestible solid, the emptying of the indigestible solid is delayed because feeding decreases the movements [2].

The emptying of solid foods may depend more on physical characteristic such as specific gravity and viscosity. A review about

the methods used for the measurement of the gastric emptying and about the disturbances which can affect the rate of emptying was carried out by Sheiner [4]. The liquid – phase gastric emptying was analyzed both in healthy subjects and in systemic sclerosis affected subjects [5]. From these studies seems to be evident that the measurement of stomach emptying based on the assumption of a single compartment system is likely to be misleading.

1.1.2 The small intestine

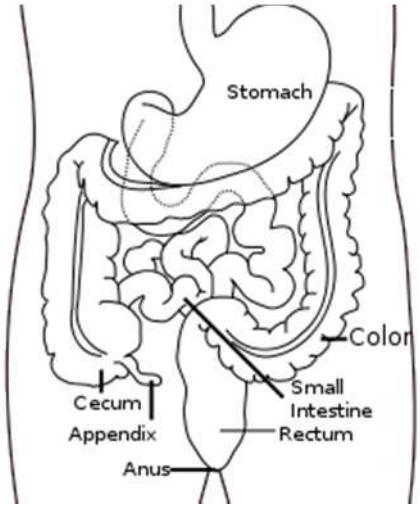

Figure 2. Gastrointestinal tract physiology.

The small intestine is made up of *duodenum*, jejunum, and *ileum*. In human beings, *duodenum* measures approximately 20 cm, while jejunum and *ileum* are approximately 2.5 and 3 m long respectively. The small intestine is strategically located at the interface between the systemic circulation and the environment, and it plays a major role as a selective permeability barrier. It permits the absorption of nutrients such as sugar, amino acids, peptides, lipids, and vitamins and it limits the absorption of xenobiotics, digestive enzymes, and bacteria. It is approximately 2.5-3 cm in diameter. Digested foods are able to pass into the blood vessels across the intestinal walls by diffusion. The small intestine is the site where most of the nutrients from ingested food are absorbed. The inner wall, or *mucosa*, of the small intestine is lined with simple columnar epithelial tissue. Structurally, the *mucosa* is covered in wrinkles or folds called *plicae circulares*, which are considered permanent features in the wall of the organ. From the *plicae circulares* microscopic finger-like pieces of tissue called *villi*

project. The individual epithelial cells also have finger-like projections known as *microvilli*. The function of the *plicae circulares*, the *villi* and the *microvilli* is to increase the surface area available for the absorption of nutrients.

Each *villus* has a network of capillaries and fine lymphatic vessels called lacteals close to its surface. The epithelial cells of the *villi* transport nutrients from the lumen of the intestine into these capillaries (amino acids and carbohydrates) and lacteals (lipids). The absorbed substances are transported via the blood vessels to different organs of the body where they are used to build complex substances such as the proteins required by the body. The food that remains undigested and unabsorbed passes into the large intestine.

Most drugs are weak organic acids or bases, existing in un-ionized and ionized forms in an aqueous environment. The un-ionized form is usually lipid soluble (lipophilic) and diffuses readily across cell membranes. The ionized form has low lipid solubility (but high water solubility – e.g., hydrophilic) and thus cannot penetrate cell membranes easily. The proportion of the un-ionized form present (and thus the drug's ability to cross a membrane) is determined by the pH and the drug's pKa (acid dissociation constant). The pKa is the pH at which concentrations of ionized and un-ionized forms are equal. When the pH is lower than the pKa, the un-ionized form of a weak acid predominates, but the ionized form of a weak base predominates. Thus, in plasma (pH 7.4), the ratio of un-ionized to ionized forms for a weak acid (e.g., with a pKa of 4.4) is 1:1000; in gastric fluid (pH 1.4), the ratio is reversed (1000:1). Therefore, when a weak acid is given orally, most of the drug in the stomach is un-ionized, favoring diffusion through the gastric mucosa. For a weak base with a pKa of 4.4, the outcome is reversed; most of the drug in the stomach is ionized. Theoretically, weakly acidic drugs (e.g., aspirin) are more readily absorbed from an acid medium (stomach) than are weakly basic drugs (e.g., quinidine). However, whether a drug is acidic or basic, most absorption occurs in the small intestine because the surface area is larger and membranes are more permeable.

The knowledge about the normal transit of chime along the small bowel and its regulation is still lacking. The reasons for the relative ignorance are the variability of the chime input into the small bowel is variable and its dependence from the gastric emptying. Some parts of the meal pass through the colon faster than others. Therefore,

physiologically there is no a single transit time but rather a distribution of residence times that cannot be easily quantified. In spite of that, the small intestinal transit time is assumed to be independent of external influences, and more consistent. As reported by McConnell et al. [6], the small intestine transit time of dosage forms is almost invariably quoted at 3 – 4 h, with no differences between tablets, pellets, and liquids. Intra-subjects variability was also observed, with a transit time varying between 1.5 and 5.4 h, the average transit time is indeed 3.2 h. The small intestinal of a dosage form is much more complex than simply being a function of intestinal motility and flow because it is not continuous. Weitschies et al. [7] were able to describe the movement of a non-disintegrating capsule along the tract by the use of a magnetic marker. The movements of this marker are characterized by a complex sequence of phases of rest, slow movements, and rapid movements. Behavior of drugs and delivery systems in the intestine depends on many physiological factors including fluid volume, fluid composition, transit, motility, *bacteria*, and pH, which are further influenced by food, gender, and age.

1.1.3 The colon

The colon is the part of the intestine from the *cecum* to the *rectum*, it is also called large intestine or large bowel. It consists of *cecum*, ascending colon, transverse colon, descending colon, sigmoid colon, and *rectum*. The colon in humans measures approximately 1.5 m in length, its diameter varies between 6 cm (in the *cecum*) and 2.5 cm (in the sigmoid colon). The colon is constituted of four layers which, from the inner to the outer, are represented by the *mucosa*, the *submucosa*, the *muscularis*, and the *adventitia*. There are many similarities in the histological structure of the *mucosa* in the colon and in the small intestine. The most important difference is that the *mucosa* of the large intestine is devoid of *villi*. The large intestine is mainly responsible for storing waste, reclaiming water, maintaining the water balance, and absorbing some vitamins. By the time the chime has reached this part of intestine, almost all nutrients and 90% of the water have been absorbed by the body. As the chime moves through the large intestine, most of the remaining water is removed, while the chime is mixed with *mucus* and *bacteria* and becomes feces. The large intestine produces no digestive enzymes because chemical digestion is completed in the small intestine. The pH in the colon

varies between 5.5 and 7. Like the small intestine, movements through the colon is not continuous, and in the transverse colon, the dosage forms were observed to be often at rest; spending 5 – 30 min periods with no or minimal propagation [7]. A mass movement was observed starting 6 h post ingestion, which transported the capsule from the distal ascending colon, to the descending colon in one movement within less than 1 minute.

Diakidou et al. [8] analyzed and characterized the contents of ascending colon to which drugs are exposed after oral administration in healthy adults under fasting and fed state. They found that free water content, pH, surface tension, and isobutyrate levels were lower in the fed than in fasted subjects. On the other hand, buffer capacity, osmolarity, acetate, and butyrate were higher in fed subjects. Carbohydrate content, protein content, and the levels of long chain fatty acid and of cholesterol are not significantly affected by the fed state. In conclusion, they found that composition of fluids in the ascending colon is affected by feeding. This may influence the performances of a dosage form designed to release in the colon.

With the aim to simulate the composition of biorelevant media as closely as possible to the composition and to the physicochemical characteristics of the gastrointestinal fluid, a set of four dissolution media was presented [9]. These media was found to be able to simulate the condition of the fasted stomach, of the postprandial stomach, and of the upper small intestine both in the fasted and in the fed condition.

1.2 Dissolution and absorption

The oral route is the most important drug administration route. Oral bioavailability is a fundamental requisite for any orally administrated drug to be effective. Systemic bioavailability is influenced by a variety of factors, which are summarized in Table 1.

Table 1. Factors influencing bioavailability [10].

Physiological factors	Membrane transport
	GI motility
	Stomach emptying
	Disease state
Formulation	Crystal form (polymorphism)
	Particle size
	Absorption enhancers
	Dissolution rate
	Solution, capsule, tablet or other
Pharmacokinetic factors	GI and liver metabolism
	Chemical instability
	Absorption
	Distribution and elimination
Physiochemical properties	Lipophilicity
	Solubility
	Degree of ionization
	Molecular size and shape
	Hydrogen-bonding potential

The key phenomena involved in the administration of a solid dosage forms are the dissolution and the absorption of the drug. Dissolution is defined as the process by which a solid substance enters in the solvent to yield a solution. To determine the dissolution rate of the drugs from solid dosage forms, several physicochemical processes in addition to the dissolution of pure chemical substances have to be considerate. The first step consists of the contact between the solvent and the solid surface (wetting), which leads to the production of a solid – liquid interface. The breakdown of the molecular bonds of the solid (fusion) and passage of molecules of the solid – liquid interface (solvation) are the second and third steps, respectively. The final step implies the transfer of the solvated molecules from the interfacial region into the bulk solution (diffusion) [11]. The physical characteristics of the dosage form, the wettability of the dosage unit, the penetration ability

of the dissolution medium, the swelling process, the disintegration and deaggregation of the dosage form are some of the factors that influence the dissolution features of the drug.

The dissolution and the absorption of the drug are the main phenomena involved in the administration of a solid dosage form. Indeed, the Biopharmaceutical Classification System (BCS) identifies the solubility and the permeability as the key parameters to describe the drug fate once ingested. According to BCS, drug substances are classified as: Class 1 drugs (high solubility and high permeability), class 2 drugs (low solubility and high permeability), class 3 drugs (high solubility and low permeability), and class 4 drugs (low solubility and low permeability) [12], as shown in Figure 3.

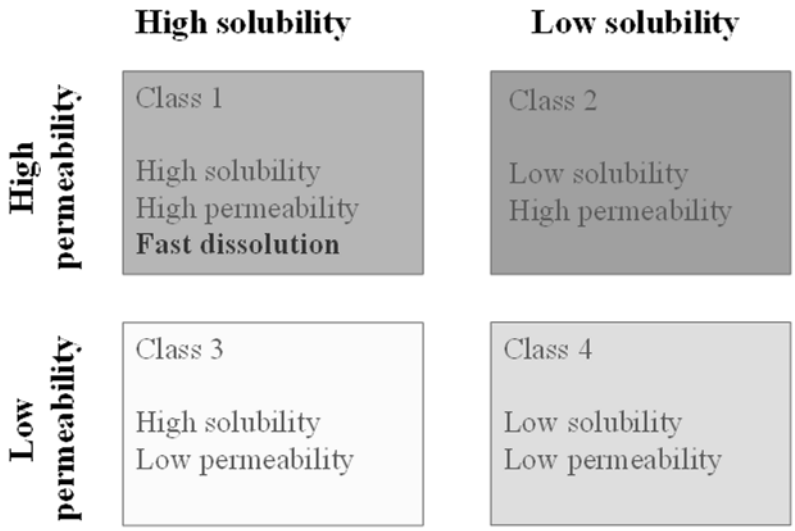

Figure 3. BCS substances classification in term of solubility and permeability.

According to these criteria, drugs are considered highly soluble when the highest dose strength of the drug substance is soluble in less than 250 mL of water over a pH range of 1-6.8; drugs are considered highly permeable when the extent of absorption in humans is determined to be greater than 90% of the administered dose.

When a solid dosage form arrives in the gastrointestinal tract, there are two possibilities of rate – limiting step. The solid form must first dissolve and then the drug in solution must pass through the gastrointestinal membrane. Freely water soluble – drugs dissolve rapidly, making the passive diffusion of the drug or its active transport

the rate limiting step for the absorption. Conversely, the rate of absorption of poorly soluble drugs is limited by the rate of dissolution of the undissolved drug or disintegration of dosage form [13]. The rate of dissolution of the pure drug substance is determined by the rate at which solvent – solute forces of attraction overcome the cohesive forces present in the solid. This process is rate limiting when the release of the solute into the solution is slow and the transport into the bulk solution is fast. In this case dissolution is named "interfacially controlled" dissolution. Dissolution may also be "diffusion controlled", when the solvent – solute interactions are fast compared to the transport of solute in the bulk solution.

Both dissolution and disintegration are key parameters in the product development strategy. Disintegration usually reflects the effects of formulation and manufacturing process parameters, whereas the dissolution from drug particles mainly reflects the effects of solubility and particle size, which are properties of the pharmaceutical raw material, but the dissolution can also be influenced significantly by processing and formulation. Therefore, dissolution testing provides the means to evaluate the critical parameters such as adequate bioavailability and it provides information necessary to the formulator in development of more effective dosage forms.

Hence, dissolution analysis of pharmaceutical dosage forms has emerged as the most important test that will ensure the quality and the bioavailability of a product. The knowledge of critical operating variables for a dissolution testing device is important for product development, quality control, and research application.

The development and the use of *in vitro* dissolution tests to evaluate and to describe *in vivo* dissolution and absorption is useful to screen potential drugs and their formulations for their dissolution and absorption characteristic and to improve the quality control procedures.

1.3 Pharmacokinetic modeling

The prediction of the drug concentration in the blood, tissue, and organs is the goal of the *in silico* pharmacokinetic modeling. The approaches to the modeling of the physiological phenomena can be different on the basis of the details used. The description of the phenomena taking place in the body is much closer to the real physiology if more details are considered.

The processes which a drug follows after the administration are absorption, distribution, metabolism, and excretion (ADME); these processes determine the evolution of the drug concentration in the body. The route of administration, the physical and chemical properties of the substance, the characteristics of the dosage form, and the physiological conditions are the factor with the most important effect on the entity and the rate of the ADME phenomena. The age, the gender, and the weight of the subject influence the ADME phenomena.

The absorption of a drug is rapid and complete in the case of intravenous injections, while it is generally delayed and incomplete in the case of oral administration. The absorption is characterized by the mechanisms of passive diffusion, facilitated diffusion, and active transport. The fraction of the drug which overcomes the biological barriers by passive diffusion enhances with the increase of the solubility of the drug in the gastrointestinal fluid, with the increase of the affinity of the substance for the phospholipids which constitute the living membrane, with the decrease of the drug molecular weight, and with the increase of the residence time in the gastrointestinal tract. The rate of the absorption phenomenon increases with the increase of the diffusion coefficient of the drug and with the decrease of the dimensions of particles which constitute the pharmaceutical formulation. The facilitated diffusion and the active transport are more complex absorption mechanism in which a carrier is involved.

The distribution of a drug is faster if the rate of absorption increases: the time of appearance of the drug in tissues and organs is lesser in intravenous injections than in oral assumptions. The mechanisms by which the drug is distributed in the organs and in the tissues are the same which characterize the passage through the gastrointestinal *mucosa*. Therefore, in the passive diffusion, a higher affinity for the constituent of the biological membranes causes an increase in the rate of the phenomenon. The amount of the drug which can be contained in a tissue or an organ increases as the real volume of the tissue or organ increases and as the fraction of the species bound to the plasma proteins decreases. The higher is the blood perfusion in the tissue or organ, the faster is the drug reaching and leaving it.

The metabolism of the drug is strongly dependent on the route of administration: if the substance is taken by intravenous injection, it is introduced in the systemic circulation and directly distributed to the

tissue. Indeed, if the substance is taken by oral administration, it undergoes the first – pass effect in which a fraction of drug is metabolized before reaching the systemic circulation. Different enzymatic reactions are involved in the metabolism. They occur mainly in the liver but also in other tissue and organs such as the intestinal *mucosa* and the kidneys. The fraction of the drug metabolized increases with the increase of the number of metabolizing sites, the rate of the biotransformation increases also with the decrease of the fraction of the substance bound to plasma or tissue proteins.

The excretion of a drug takes place by two main routes: the liver and the kidneys which produce the bile and the urine, respectively. The mechanism of the substance removal from the body depends on its molecular weight: smaller particles are removed mainly in the urine. The liver metabolizes the species by secretion, the kidneys by filtration (passive transport) and by secretion (active transport). The more hydrophilic are the substances administered, the higher is the percentage of the dose excreted. The rate of elimination increases with the increase of the unbounded to plasma and tissue proteins.

All these transport phenomena described must be taken into account in the development of an *in silico* model.

Three different approaches can be followed to build an *in silico* model to predict the fate of administered drug:

1. **The pure compartment modeling**. The compartment approach is based on the schematization of the body by a system of interconnected volumes, the compartments, which can be easily identified as chemical reactors or as a physical contacting units. In the pure compartmental models, the compartments do not represent necessary anatomical units.
2. **The physiologically based pharmacokinetic modeling (PBPK)**. In the physiologically based models, the compartments are representative of a tissue, an organ or a group of organs, each with a specific function, and the interconnection between the compartments reproduces the effective one between tissue and organs.
3. **The purely mathematical modeling**. The pure mathematical models are able to correlate the results of an *in vitro* dissolution tests to the *in vivo* drug concentration in the blood. Such correlations are the IVIVC (*in vitro/in vivo* correlations).

The IVIVC are classified in four levels: level A, level B, level C, and multiple level C correlations [14]:

1. A level A correlation is a point to point relationship between the *in vitro* dissolution profile and the *in vivo* plasma evolution of a drug.
2. A level B correlation is a relationship between the mean *in vitro* dissolution time and the mean *in vivo* residence time, obtained by considering the full profile of *in vitro* dissolution and the full *in vivo* plasma evolution.
3. A level C correlation is a single point relationship between a dissolution parameter (e.g. the percent dissolved after 4 h) and a PK parameter (e.g. the maximum of plasma concentration).
4. A multiple level C correlation is a relationship between several points of the dissolution profiles with several PK parameters.

Regulatory boards (FDA, USP) accept only Level A IVIVC for Scale-Up and Post-Approval Changes (SUPAC) which can be justified without the need for additional human studies. A PK model able to correlate the *in vitro* dissolution profile and the *in vivo* plasma evolution, will play the same role of a Level A IVIVC, but it is of great interest since it is more physically based.

Chapter Two

State of the art – *in vitro* and *in silico* models

In this chapter the analysis of the in vitro models found in literature, both USP and not USP approved, is faced. Moreover, several models used to simulate the gastric motility are described. Furthermore, the analysis of the in silico pharmacokinetic models found in literature is faced.

2.1 USP apparatuses

It has long been recognized that solid drug orally administrated are not immediately available to the biological system since they are absorbed only from a solution. During the development of the dosage form, the *in vitro* tests serve as a guide in estimating the amount of drug released per unit time in a given dissolution medium. *In vitro* dissolution tests seems to be the most sensitive and reliable predictors of *in vivo* performances and they offer a meaningful indication of physiological availability.

Many devices have been reported for determination of the dissolution rate, some of them accepted and classified by the Pharmacopeia(s). The procedures differ in degree rather than in basic principles. The apparatuses used for dissolution testing are the USP (United States Pharmacopeia) apparatuses 1, 2, 3, 4, 5, 6, and 7 [15].

The USP Apparatus 1 (basket apparatus) consists of a wire-mesh basket that is attached to a rotation shaft, which is then immersed into a dissolution vessel for the duration of the dissolution test. Since the dosage form is in direct contact with the basket, the physical dimensions and the motion of the basket can have a strong impact on the dissolution rate of the solid dosage unit. The basket height, the diameter of the basket opening, height of the open screen, and size of the mesh are specified in USP chapter <711>.

Figure 4. USP apparatus 1 (basket apparatus).

The advantages of this apparatus are the breadth of experience in its use, the possibility to obtain easily pH changes during a test, and the ease of automation, which is important for routine investigations. On the other hand, the dosage form is subjected to

dissolution/disintegration interactions, which could influence the rate of dissolution. Furthermore, other critical points are the presence of an hydrodynamic "dead zone" under the basket and the presence of a limited volume which could not ensures the perfect sink, especially for poorly soluble drugs.

Another official method is the USP apparatus 2, the paddle method. For these apparatuses, vessels should be uniform with respect to their weight, inside diameter, and inside curvature. Statistically significant differences in dissolution rates have been reported when the same product was tested in different vessels. In this official method, the sample container itself serves as a liquid stirring device. Under these conditions, there can be strong abrasion and wear of the sample due to mechanical impacts with the container surface.

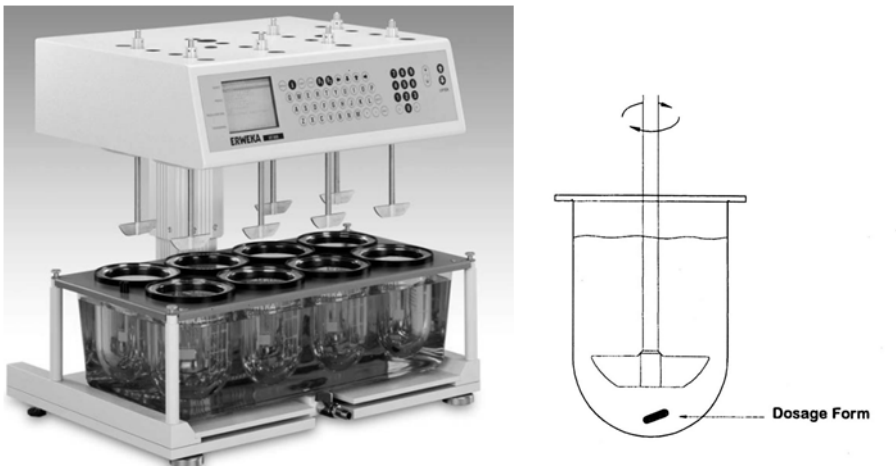

Figure 5. USP apparatus 2 (paddle method).

Instead of the simplicity of use, its high degree of standardization, and its robustness, this apparatus is characterized by ease to realize pH changes and the fluid dynamic is very complex and can vary with site of dosage form in the vessel and therefore may significantly affect drug dissolution.

The USP apparatus 3, the reciprocating cylinder, was based on the recognition of the need to establish *in vitro* - *in vivo* correlation (IVIVC), since the dissolution results obtained with USP apparatuses 1 and 2 may be affected by mechanical factors, such as shaft wobble, location, centering, deformation of the basket and paddles, and presence of bubbles in the dissolution medium. The design of this

apparatus provides capability agitation and media composition changes during a run as well as full automation of the procedure.

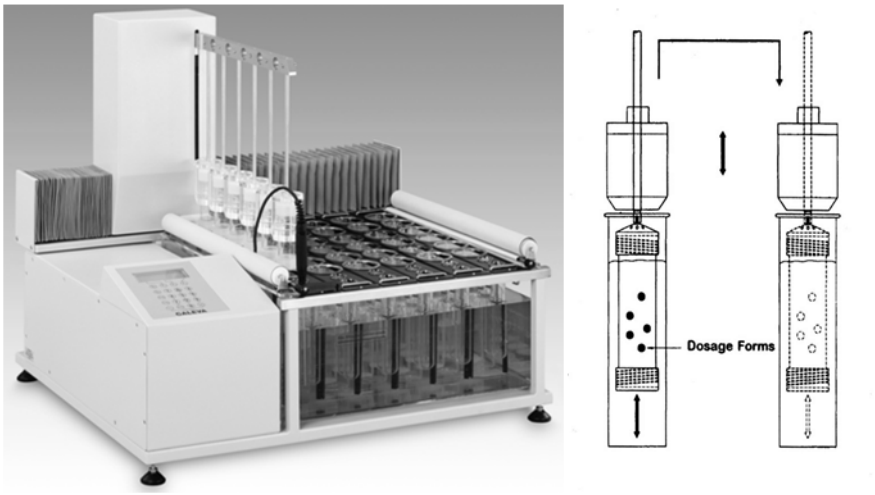

Figure 6. USP apparatus 3 (reciprocating cylinder).

Furthermore, the reciprocating cylinder allows to obtain a good correlation for extended-release formulations because of the ease of sampling, and because of the ease of pH changing during the test run which offers the advantage of mimicking the changes in physiochemical conditions. The deformation rates are higher than those of the apparatuses 2 but the apparatus 3 is less diffused and used.

The USP apparatus 4, also known as the flow – through cell, is composed by a small volume cell containing the sample solution which is subjected to a continuous stream of dissolution medium. The dissolution medium flows through the cell from bottom to top. The pulsating movement of the piston pump supplies the need of further stirring or shacking elements. A filtration device at the top of the cell retains all the undissolved material. The flow-through cell system usually operated as an open loop, therefore new dissolution medium is continuously introduced into the system. In this way, all the drug dissolved is immediately removed along the flow of the dissolution medium. This apparatus is reliable not only for the determination of the dissolution rate of tablets but also of capsules, semisolids, powders, and granules.

Figure 7. USP apparatus 4 (flow – through cell).

Some advantages of the apparatus 4 are: the possibility of generating rapid pH changes during the test, continuous sampling, unlimited solvent volume, minimizing downtime between two tests, ability to adapt test parameters to physiological conditions, and retention of undissolved particles (without of additional step of filtration or centrifugation). Instead of the fact that the apparatus is very versatile, the realized fluid dynamic is very far to the real one, it requires high volume of dissolution media, and deareation is necessary.

Transdermal or patching testing is carried out using USP method 5 (paddle over disc) or USP method 6 (rotating cylinder). With paddle over disc, the transdermal patch is placed between a glass disc and an inert mesh. This is placed at the bottom of the vessel, with the meshing faced upwards, under a rotating paddle. Unlike dissolution testing, transdermal testing is carried out at 32°C to reflect the lower temperature of the skin. Other variables such as the height setting and sampling requirements are the same as dissolution testing. The rotating cylinder is very similar to USP method 1 (the rotating basket). With USP method 6, however, the basket assembly is replaced by a solid stainless steel cylinder. The cylinder consists of two parts that fit together: the main shaft/cylinder assembly plus an extension. The extension is used when the transdermal patch requires a larger area.

Figure 8. USP apparatuses 5 and 6 (paddle over disc and rotating cylinder, respectively).

The advantage of these apparatuses is the possibility to use a standard equipment (paddle) but, conversely, the disk assembly restricts the patch size.

Originally introduced in the USP as small-volume option for small transdermal patches, the USP apparatus 7 (reciprocating disk apparatus) was later renamed the reciprocating holder apparatus with the adoption of four additional holders for transdermal system, osmotic pumps and other low dose delivery systems.

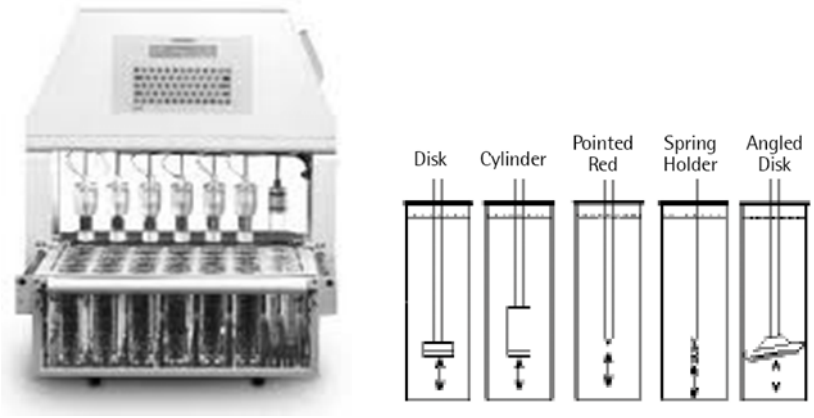

Figure 9. USP apparatus 7 (reciprocating disk).

With this apparatus, switch to different pH buffer is easy and provides deformation rates higher than apparatus 2 but it is less diffused and used.

2.2 Non USP apparatuses

There are a lot of devices used in dissolution testing. Many of these suffer from deficiencies, such as too poor agitation, absence of sink condition, and inability to program progressive changes in the dissolution environment. Different apparatuses (not USP approved) were built to overcome these difficulties. The benefits of alternative dissolution approaches to the currently recommended USP methods applied to swellable/floatable delivery systems were shown by Pillay and Fassihi [16]. They used a new device in conjunction with the paddle method to study the influence of the position of various dosage forms on release behavior. This device was accomplished by placing the delivery system over a ring/mesh assembly.

2.2.1 The Sartorius absorption model

The Sartorius Absorption Model was introduced in 1973 [17].

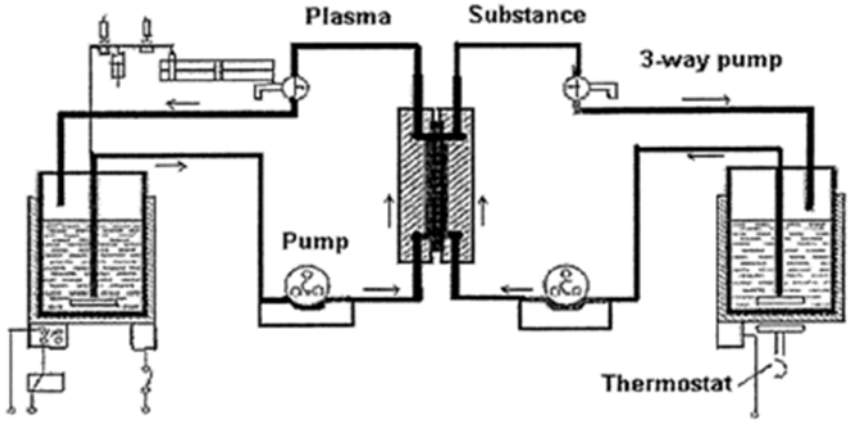

Figure 10. Schematization of the sartorius Absorption Model.

It simulates concomitant release from the dosage form in the gastrointestinal tract and drug absorption through the lipid barrier. The most important features of this model are the two reservoirs for holding different media at 37°C, a diffusion cell with an artificial lipid barrier of known surface area, and a connecting peristaltic pump which aids the transport of the solution or the media from the reservoir to the compartment of the diffusion cell. The two media typically used include Simulated Gastric Fluid and Simulated Intestinal Fluid. The drug substance under investigation is introduced, and its uptake in the diffusion cell is governed by its hydrophilic-lipophilic balance.

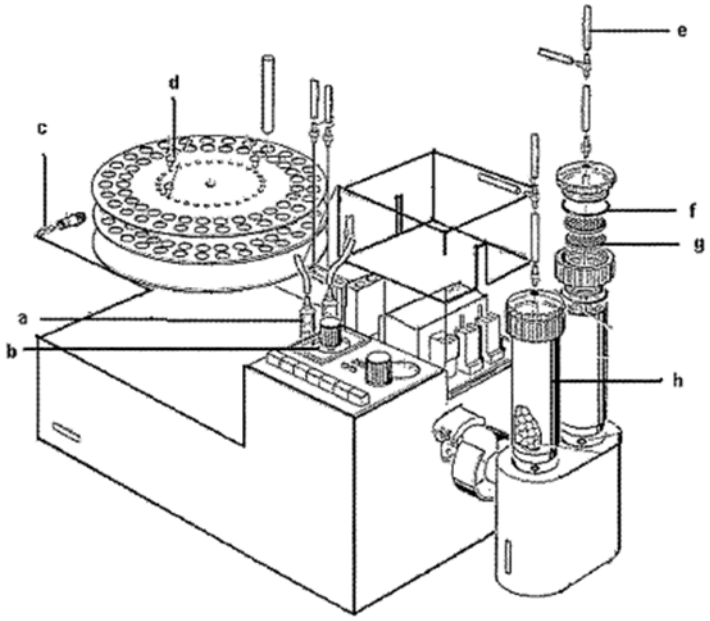

Figure 11. Sartorius dissolution model. a) plastic syringe, b) timer, c) safety lock, d) cable connector, e) silicon tubes, f) silicon O-rings, g) metal filter, h) polyacril reaction vessel.

Despite the simulation of both the dissolution and the absorption, the fluid dynamic of the system is very far from the real one and the pH changes are very difficult to be realized.

2.2.2 In vitro simulation of gastric digestion

Savalle et al. [18] proposed a simple *in vitro* method to simulate the gastric emptying of digestive product in 1989. To overcome the accumulation of digestion product and inhibition of proteolysis, a method based on the enzymatic hydrolysis of proteins with simultaneous dialysis of digested products was developed to simulate the pancreatic digestion. The aim of this work was to simulate several of the most important phenomena observed *in vivo* in the stomach during digestion of milk proteins, to obtain an *in vitro* model for studying gastric digestion of proteins. The gastric digestion unit was composed of a thermostated fermentor regulated at 37°C. Acidification of the medium and enzyme supply were ensured through two peristaltic pumps with variable flow rates and the pH of the incubation medium was measured, but not controlled, during digestion. HCl was added at constant flow rate together with diluted

enzymes at variable flow rate, then variable emptying rates are requested to maintain a constant volume in the fermentor. The contents were shaken to homogenize the mixture and to ensure the formation of coagulum. The effluents were collected and immediately precipitated and centrifuged. The authors found that, at high acidification rate, the pH drop was too fast, whereas the acidification was incomplete with a low acidification rate. The results are reported in the following figure:

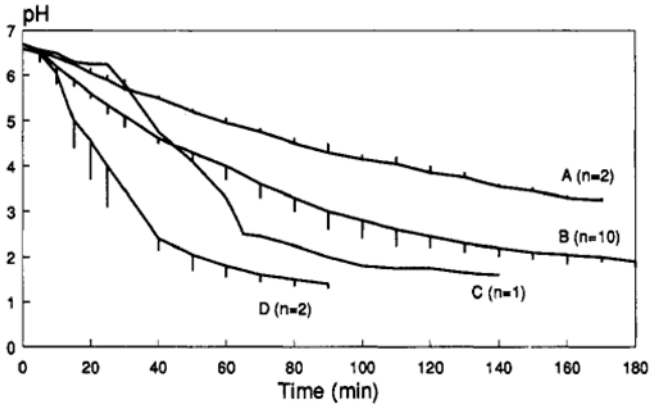

Figure 12. pH decrease during *in vitro* gastric digestion of milk. n = number of experiments. A) 143 mM HCl, 1.5 mL/min, constant shaking; B) 143 mM HCl, 2.0 mL/min, constant shaking; C) 143 mM HCl, 2.0 mL/min, irregular stirring; D) 286 mM HCl, 3.0 mL/min, regular stirring.

The choice of pH conditions is a very important factor affecting the enzymes activity and thus the composition of the evacuated products. The slow decrease of the pH is necessary to ensure emptying of intact proteins or large peptides. Finally, the authors, by means of biochemical techniques, followed and reproduced the kinetics of the gastric digestion of milk proteins. This apparatus is very simple and pH changes are very easily obtained, even if only a constant adding of acid is allowed. However, the agitation and the fluid dynamic are very far from the real one.

2.2.3 A multicompartmental model simulating the stomach and small intestine

Minekus et al. [19] developed a completed and detailed *in vitro* model which simulates the dynamic physiological processes which occur in the lumen of stomach and small intestine of men in 1995. They described this model and its accuracy and reproducibility in

simulating gastrointestinal transit, pH, bile salts concentrations and the absorption of glucose. The model consists of four successive chambers simulating the stomach, duodenum, jejunum, and ileum.

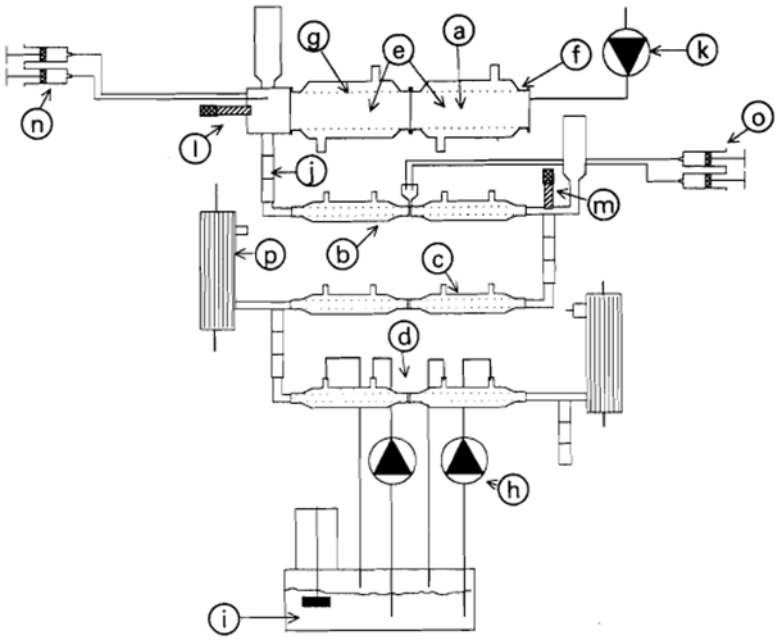

Figure 13. ***In vitro*** **model developed by Minekus et al. a) gastric compartment; b) duodenal compartment; c) jejuna compartment; d) ileal compartment; e) basic unit; f) glass jacket; g) flexible wall; h) rotary pump; i) water bath; j) peristaltic valve pump; k) peristaltic pump; l, m) pH electrodes; n, o) syringe pumps; p) hollow fibre device.**

Each compartment is formed by two connected units consisting of a glass jacket with a flexible wall inside. Water is pumped from a bath into the glass jacket around the flexible walls to control the temperature in the unit. This ensure also the mixing of the chime by alternate compression and relaxation of the flexible wall.

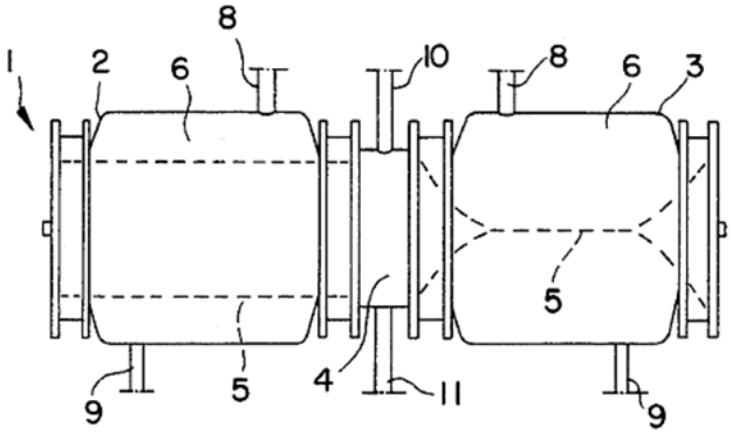

Figure 14. Simulation of the peristaltic waves in the Minekus model. 1) unit 2, 3) pressure chamber; 4) intermediate piece; 5) flexible wall; 6) space between rigid and flexible wall; 8, 9, 10, 11) connectors [20].

In fact, the space between the rigid and the flexible wall of the chamber has been filled with a liquid or a gas under pressure and, as a result, the flexible wall is pinched. The mixture of the substances which was present in the hose of the pressure chamber will be driven out of this hose and forced through the intermediate piece into the unpinched hose of the pressure chamber. Then, the liquid is discharged through the outlet and the same operation is repeated for the other chamber. In this way, the substances present inside the flexible wall will flow back again. With this continuous movement, the peristaltic movements of the stomach and the intestinal tract are simulated and homogenization is ensured.

The compartments are connected by peristaltic valve-pumps. The pH values are controlled via computer by secreting acidic or basic solutions. The jejunal and ileal compartments are connected with hollow fibers to absorb digestion products and water from chyme and to modify electrolyte and bile salt concentration. The accuracy and reproducibility of the model was verified, as well as its ability to mimic the gastrointestinal transport of chyme. The model mimics gastrointestinal peristalsis, which results in physiological mixing. The pH and the enzymes and bile salts concentrations simulate the dynamic physiological patterns found *in vivo*. The hollow fiber devices appeared almost as efficient at absorbing glucose as the active process *in vivo*.

The authors tested the model reliability to reproduce predetermined physiological parameters, such as meal size and duration, pH, gastric and intestinal secretions, gastrointestinal transit, and adsorption of digested product and water [19]. Water and metabolites were absorbed adequately through hollow – fibre membranes inside the compartments. Experiments were performed to demonstrate that the short chain fatty acid could be dialyzed efficiently and that their concentration could be maintained within physiological limits [21]. The stability of the *microflora* in the system was tested after inoculation with fresh fecal samples and after inoculation with a *microflora* that was maintained in a fermenter. This *in vitro* model was used for several studies including the absorption of the products of digestion, the bioavailability of minerals, the survival rate of microorganism, the composition and enzymatic activities of the *microflora*, and the functionality of recombinant microorganism in the digestive environment [22]. This apparatus was also used to evaluate *in vitro – in vivo* correlation [23].

Despite the accurate reproduction of the biochemistry of the gastrointestinal tract, the fluid dynamic, particularly in the stomach compartment, is still far from the real one.

2.2.4 Simulated biological dissolution and absorption system

Tam and Anderson developed a method for assessing simulated biological dissolution of a pharmaceutical formulation and absorption of a pharmaceutically active compound [24].

According to the invention, this system comprises a dissolution chamber for determining the dissolution profile of the pharmaceutical formulation in a medium to be supplied to the apical surface of a cell monolayer, and a cell culture chamber wherein absorption may occur.

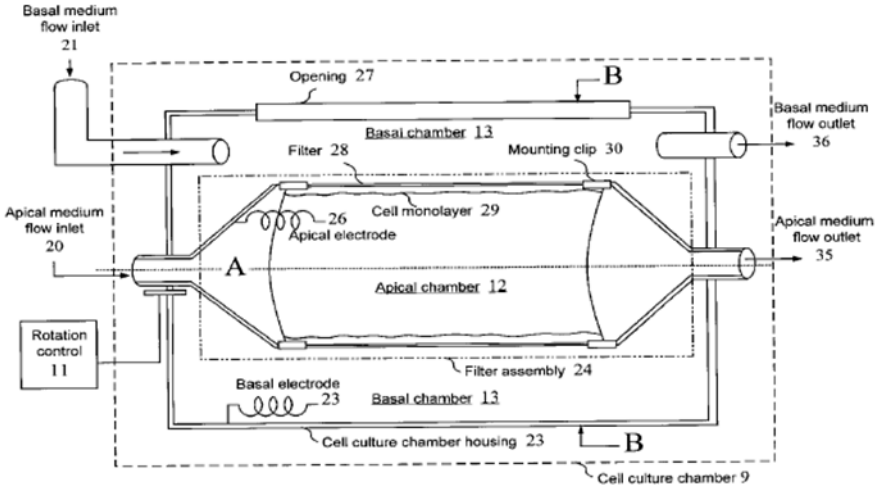

Figure 15. Simulated biological dissolution and absorption system by Tam and Anderson.

Medium is provided from an apical medium source chamber to a dissolution chamber using a gradient and flow control. Parameters such as pH and osmolarity may be measured by the gradient and flow control system. The apical medium will include bile salts, lipid or carbohydrates. The basal medium, which flows to the basal chamber of the cell culture chamber, may be of any type used to support cultured cells, and may comprise growth media, sera, buffers, minerals, nutrients, hormones, growth factors, and antibiotics. An automatic flow control system controls the temperature and partial pressure of the gas. In the dissolution chamber a dosage form is dissolved in the apical medium. The mixing rate in the dissolution chamber influences the unstirred water layer surrounding the dosage form, and thus is under automated control. Only a portion of the medium enters in the cell culture chamber to maintain a standard flow rate and to prevent excess shear stresses on the cell monolayer within the cell culture chamber. A filtration device may be incorporated into the dissolution chamber to control the size of the particles leaving the dissolution chamber. The basal surface of the cell monolayer is exposed to basal medium through the filter which is permeable to media.

Transepithelial electrical resistance analysis means may be used to determine the viability or integrity of the cell monolayer. Rotation of the filter ensures good mixing and minimizes the unstirred water layer adjacent to the cell monolayer.

According to the system, parameters such as mechanical stresses, intestinal distention, shear forces, and interspecies variability can be addressed by adjusting flow rates of the media through the cell culture chamber.

2.2.5 Three staged gastrointestinal model

Wickham and Faulks proposed an *in vitro* model which may include different stages in 2005 [25]. To ensure the reproducibility in size reduction, a precision cutting device was designed. The designed piece of the apparatus cuts food material into cubes of approximately 3 mm^3 dimensions, representing the approximate size of food produced by human chewing prior to swallowing. Food materials was first cut and then exposed to low levels of α-amylase at 37°C (model *saliva*).

First stage simulates the main body of the stomach (the *fundus*), a region with inhomogeneous mixing behavior, distinct acid and enzyme additions. This apparatus comprises an outer vessel into which fluids can be introduced and removed and an inner digestion chamber comprising a rigid portion through which the foodstuff can be introduced and a flexible portion. Reversible alternation of fluid pressure within the outer vessel causes reversible partial compression of the flexible portion for mixing foodstuff present therein. The mixing achieved in this stage is inhomogeneous. The contractions produced by the fluid in the outer vessel facilitates also the penetration of digestive additives. Long after ingestion, the meal remains heterogeneous, so gastric secretions only penetrating around the outside of the food bolus, which is not diluted by secretions for an appreciable time. The inner chamber has a plurality of pH electrodes disposed within it, designed and positioned to minimally interfere with mixing. The additive will generally be one or more of acid, alkali, enzymes, phospholipids, and bile.

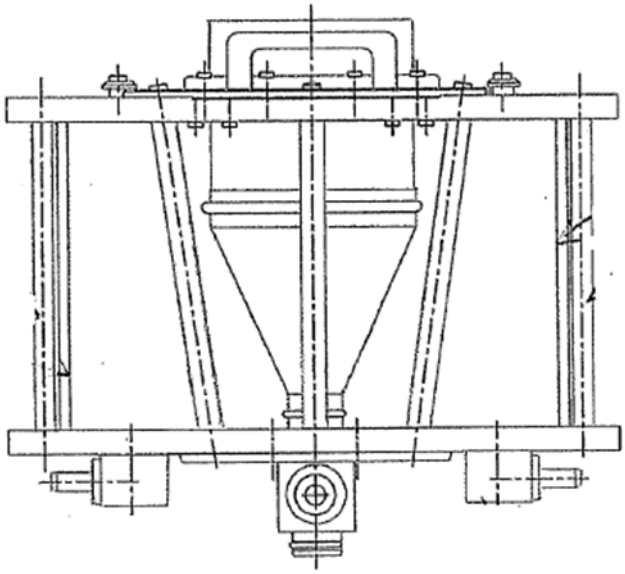

Figure 16. First stage (the *fundus*) of the Wickham and Faulks model.

Second stage of the model provides a simulation of the region of high shear (the *antrum*), mimicking both the rate and strength of contractions evaluated *in vivo*. This stage comprises a system of nested cylinders, as shown in Figure 17. An outer cylinder includes in a first end wall an entry port through which foodstuff can be introduced, and at the opposite end wall an exit port from which the foodstuff can be removed. The inner sliding cylinder mounted within the outer cylinder and including an aperture through which the foodstuff can be reversibly forced between the inner and the outer cylinders. A plunger is mounted within the inner cylinder for drawing the foodstuff through the entry port and the aperture into the inner cylinder. The aperture in the inner cylinder through which the foodstuff can be reversibly forced creates a shearing force. A piston defines the end wall of the chamber which remains at a predetermined distance. By repeated strokes of chamber forcing the foodstuff trough aperture, the foodstuff is subjected to sufficient shear to break the foodstuff down. When sufficiently broken down to mimic physiologic processes and foodstuff size, valve (the pylorus) is opened and plunger is pushed upward and the processed food can go out.

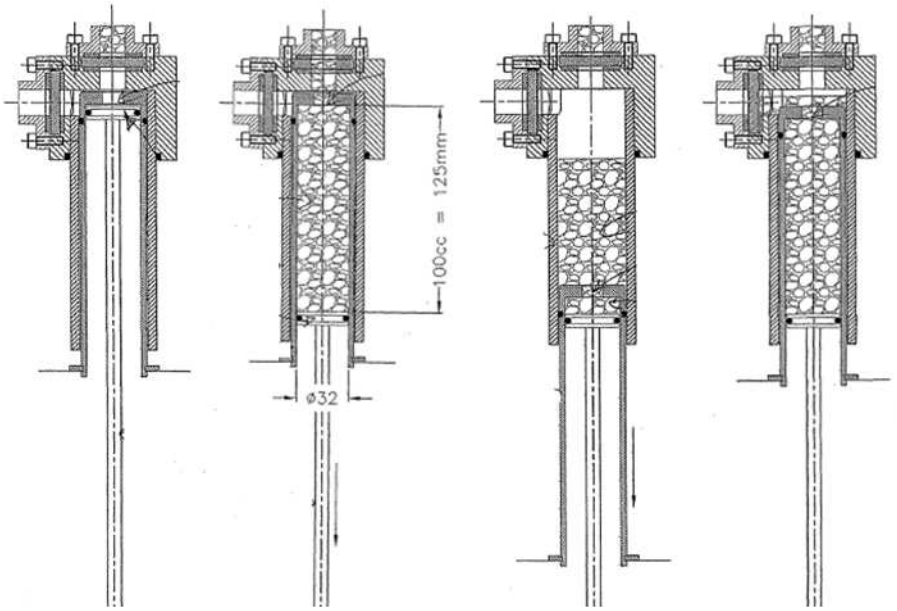

Figure 17. Second stage (the *antrum*) of the Wickham and Faulks model. The movement of the piston simulates the high shear stress of the stomach bottom part.

Nutrient absorption and finally excretion may then optionally be studied, for example, using the apparatus developed by Tam and Anderson previously described.

The real fluid dynamic in this model is well approximated but the simulation is limited to the stomach region, which are not too much relevant in drug delivery, since most of the absorption takes place in the intestine.

2.2.6 Use of hollow fiber to simulate the intestinal absorption

An artificial gut comprising a multilayer of hollow fibers was developed by Rozga and Demetriou in 2002 [26]. The artificial gut comprises a first hollow fiber having an inner surface which is lined with at least a layer portion of a plurality of biological components. Further, a second hollow fiber is adjacent to the first hollow fiber. The biological components consist essentially of enterocytes. The enterocytes inner surface is perfused with a feeding solution containing nutrients, and the enterocytes absorb, process, and transport the nutrient across the wall of the first hollow fiber. The nutrients eventually diffuse into the second hollow fiber. A perfusate selected from the group consisting of culture medium, blood, and

plasma can perfuse an inner surface of the second hollow fiber, whereby the perfusate is nourished by the nutrients. The housing and the outer surfaces of the first system of hollow fiber and the second system of hollow fiber define an extra – fiber space. The housing includes a first set of perfusion ports coupled with the first system of the hollow fiber, and a second set of perfusion ports coupled with the second system of hollow fibers. Thus, the enterocytes absorb the nutrients and pass them into the extra – fiber space. The nutrients in the extra – fiber space then diffuse into the second system of hollow fibers.

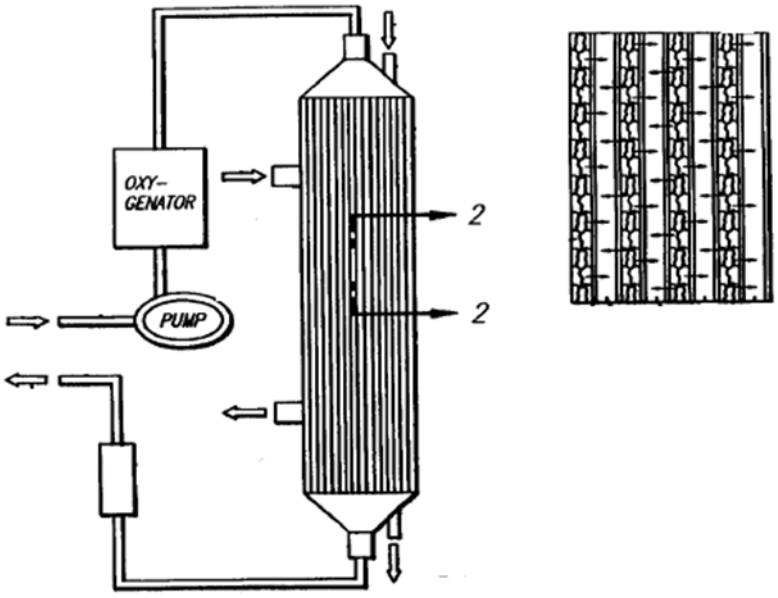

Figure 18. Elevation view of the Rozga and Demetriou artificial gut.

2.2.7 Dissolution test apparatus by Garbacz et al.

Garbacz et al. [27] proposed a new apparatus mimic hydrodynamic and mechanical condition in gastrointestinal tract to improve the predictability of dissolution testing in 2008. This included the simulation of the pressure forces due to gut motility, of the shear forces generated during the propagation, and of the loss of water contact when the dosage form is located in an intestinal air pocket. The device consists of a central pipe, with six steel netting spheres (chambers) of 35 mm diameter where the dosage forms are hosted. The central axle is coupled at one end to a pressure regulation unit by

a rotating joint and on the other end to a stepping motor. Pressure waves are generated by a pulsatile inflation and deflation of a balloon inside the chambers that is tightly attached to the nozzle. The inflactions are controlled by synchronized switching of solenoid valves. The pressure is regulated by a computer – controlled pressure reducing device. The central axle is driven by a computer – controlled stepping motors.

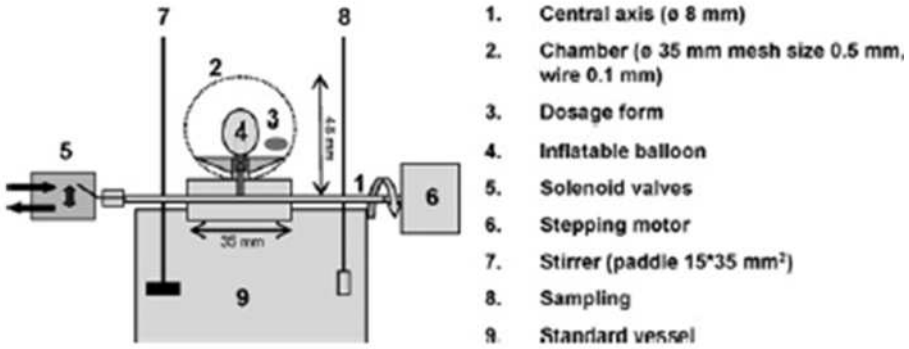

Figure 19. Schematic representation of dissolution stress test device developed by Gabacz et al.

The composition of dissolution medium was based on the results of analytical characterization of human gastrointestinal tract. The dissolution test device exposes the dosage form to an arbitrary sequence of movements, pressure waves and phase of rest as occur under *in vivo* condition. During rotation, the spheres are for 50% of the time immersed in the medium and for 50% of the time exposed to air. The medium was continuously homogenized. This device allow to generate a discontinuous movement of the dosage form within the gastrointestinal tract and to mimic the agitation caused by the gastrointestinal pressure waves as observed *in vivo*. In this apparatus, the simulation of pressure waves and alternate exposition to solvent/air are introduced and the mechanical behavior is very simple to control but pH changes are difficult to be realized and the fluid dynamic is far to the real one.

Different nifedipine extended release formulations were tested using the paddle apparatus, the reciprocating cylinder, the rotating beaker apparatus, and the new stress test device [28] [29]. These studies show that besides pH dependency the aspect of the mechanical robustness may be an essential factor affecting the dissolution characteristic of hydrogel matrix formulations. Furthermore, the authors found that

drug dissolution from all the formulations is not controlled by the properties of the tablet matrices but is determined by the dissolution characteristics of the nifedipine crystals which are release during the spontaneous disintegration of the tablet matrices.

2.2.8 Stirring device for dissolution testing

Recently, Bogataj et al. [30] developed a dissolution stirring device which simultaneously enables gentle mechanical contact of solid dosage form with grounding and its peristaltic movement due to the movement of the grounding. This apparatus comprises a thermostated round bottom vessel in which the stirring is performed by a cylindrical stirrer bar. The length of the stirring bar is about 8-10 mm shorter than the inner diameter of the vessel. At the bottom of the vessel there are small beads which are mechanically pushed by the stirrer bar and thus provide peristaltic movements during stirrer in a suitable medium. The preferred quantity of the beads used is to achieve the minimum amount which covers the bottom of the vessel in one layer to maximum amount which represents the height of about 400% of the stirring bar diameter. The beads are spherical and made of glass or other inert material which does not react with the vessel or with any substance in it. Additionally, beads must not adhere on the surface of the dosage form and they must have suitable density to settle on the bottom of the vessel. Dissolution profile obtained in pharmacopoeial apparatus with paddle stirring element is compared with the profile obtained using the this device. Differences in the dissolution profiles from 120 minutes on are probably in a great extent a consequence of the way of movement and the mechanical contact of the tablet with glass beads in the device.

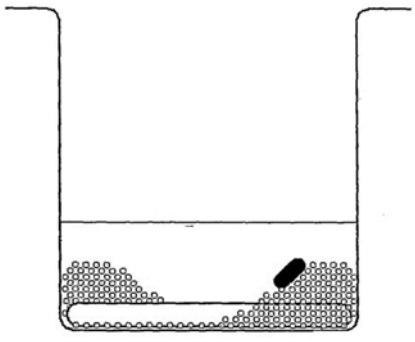

Figure 20. Front view of the vessel with stirrer bar and beads when no stirring is applied.

2.3 Gastric motility

Digestion is well studied in terms of the secretion of gastric acid, bile salts and digestive enzymes. Similarly, the mechanical functions of the stomach and duodenum are well defined in terms of viscoelastic properties, movement patterns of their walls, neuronal and electrical controls, and the dynamics of gastric emptying [5]. Less well understood are the flow processes that extract small molecules from complex foods: secretions have to penetrate food, particles have to be rendered less compact and suspended in liquid medium, substrate has to be transformed into thin sheets for enzymatic attack, the epithelial boundary has to be replenished with nutrients. These processes are susceptible to fluid-mechanical analysis [31]. The shape of the stomach and duodenum is influenced by its contents and by surrounding organs. These anatomical features have likely implications for the distribution of luminal contents and their motions in response to contractions, and they depend also on the inter-individual and inter-racial differences [32]. The first computations of flow and mixing in the human stomach was published by the group of James Brasseur [33]. Their model of the human stomach applies the 'lattice-Boltzmann' algorithm that is particularly well suited to fluid flows with complex geometry. A separate numerical model is used to parameterize the time changing geometry of the gastric lumen that must be provided to the lattice-Boltzmann algorithm as 'boundary conditions'. Fluid motions within the stomach are generated primarily by the gastric wall motions associated with antral contractile activity, pyloric opening and fundic contraction. It was necessary, therefore, to extend the basic lattice-Boltzmann algorithm to include 'moving boundary conditions'. The combined stomach model predicts gastric fluid motions, intragastric pressure, particle dispersion and mixing in the stomach for specified variations in the geometrical characteristics that underlie gastric motility. To analyze the movements of the stomach, a large number of MRI were studied. The geometry of the stomach was modeled in two dimensions (2D) to reduce the high level of complexity in full threedimensional (3D) models. Previous model studies of peristaltic transport in 2D versus axisymmetric geometries reported by Pal et al. [33] show that the 2D model has the same qualitative behavior as the corresponding 3D model, with modest quantitative differences in pressure and velocity. Most importantly, the fluid motions arising from lumen-deforming muscle contractions are captured by the 2D model. A realistic geometry model of the

stomach was designed from MRI movies of gastric motility, with physiological ranges of anatomical and physiological parameters obtained from the literature, as reported in Figure 21.

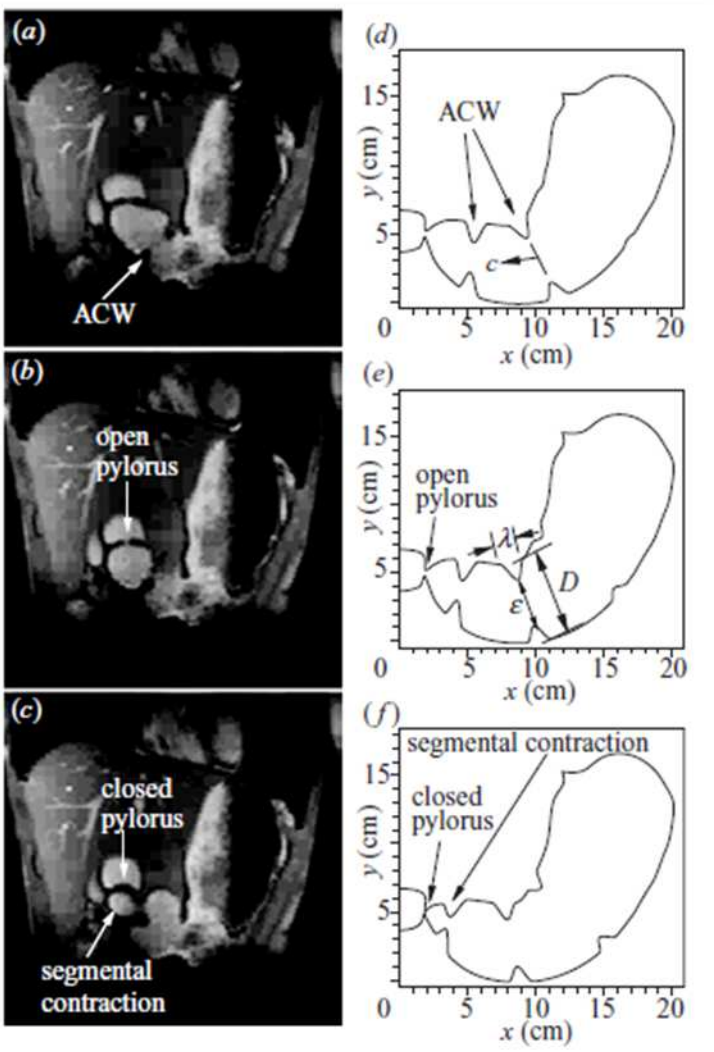

Figure 21. The stomach geometry reconstructed by the use of MRIs [33].

The reconstructed geometries on the right were obtained using a cubic spline curve passed through selected points of the respective figure on the left. A uniform grid was then placed over the gastric volume. All simulations assumed a liquid density of 1 g·cm^3 and a viscosity of 1000 cP. The results of these simulations are shown in Figure 22.

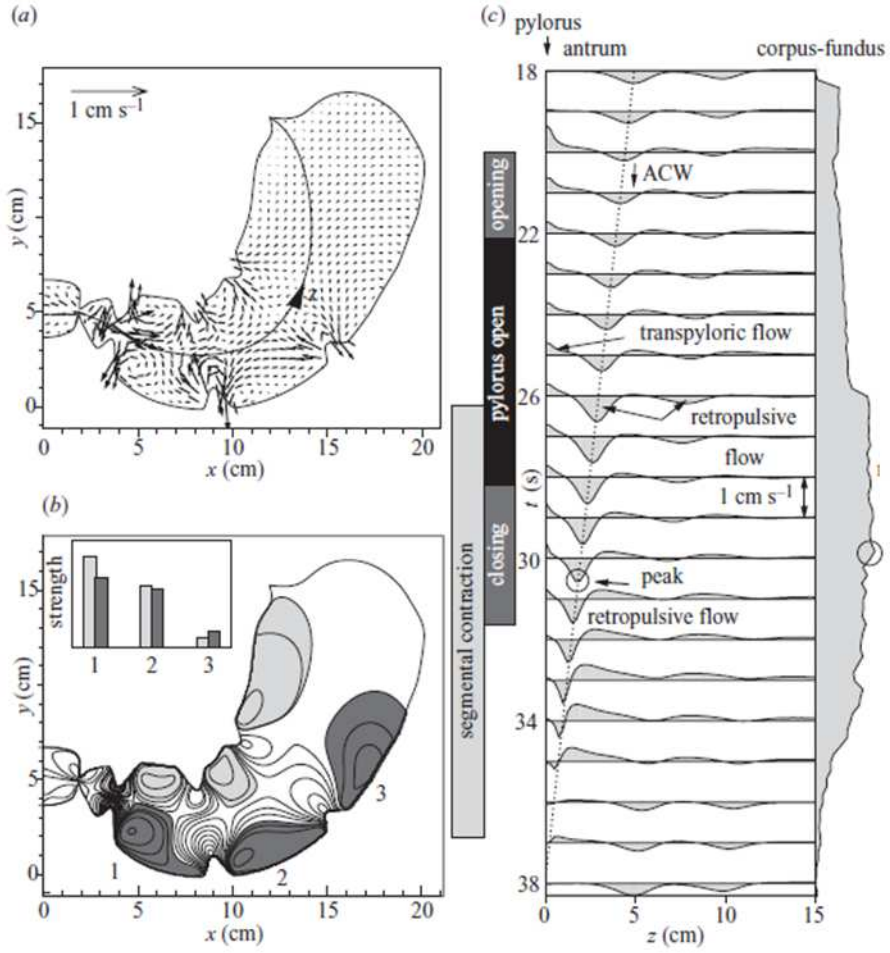

Figure 22. (a) Predicted gastric flow velocity vectors at one time instant, (b) Instantaneous streamlines, (c) Flow velocity along the z-axis shown in (a), plotted at 1 s intervals. The filled curve on the right is the maximum retropulsive flow velocity through the contractions as a function of time. The dotted line follows the propagation of the distal contraction in space–time [33].

These results are obtained with the hypothesis of open pylorus and the coexistence of 3 peristaltic waves. The velocity vectors (Figure 22-a) show that the strongest fluid motions are in the antrum, and two basic antral flow patterns are produced by the propagating contractions, retropulsive jet-like motions with the highest velocities and recirculating flow patterns between pairs of contractions. In Figure 22-b the streamlines of gastric fluid flow at a fixed instant in time are shown. Figure 22-c quantifies the magnitude of retropulsive jet velocity as a contraction approaches the pylorus. Velocity profiles

along the z-axis are shown at 1 s intervals. Using the model described also the mixing behavior of the stomach could be simulated.

Using these model of the human stomach, the same authors discover a new function of these contraction waves apart from grinding and mixing [34]. In coordination with fundic contractions, antral contraction waves move liquid content from the fundus along a very narrow path to the duodenum through the center of the antrum. Using physiological data, it was shown that this gastric emptying ‘‘Magenstrasse’’ can funnel liquid gastric content from the farthest reaches of the fundus directly to the intestines within 10 min. Consequently, drugs (tablets, capsules, liquid) released off the Magenstrasse may require hours to enter the duodenum. On the contrary drugs released on the Magenstrasse the drug can enter the duodenum and activate within 10 min at high concentration. This discovery might explain observed high variability in drug initiation time, and may have important implications to both drug delivery and digestion, as well as to other wall-driven emptying of elastic containers.

More recently a computational fluid dynamics (CFD) was used to develop a 3D model of the shape and motility pattern of the stomach wall during digestion, and it was used to characterize the fluid dynamics of gastric contents of different viscosities [35]. A geometrical model of an averaged-sized human stomach was created, and its motility was characterized by a series of antral-contraction waves of up to 80% relative occlusion. The flow field within the model strongly depended on the viscosity of gastric contents, as shown in Figure 23.

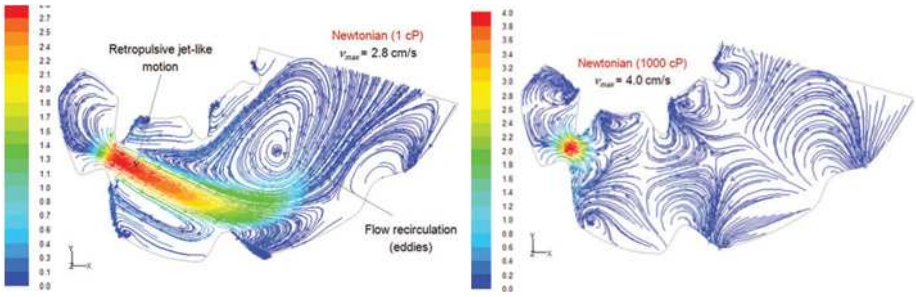

Figure 23. Effect of viscosity on the formation of the retropulsive-jet like motion and eddy structures [35].

By increasing the viscosity, the formation of the 2 flow patterns commonly regarded as the main mechanisms driving digestion (i.e., the retropulsive jet-like motion and eddy structures) was significantly decreased, while a significant increase of the pressure field was predicted. These results were in good agreement with experimental data previously reported in the literature, and suggest that, contrary to the traditional idea of a rapid and complete homogenization of the meal, gastric contents associated with high viscous meals are poorly mixed. This study illustrates the capability of the model to provide a unique insight into the fluid dynamics of the gastric contents, and shows its potential to develop a fundamental understanding and modeling of the mechanisms involved in the digestion process. To fully characterize and model food digestion, the knowledge of the relationship between the disintegration rate of food structures and the dynamics of gastric contents during digestion is necessary. Hence, a further improvement of the model was developed by the same authors [36].

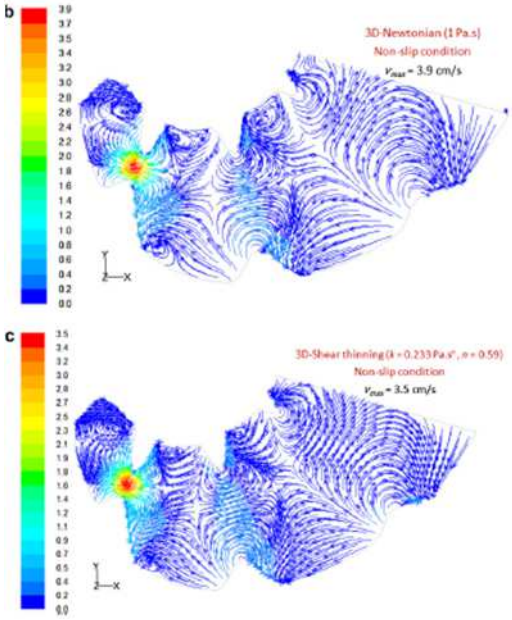

Figure 24. Streamlines of the fluid flow within the stomach's middle plane. b) Newtonian fluid with viscosity of 1 Pa·s; c) Shear thinning fluid (k = 0.233 Pa·s, n = 0.59) [36].

The rheological properties of the fluid can have a significant effect on the dynamics of gastric flows during digestion. To investigate this effect, the flow behavior of two Newtonian fluids of different

viscosities, and a non-Newtonian shear-thinning fluid, were analyzed. The behavior of the shear-thinning fluid was characterized in terms of the Power Law model and the results are shown in Figure 24.

The local flow behavior was significantly influenced by the rheological properties of the gastric fluid, especially in the antropyloric region. By increasing the viscosity of the gastric fluid, higher retropulsive velocities are developed (Figure 23), but their development was confined to a smaller region at the location of the contraction peak, and the formation of the retropulsive jet-like motion was arguable [35]. A similar flow behavior was predicted in the case of the shear-thinning fluid (Figure 24-c). However, due to its lower viscosity at the region of the ACW's peak, smaller retropulsive velocities were predicted within the system. Rheological properties also affected the formation and strength of eddies. By increasing the viscosity of the fluid or changing its Newtonian characteristics, the development of circular motions was confined to regions closer to the contraction. In addition, the authors proposed the development of a new *in vitro* system to determine and model the disintegration rate of different food structures, under different physiological conditions. An experimental system capable of reproducing the main features of gastric motility, while supporting the use of a non-intrusive flow measurement technique (Particle Image Velocimetry) was developed. The system consisted of a polycarbonate chamber, where one of its walls was substituted by a neoprene sheet that was continuously deformed by the movement of a stainless steel cylinder. The flow behavior of two Newtonian fluids and one shear thinning fluid were experimentally and numerically investigated, as shown in Figure 25.

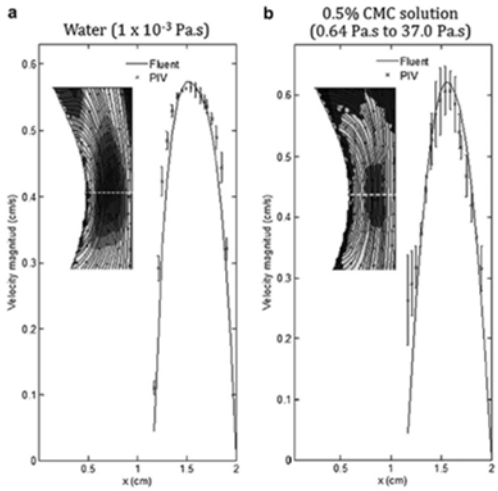

Figure 25. Predicted versus experimental velocity profiles along a horizontal line [35].

Similar to the numerical prediction obtained within the stomach model, as the viscosity increases, higher and more localized retropulsive velocities are.

2.4 Pharmacokinetic models

The prediction of the drug concentration in the blood, tissue, and organs is the goal of the *in silico* pharmacokinetic modeling. The approaches to the modeling of the physiological phenomena can be different on the basis of the details used. The description of the phenomena taking place in the body is much closer to the real physiology if more details are considered.

2.4.1 The first whole body physiologically based pharmacokinetic model

There are several examples of pharmacokinetic compartmental models, the most important is the first whole body physiologically based pharmacokinetic model proposed by Jain [37]. Mass transfer is modeled by a set of interconnected lumped compartments representing the various tissues. Each compartment is divided into three compartments representing the vascular, interstitial, and intracellular space, and drug concentration within each compartment is assumed to be uniform.

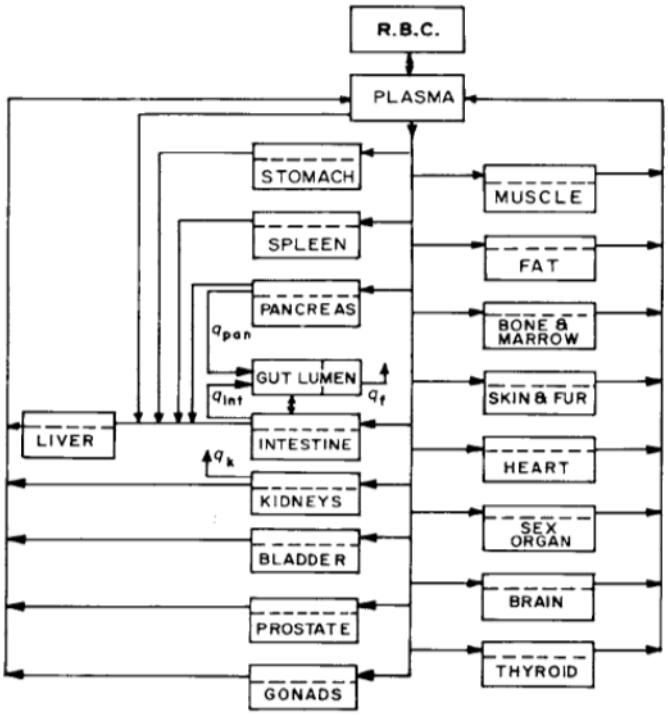

Figure 26. Schematization of the Jain absorption model.

The model is based on the schematization of the rat body into 21 compartments, each representative of an anatomical part. The mathematical structure of the model is made up by a system of 38 coupled ordinary differential equations, solved with the initial condition that all the concentration, but the plasma one, are zero. The simultaneous resolution of the equations requires the knowledge of 98 different model parameters. An application of the model was carried out by the authors in a case of intravenous injections of zinc sulfate in rats and a good agreement between the prediction of the model and the experimental data was found. In applying the model to zinc, the following assumption are made: there is instantaneous mixing of drug in the plasma after the intravenous injection, the effluent plasma concentration is equal to the drug concentration of the vascular subcompartment, and the capillary endothelial layer is more permeable than the cellular membrane.

In spite the fact that the model gives a complete description of the physiology and is very accurate, it is too difficult to be adopted for predictive purposes because of the high number of parameters which have to be fitted. Furthermore, the model concerns only the case of

intravenous injection in rats and, then, it cannot be used for the simulation of oral administration or for human physiology.

2.4.2 The simplified model inspired by Jain et al.

To overcome the complexity of the Jain model, an algorithm to identify the best lumped model was proposed [38]. The procedure provides i) the grouping of tissue and organs, on the basis of their time constants, obtaining some competing lumped model; ii) a global sensitivity analysis to find the parameters with the most important effects on the pharmacokinetic profiles; iii) the selection of the model with the same mean and variance of the arterial concentration time profile obtained by the complete model. The comparison between the performances of the simplified model with those of the complete helped to choose the more efficient.

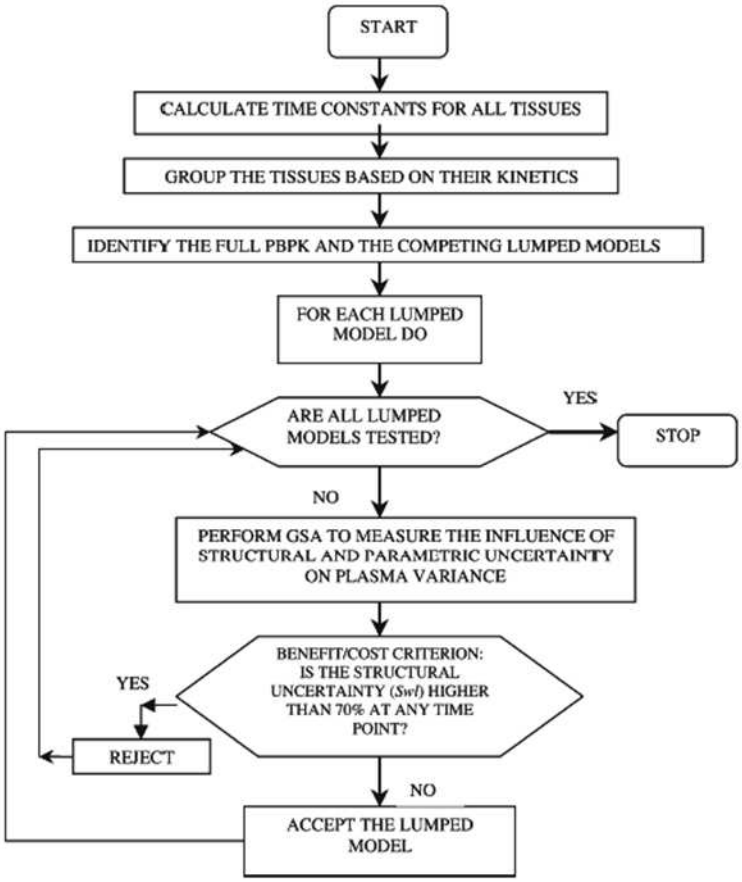

Figure 27. Algorithm employed for whole body PBPK model reduction.

A lumped model composed of six compartments was proposed and applied in the case of intravenous injections of barbiturates in rats [39]. The authors found that the sensitivity applied may be extended to other models with similar structure and parameter values. However the ranking of the parameters is a dynamic property and refers to the transient phase of the processes, essentially before the equilibrium in the tissue is achieved. Some failure in this approach (e.g. the failure to predict the importance of the liver flow and partition coefficient), however, suggest that alternative approaches should be used when more detailed information are crucial.

2.4.3 Compartment Absorption and Transit model

The complete model developed by Yu et al. [40], [41] is defined as the "Compartment Absorption and Transit" (CAT) model. The schematization of the gastrointestinal tract is made up by 10 compartment, then the mathematical structure is made up by 10 ordinary differential equations which have to be solved with the initial conditions (on the fraction of the dose in the gastrointestinal tract and on the plasma concentration) to characterize the time profiles of the drug levels in each compartment. The knowledge of 18 parameters, of the absorption rates, of the degradation rate constants, of the elimination constant and of the distribution volume is required to solve the equation.

The CAT model was applied to simulate cases of oral drug administration (both in immediate and in controlled release formulations) and it showed a satisfying agreement between the model prediction and the experimental data. The CAT model is useful in the design of the controlled release delivery systems and has the potential to investigate the effects of physicochemical, physiological and dosage form variables on the oral drug absorption. The main drawback of this model is that it can be applied only for oral administration. Furthermore, many other factors such as solubility, crystal form, blood flow, gastrointestinal pH, and dosage form factors have not been completely considered.

2.4.4 Advanced Compartmental Absorption and Transit model

The CAT model constituted the starting point for the development for the "Advanced Compartmental Absorption and Transit" (ACAT) model [42]. For drugs with low permeability and solubility, absorption

may be not complete in the small intestine and the CAT model can be more accurate by treating the colon as an additional absorbing compartment. This model was implemented into a simulation software, *GastroPlus*. *GastroPlus* was tested as an *in silico* tool for the prediction of the effects of the physiological conditions on physicochemical parameters of some therapeutic substances. A basic assumption of ACAT model is that drug passing through the small intestine will have equal transit time in each of the compartments. The luminal barrier has been modified, respect to CAT model, by the addiction of compartments corresponding to the enterocytes and surrounding tissue. In addition, the ACAT model uses the concentration gradient across the apical and basolateral membranes to calculate the rate of drug transfer into and out of an enterocyte compartment for each gastrointestinal tract lumen compartment.

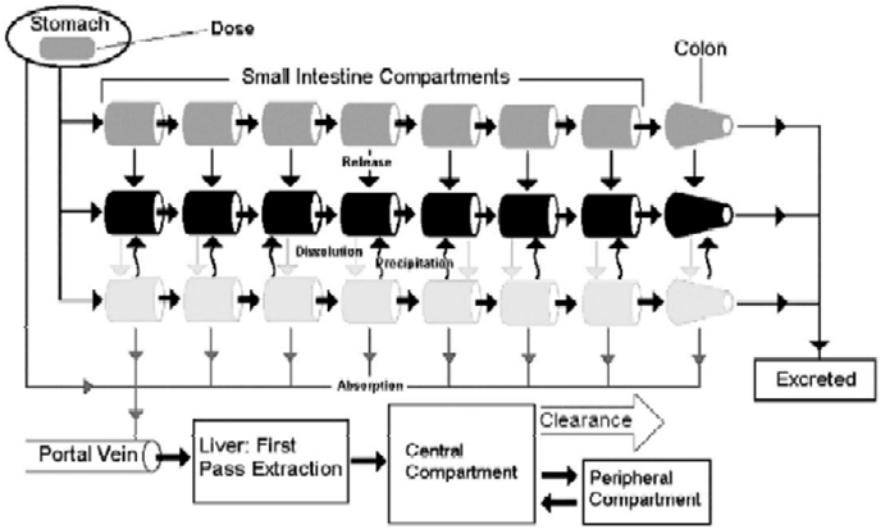

Figure 28. ACAT model schematic.

Satisfying prediction of the absorption, distribution, metabolism, and excretion (ADME) phenomena were obtained but this model can be used only after a lot of careful *in vitro* and *in vivo* measurements.

2.4.5 The Advanced Dissolution, Absorption and Metabolism model

While several models and algorithms have been developed to predict bioavailability in an average person, efforts to accommodate intrinsic variability in the component processes are less common. An approach

which incorporates such variability for human populations within a mechanistic framework is described, together with examples of its application to drug and formulation development by Jamei et al [43]. The ADAM (Advanced Dissolution, Absorption and Metabolism) model is a development of a succession of representation of drug absorption from the human gastrointestinal tract ACAT model. It divides the gastrointestinal tract into nine anatomically defined segments from the stomach through the intestine to colon. Drug absorption from each segment is described as a function of release from the formulation, dissolution, precipitation, luminal degradation, permeability, metabolism, transport, and transit from one segment to another. It is assumed that absorption from the stomach is negligible, that the movements of solid and liquid drugs through each segment of the GIT may be described by first order kinetics, and that the metabolism in the colon is negligible. Finally, the transit time in each segment of the small intestine is assigned as a fraction of the total small intestine transit time, proportionally to the length of the segment.

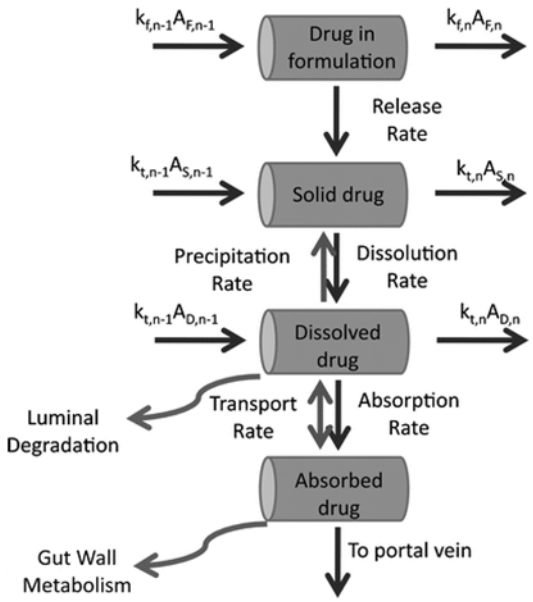

Figure 29. Kinetic processes within each intestinal segmento f the ADAM model.

Furthermore Jamei et al. [44] used a mechanistic approach implemented in the Simcyp Simulator to simulate complex absorption,

distribution, metabolism, and excretion. The Simcyp Simulator can be used at different stage of drug discovery and development for a variety of purposes.

2.4.6 Physiologically Based PharmacoKinetic model

Di Muria et al. [45] proposed a PKPB model based on a simple representation of the body. It provides 7 compartments, each of them representing an organ, a tissue, a fluid of the body or a group of them.

The gastrointestinal tract is split into the stomach, the small intestine, and the large intestine; the gastrointestinal circulatory system, the liver block, the plasma block, and the tissue compartment describe the rest of the body. The PBPK model was conceived to be applied in the cases of both single and multiple administration. The initial conditions have to be diversified on the basis of the route of administration, the kind of pharmaceutical form, and the frequency of the administration.

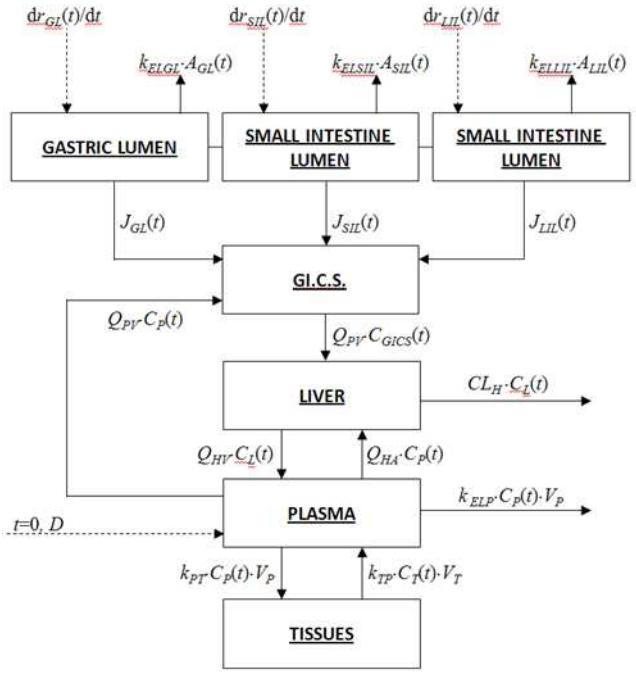

Figure 30. Schematic reproduction of the model proposed by Di Muria et al.

This model consists of the mass balance equations on the compartments (7, one for each compartment) and their initial conditions. 22 physiological parameters are used in the model but a very limited number of them (up to 5) has to be optimized. The model

is able to predict the drug hematic levels for several administration routes. The capabilities of the model were confirmed by the comparison between the model predictions and the experimental data from literature for several case histories.

2.4.7 Other physiologically based models

Models to predict the absorption from the human intestine have ranged in type and complexity from simple correlation to single experiment, to mathematical calculations using a variety of parameters, including mass balance approaches. A description of a physiologically based model of drug absorption in the human gastrointestinal tract was carried out by Grass [46]. The simulation combines a model of fluid movement in the gastrointestinal tract with a calculation of drug absorption (flux) in each intestinal segment (modeled as a separate compartment) over time. The evaluation of three parameter (solubility, surface area, and permeability) taken from literature allows the calculation of the theoretical flux in each segment. The flux estimated in each compartment over time was combined to construct an absorption rate prediction.

Willmann at al. developed a physiologically based absorption model for orally administrated drugs in rats [47] and monkeys [48]. The gastrointestinal tract is modeled as a continuous tube with spatially varying properties. The mass transport through the intestinal lumen is described via an intestinal transit function. The only substance specific input parameters of the model are the intestinal permeability coefficient and the solubility in the intestinal fluid. With this information, the complete temporal and spatial absorption profile can be calculated. The described model was used as a starting point for the development of a model simulating the gastrointestinal transit and passive absorption of a compound administered in solution in a fastened subject [49]. The overall performance of the model was investigated by calculating the fraction dose absorbed for a broad range of the input parameters.

Plusquellec et al. [50] built a pharmacokinetic model taking into account a discontinuous absorption along the gut, from n successive sites, a non-absorbing intestinal segment being always in between two successive sites. An analytical expression of plasma concentration was obtained. This model is able to deal with areas under curve,

bioavailability, clearance and to point out the contribution of each site to the total absorption of the drug.

Chapter Three

State of the art – Absorption models

This chapter deals with the absorption models which are described in literature. In vitro methods to predict the absorption, animal, and human perfusion studies are analyzed.

3.1 Absorption models

During the years several methods to estimate the absorption in the gastrointestinal tract have been developed. These methods could be based on theoretical prediction, on *in vitro* methods, on animal or human perfusion, on biological or artificial membranes [10].

3.1.1 Absorption prediction from theory

An estimation of the intestinal permeability, and, as a consequence, of the absorption across the intestinal wall, can be made with the knowledge of the molecular properties (structural features and physicochemical properties). The most relevant properties affecting the intestinal absorption are the lipophilicity, molecular size, charge, hydrogen bonding, and solubility. These properties can be evaluated by experimental or computational approaches. An important feature of these properties is the fact that they are inter-depending properties, in fact, changing one of them usually affects the others. The link between these properties is shown in Figure 31.

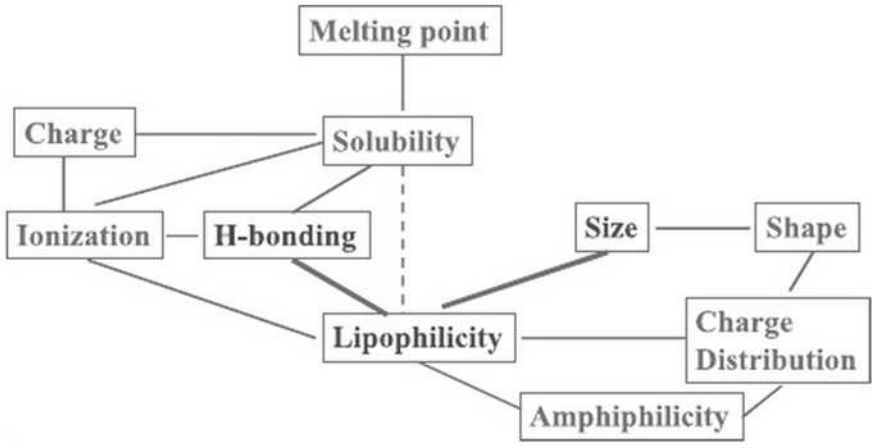

Figure 31. Physicochemical properties affecting intestinal absorption [10].

In the absorption studies, a relation of particular interest is the one between the partition (*log P*) and distribution (*log D*) coefficients. These coefficients are related principally to two major contributions: the size of the compounds and the capability to form hydrogen bonds.

Rule of five

Lipinski's rule states that, in general, an orally active drug has no more than one violation of the following criteria:

1. There are more than 5H-bond donors (expressed as the sum of OHs and NHs);
2. There are more than 10 H-bond acceptors (expressed as the sum of Ns and Os);
3. The mass weight is over 500;
4. The *log P* is over 5;

All numbers are multiples of five, which is the origin of the rule's name. As with many other rules of thumb, there are many exceptions to Lipinski's rule, i.e. compound classes that are substrates for biological transporters are exceptions to the rule.

The respect of the rule-of-5 is fundamental for the design of orally administered compounds and it is based on purely computational evaluations.

Solubility evaluations

Concerning the solubility, this property is linearly related to the dissolution rate. Therefore, poorly soluble compounds are expected to have dissolution-limited absorption. Moreover, the solubility could be related to the lipophicility (*log P*) and the melting point [10]. The disadvantage of this relation is that it could not be used prospectively. Kamlet and his coworker [51] demonstrated that solubility depends on a number of factors, the major contributes are due to molecular size, polarity, and hydrogen bond formation.

Lipophylicity evaluations

Concerning the lipophilicity, the main parameters which have to be taken into account are the 1-octanol/water distribution coefficient at a certain pH (defined as *log D*) and the 1-octanol/water partition coefficient (defined as *log P*). The estimation of *log D* and *log P* could be made by computational approaches based on the molecular size and on the hydrogen bonding. Immobilized artificial membranes could be used instead of *log D* because they better mimic the membrane partitioning. The disadvantage of this technique is that the correlations found between the permeability and the immobilized artificial membranes is not always reliable.

3.1.2 In vitro methods for absorption predictions

In this paragraph the biological *in vitro* methods are briefly described. These methods consist in cultured cells or intestinal tissue of human or animal origin which are used to determine the permeability in the gastrointestinal tract of a drug. One of the advantages of these methods is that they are not based only on the computational analysis but they could be applied to investigate the influence of additives for example and they are more versatile than the others. Obviously, all the methods cover only a part of the aspects involved in the gastrointestinal absorption and not all the factors involved are taken into account by each method.

Brush Border Membrane Vesicles

The Brush Border Membrane Vesicles (BBMV) preparation is based on the homogenization and differential precipitation, fractionation, and analysis using marker enzymes. The final pellet contains the luminal wall-bound proteins and phospholipids, which contain most of the brush border enzymatic and carrier activity. Re-suspension of the pellet in buffer results in the formation of vesicles. The vesicles are mixed with the compound of interest and filtered, the amount of the compound taken up by the vesicles is then determined. This methods has many drawbacks such as the need of a radiolabeled compound for the analysis and day-to-day variation in preparation, this method is useful for mechanistic study of drug absorption process.

Everted intestinal rings

A simple method used for absorption measurements is using intestinal rings. A section of the intestine is isolated immediately after the death of the animal, washed to eliminate digestive by-products, and saturated at one end. The closed side is then pushed through the intestine resulting in eversion of the intestine, which is cut in small rings. This method is called “everted intestinal ring”. The slice are then incubated in a medium containing the compound of interest and shaken in a waterbath. After a certain time the tissues are withdrawn, dried, weighed, and then dissolved. After the dissolution the uptake of the compound is measured. The advantages of this method are the ease of preparation and the fact that from one segment of intestine a large amount of rings could be prepared. With this method both passive and carrier-mediated transport have been tested.

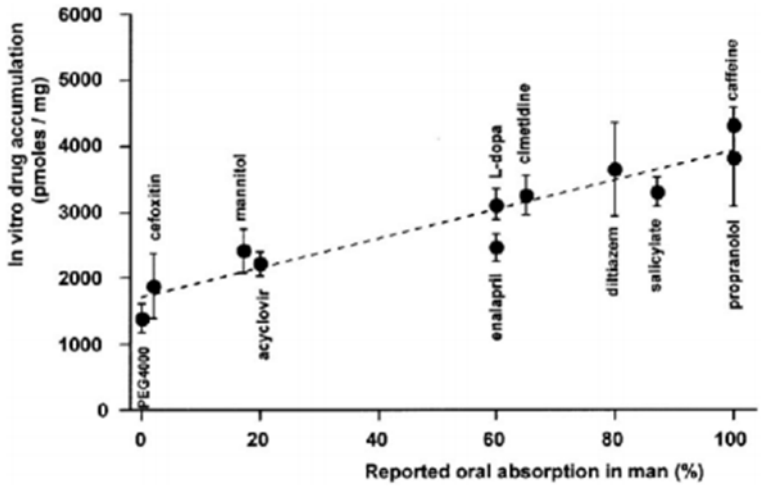

Figure 32. Correlation of oral availabilities in humans and measured uptake *in vitro* in everted intestinal rings [10].

A good correlation was found between oral availability and the *in vitro* uptakes. Despite the simplicity of use, it could be taken into account the fact that the transport of the solute into the slices includes all areas, hence connective and muscles tissue are exposed to drug solution. This could overestimate the solution uptake, which is the major drawback of the method.

Everted intestinal sac

An evolution of the previously described method is the "Everted intestinal sac" method. A section (2 to 4 cm) of the intestine is tied off at one end and everted. The mucosa becomes the outer side of the sac and is in contact with the incubation medium but, in this case, only the mucosa is in contact with the permeant. The sac is filled with buffer and put in an oxygenate buffer containing the component of interest. At the end of the experiment the sac is cut and the serosal fluid collected. In this case the tissue is subjected to a sudden deterioration which could be avoided if the animal is anesthetized before the exportation of the intestine. The everted sac method is an inexpensive technique which is relatively simple and allows several tests using tissue from only one intestine. Another advantages are the low serosal volume compared with the area of absorption and the possibility to compare absorption of different sites by preparing segments from different parts of the intestine.

Ussing chamber

Devices which have been used since the first studies to determine the transport of compounds in living tissue are the Ussing chambers.

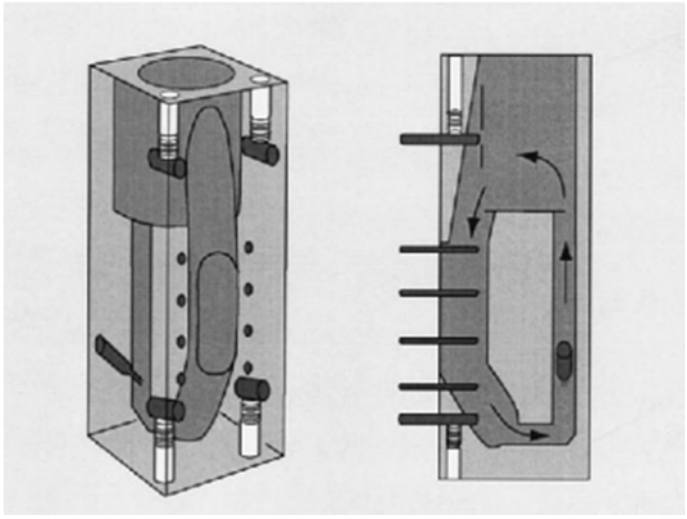

Figure 33. The Sweetana-Grass diffusion cell. The tissue is mounted between two acrylic half-cells. Buffer is circulated by gas lift.

In this method small sections of the intestine are clamped between two glass chambers filled with buffer and nutrients at a temperature of 37°C. The buffer solution is continuously gased with carbogen to maintain the viability of the tissue and to ensure the good mixing. The compound of interest is added to one compartment (donor compartment) and its accumulation at the other side of the membrane is measured as function of time evaluating the permeability value. In the original design of the Ussing chambers the setup was equipped with electrodes and a voltage clamp for monitoring epithelial potential difference. This parameter could be used to verify the tissue viability during the experiment.

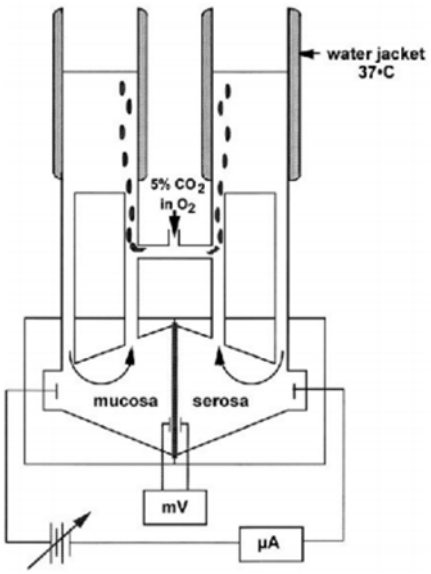

Figure 34. Original Ussing chamber. The half cells with thermostated water jacket, gas lift, and potential diffedrence and current electoredes are shown.

The integrity of the tissue can also be followed using an integrity marker in addiction or in place of the electrical parameters. The big disadvantage of this device is that the tissue, as with the everted sac, can deteriorate within 30-60 minutes. Addition of energy sources such as glucose can improve its life considerably. Proper handling and gasing with carbogen further improves the viability. By the way, information on time dependent structural changes would be necessary for a complete interpretation of the permeability data.

Isolated intestinal cells

Another *in vitro* method used to determine the drug absorption is the isolated intestinal cells. The methods used to isolate the cells are substantially two: an *in situ* method which is based on the perfusion of the intestine with enzymes solution that release the cells, and an *ex vivo* method which is based on the treatment of the cells with chelating agents. In a typical permeability measurement, the cells are separated from the buffer by centrifugation, resuspended in a solution containing the interest permeant and shaken. After a certain time, the cells are separated and extracted. The main drawback in the cell isolation is the variability of the population of cells. Since the cells have a low volume, once more the assay is based on the radiolabel counting, which constitutes a drawback for the method.

Caco-2 monolayer

The alternative to the previous method is use cultured cells [52]. One of the advantages of the cultured cells grown as monolayer is that they exhibit a polarized behavior, mimicking the intestinal environment. Most of the cell culture models are based on immortalized cell lines deriving from normal cells, from induced tumors, or from human colonic cancers. The most widely used are the Caco-2 line, which has the advantage that it can be grown on a porous filter forming a polarized cell monolayer within few days. Usually a polycarbonate filter support is used and the layer reaches the density of 60000 cells/cm^2.

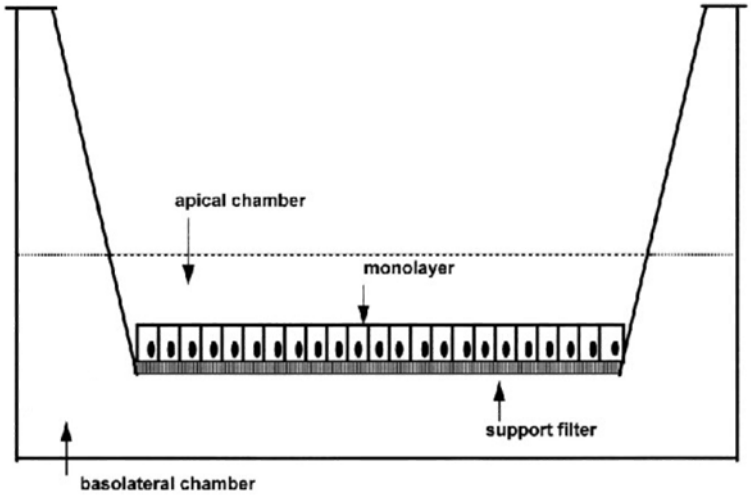

Figure 35. Caco-2 cell monolayer cultured on polycarbonate filter [10].

The tight junctions in the Caco-2 monolayers look like the junctions in the human colon, resulting in a higher TransEpithelial Electrical Resistance (TEER), which makes the Caco-2 cell line very useful for studying the influence for both the pharmacological pretreatment and direct additives on cell integrity because the paracellular permeability of a non-permeant (as mannitol) could be easily monitored. Hence, TEER is used as indicator of the monolayer integrity (Figure 36).

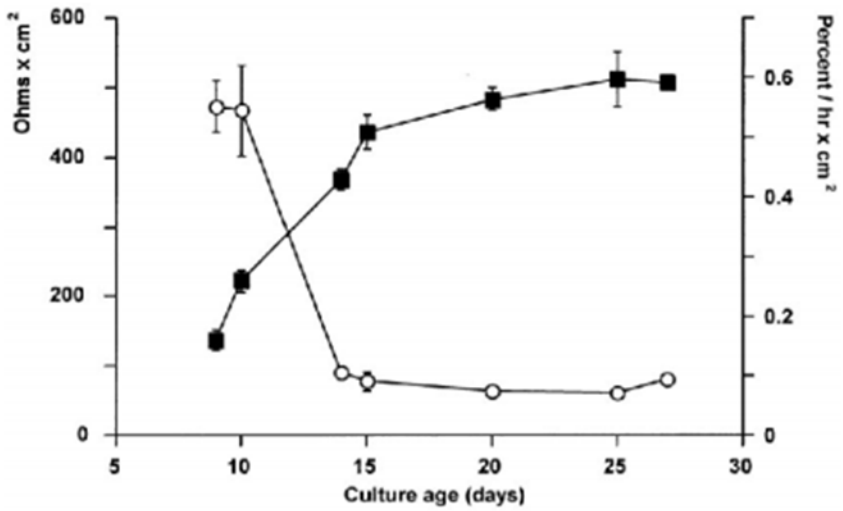

Figure 36. Transepithelial electrical resistance (■) and mannitol flux (○) as indices of monolayer integrity [10].

Another advantage of the use of Caco-2 cell line is the fact that the cells express several active transport system, such as amino acid or vitamin B12 transporters. Once grown on a porous filter, the transport of pharmaceuticals can be measured using the original culture chamber mounted on a shaker in an incubator. The culture medium is then replaced by a donor medium containing the permeant of interest and, on the other side, by the acceptor medium. One the mayor advantages of the cultured cells method is its application to high-throughput screening strategies because the cells are relatively simple to culture in high quantities. Once the culture method has been developed, the permeability measured with the Caco-2 cell line and the values measured with human large-intestinal tissue is compared for different substances [10], and the result is shown in the following figure:

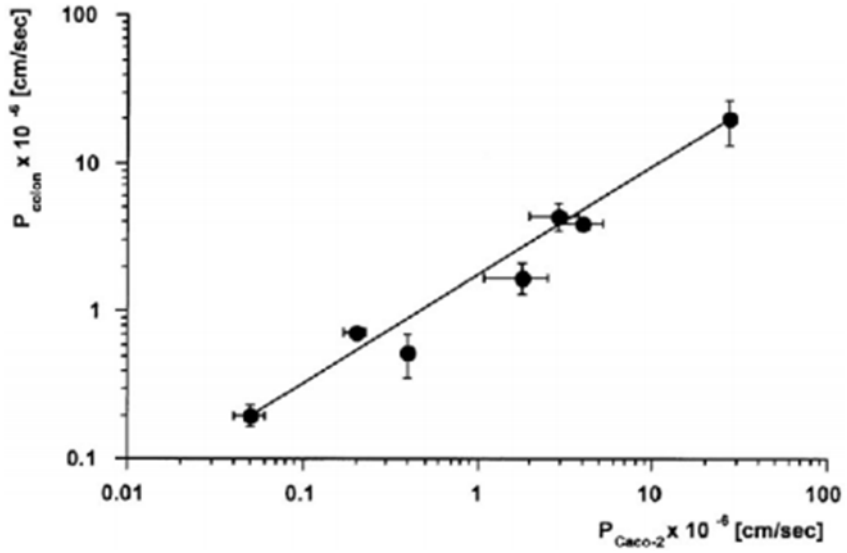

Figure 37. Relation of solute permeability of several substances across Caco-2 monolayer and human large intestinal tissue.

For the system in which Caco-2 cell monolayers are grown on permeable filter supports, with drug appearance being monitored in the receiver compartment of a side-by-side diffusion apparatus, a number of laboratories have correlated permeability with fraction absorbed [52]. This relationship, in turn, facilitates the interpolation of fraction absorbed from the permeability of New Chemical Entities (NCEs) for which in vivo studies have not been conducted (Figure 38).

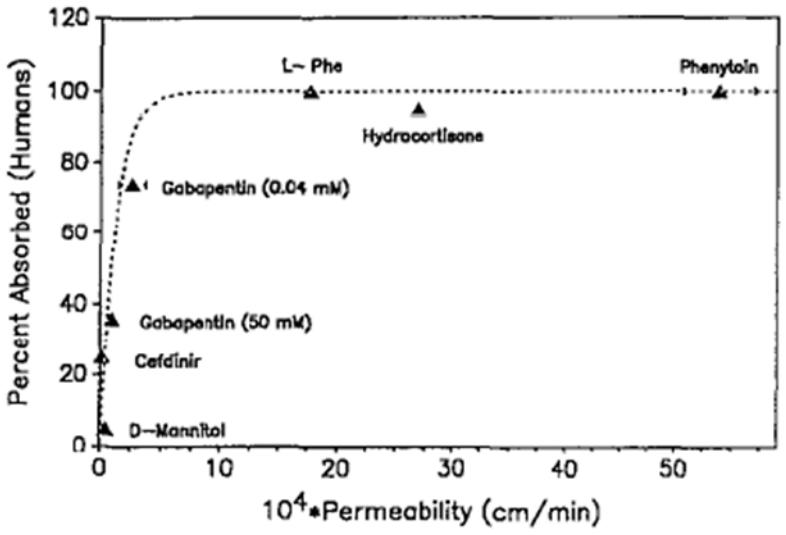

Figure 38. Comparison between percent absorbed in humans and permeability across Caco-2 cell monolayer for several molecules.

Moreover, drug transport rates in Caco-2 monolayers were compared with those obtained in the human jejunum *in vivo* [53]. Permeability coefficients were calculated in order to allow direct comparison of the two models. The rapidly (passively) transported drugs were found to have comparable permeability coefficients in Caco-2 cells and in human jejunum. The permeability coefficients of the slowly (passively) transported, hydrophilic drugs were found to be lower in Caco-2 cells than in jejunum. The carrier-mediated transport rates were also much slower in Caco-2 cells than in human jejunum. The results indicate that Caco-2 monolayers can be used to predict passive drug transport in humans, while prediction of transport by carrier-mediated systems may require a scaling factor, due to a low expression of carriers in this cell line. Hence, despite the described advantages, cultured cells based on Caco-2 line have disadvantages. The tight junctions in this cell line are closer than the colonic ones, this may result in an underprediction of the permeability of hydrophilic compounds as shown previously. Moreover, although the cells show the expression of active transport systems, this expression is quantitatively different for several transporters in the intestinal tissue. Last, batch to batch variation in expression may occur, this may result in poor predictability of the permeability values.

Madin-Darby Canine Kidney cell line

Another kind of cells which could be used for permeability studies are the Madin-Darby Canine Kidney cell line. The MDCK permeability assay has been widely used in many companies because of its many favorable characteristics. These characteristics include spontaneous differentiation into a polarized epithelial tissue in a short culture time (~3-5 days) which minimizes maintenance and reduces the chance for contamination, low expression of metabolizing enzymes and transporters, tight paracellular junctions, high monolayer integrity, and morphologic homogeneity which contributes to good inter-lab reproducibility. There are two kind of MDCK cells: the first one (MDCK I) which is characterized by an high value of TransEphiliar Electrical Resistence (TEER), and the second one (MDCK II) which is characterized by a low value of TEER. The permeability measured with these cells is been compared with the permeability measured with the Caco-2 cells, the results are shown in Figure 39.

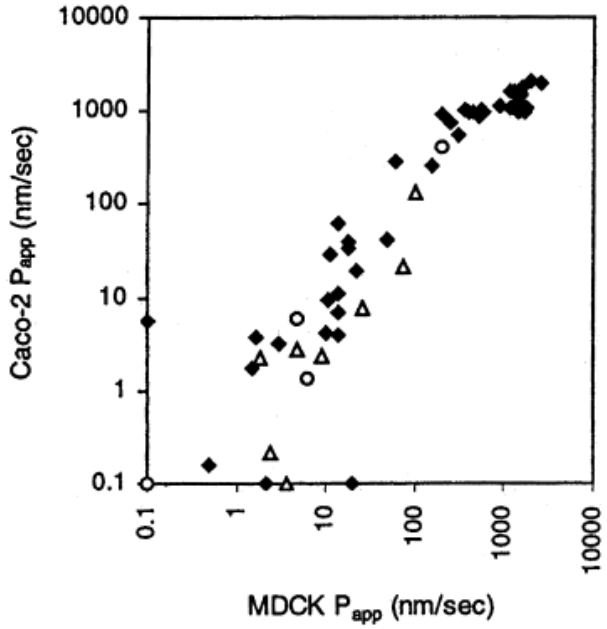

Figure 39. Correlation between apparent permeability of Caco-2 e MDCK for actively transported compounds (□), passively transported compounds (♦), and efflux substrates (○) [54].

It could be noticed that there is a good agreement particularly between the permeability values of the passively transported compounds. Because of the non-human origin of MDCK cells, the endogenous

canine transporters can have different activity and selectivity against various substrates and interfere with passive permeability measurement. The most important endogenous transporter in MDCK cells is the canine P-glycoprotein (Pgp). Compounds can be substrates for canine Pgp, but are not necessarily substrates for human Pgp and vice versa, leading to false positives in efflux transport assays. During the studies, a sub-population of the MDCK II (RRCK) cells that expresses low levels of endogenous canine Pgp to minimize the interference of canine Pgp on passive permeability measurement was isolated [55].

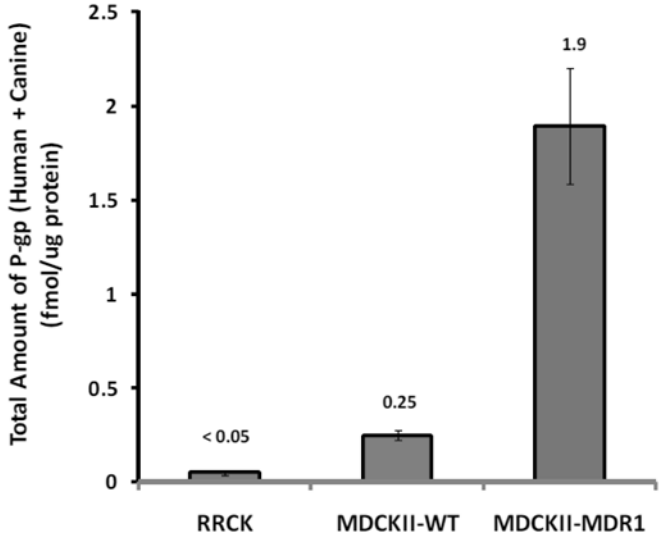

Figure 40. Total Amount of Pgp (Human + Canine) in several subpopulation of MDCK cells (RRCK, MDCKII-WT and MDCKII-MDR1Cells)[55].

It could be seen that the level of total Pgp could be significantly reduced for these cells. Although the evaluation of permeability using these cells could be more reliable than that made with the Caco-2 cells, the disadvantage of the impossibility to distinguish between canine and human Pgp is relevant and it has to be considered during their use.

2/4/A1 cell line

Although the cell lines proposed so far, research on cell culture models which better reflect both the transcellular and the paracellular permeability of the human small intestine is therefore of interest. A particularly interesting cell line in this regard is 2/4/A1, a rat intestinal epithelial cell line, which forms polarized monolayers 4–6 days after

seeding onto permeable supports. Initial results showed that the permeability of 2/4/A1 monolayers is comparable to that of the human small intestine. This led us to pose the hypothesis that 2/4/A1 cells monolayers are a suitable cells model for studies of slowly and incompletely absorbed drugs that are significantly transported via the paracellular route [56]. The general performance of 2/4/A1 monolayers was studied using 20 structurally diverse drug molecules that have an absorbed fraction after oral administration to humans (FA) ranging from 0 to 100%. The results are presented in Figure 41 and show that sigmoidal relationships were obtained for both 2/4/A1 and Caco-2 cell monolayers.

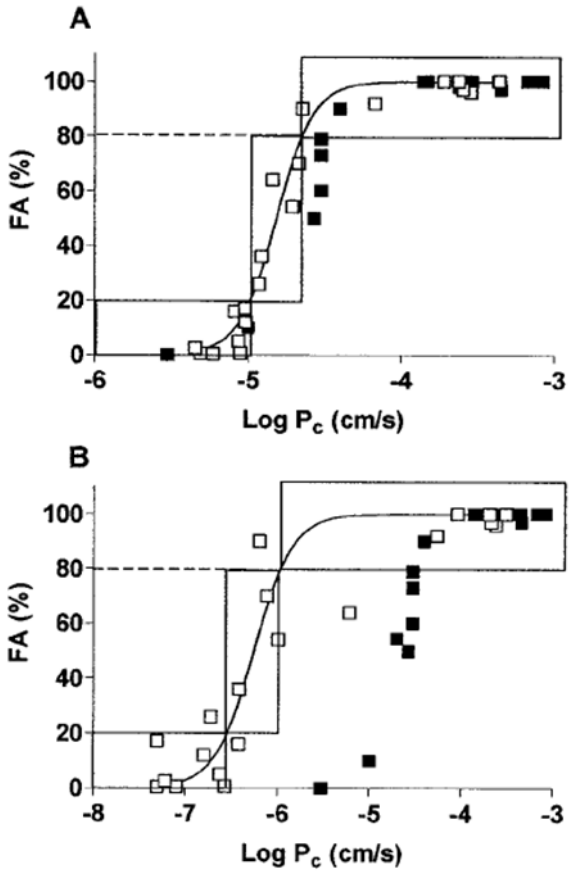

Figure 41. Relationships between FA and permeability coefficients (□) obtained in 2/4/A1 (A) and Caco-2 (B). Data from the human jejunum in vivo (■). The squares represent sparingly absorbed (FA 0–20%), intermediately absorbed (FA 20–80%) and completely absorbed (80–100%) drugs after oral administration to humans [56].

However, when the drugs were categorized as sparingly (FA 0–20%), intermediately (FA 20–80%), and completely (80– 100%) absorbed drugs (23), the permeability values (P_c) for sparingly and intermediately absorbed drugs (hereafter denoted incompletely absorbed drugs) appeared more scattered in Caco-2 than in 2/4/A1 cell monolayers. The difference between the Pc values for incompletely and completely absorbed drugs was much smaller in 2/4/A1 than in Caco-2 cell monolayers. This fact may be explained by the larger contribution of the paracellular pathway to the overall permeability in 2/4/A1 monolayers. This resulted in a less scattered relationship between FA and P_c for 2/4/A1 than for Caco-2 for the low-permeability drugs and in better predictions of FA in 2/4/A1 than in Caco-2. Furthermore, the range in P_c values obtained in 2/4/A1 cell monolayers is in excellent agreement with that obtained in the human jejunum. It could be concluded that 2/4/A1 cell monolayers have a small intestine-like permeability and that these cell monolayers predicted the intestinal absorption of a set of low-permeability drugs that are incompletely absorbed better than the Caco-2 cell monolayers. Additional advantages of the 2/4/A1 model as compared to Caco-2 include a shorter cultivation time (4–6 days compared to 21 days for Caco-2 cells using the standard cell culture procedure) and (because larger amounts of drugs are transported in 2/4/A1 cells) improved precision in the analysis of transported drug.

To compare the performances of the different cell lines mentioned, Linnankoski and his coworker [57] measured the permeability of polyethylene glycol (PEG) oligomers across the different cell lines. The results are reported in Figure 42.

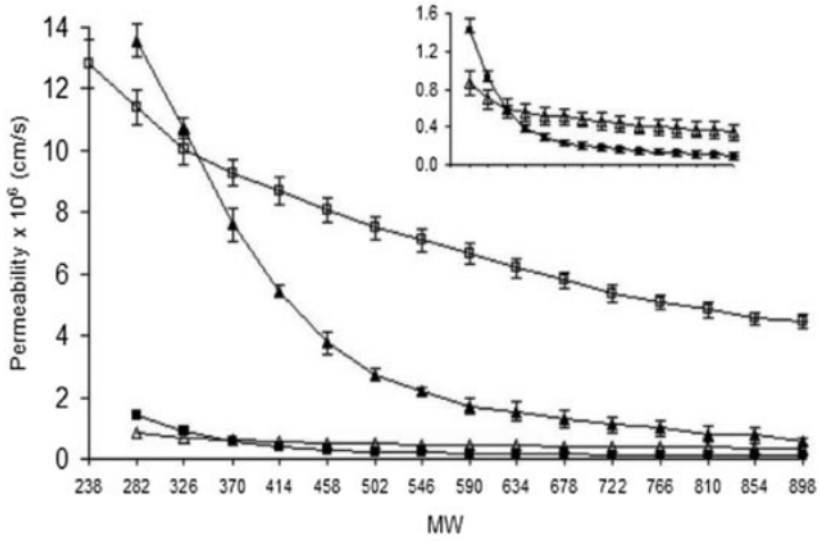

Figure 42. Permeability versus moleculare weight of PEG oligomers for different cell lines. (□) 2/4/A1 cells, (■) Caco-2 cells, (Δ) MDCKII cells, (▲) human intestine [57].

The data show that the overall paracellular permeability is the highest in the 2/4/A1 cell line, followed by the human intestine. The MDCKII and Caco-2 cell lines have the lowest permeabilities. The MDCKII and Caco-2 cell lines, and the human intestine show a biphasic relationship between permeability and molecular weight/radius of the PEG oligomers, while a linear relationship is seen between permeability and molecular weight/radius in the 2/4/A1 cell model. Furthermore, the analysis indicates that there are two distinct pore sizes in the MDCKII and Caco-2 cell models and in the human intestine. The radii of the small pores were in the same order of magnitude in the membranes (5.5–6.6 A). The radii of the large pores were 10.1–30.5 A. The 2/4/A1 monolayer was found to have pores of only one size. Of course, the porosity is an important feature for the cell line which has to mimic to intestinal permeability. The porosity of the different cell lines was compared.

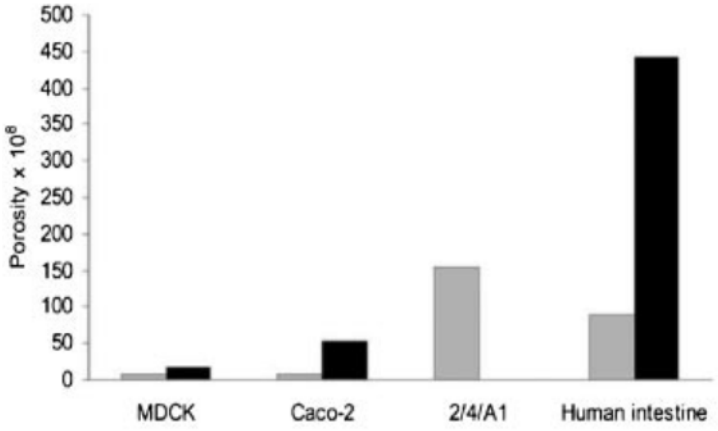

Figure 43. Porosities constituted by large pores (grey) and small pores (black) in MDCKII, Caco-2, 2/4/A1 cell lines and human intestine [57].

The total porosity of the human intestine is 20 times that of the MDCKII cell line, over 10 times that of the Caco-2 cell model and over 3 times that of the 2/4/A1 cell model. The porosity created by small pores is greater than that created by large pores in the MDCKII and Caco-2 cell lines and the human intestine, whereas the total porosity of the 2/4/A1 cell line is constituted by large pores only.

Parallel Artificial Membrane Permeability Assay (PAMPA)

The *in vitro* methods based on biological membrane are usually laboratory intensive and therefore currently are not suited for high-throughput measurements. Hence, a method able to analyze a large number of compounds at an early stage of discovery is necessary, particularly to help in the differentiation between active, paracellular, and transcellular absorption processes. Once the main phenomena is identified, the right method to study the compound of interest could be used. This was the focus of the PAMPA, which stands for "Parallel Artificial Membrane Permeability Assay". PAMPA is a simple method for prediction of transcellular drug absorption, it could be used to screen the biopharmaceutical properties of compounds at high speed, this is a big advantage compared with the biological membranes which need long culture and preparation time. Initially, to validate the PAMPA model, the analysis made with this system, were compared to a set of well-described drugs found in literature [58]. The selected set includes known passively absorbed compounds, as well as actively transported drugs. PAMPA is based on a 96-well microtiter plate technology completely artificial, without

pores and active transporter systems and 96-well microfilter plate. Each composite well is divided in two chambers: the donor chamber at the bottom and the acceptor chamber at the top, separated by a microfilter disk coated with a mixture of lecithin and an inert organic solvent (several formulation of the coating are possible). The setup is shown in Figure 44.

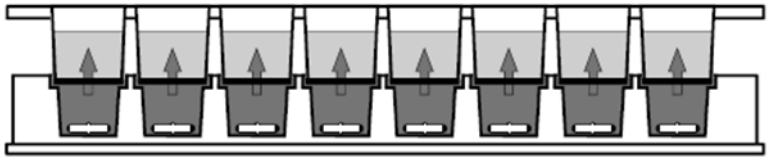

Figure 44. Cross section of PAMPA sandwich assembly [59].

Using a hydrophobic filter material as a support, the permeation of these compounds through a membrane was measured. The obtained flux values were compared with known human absorption data [58, 60]. Moreover, influences of pH changes, phospholipid composition, solubility, or effects of surfactants, like bile acids, on transport processes can be examined.

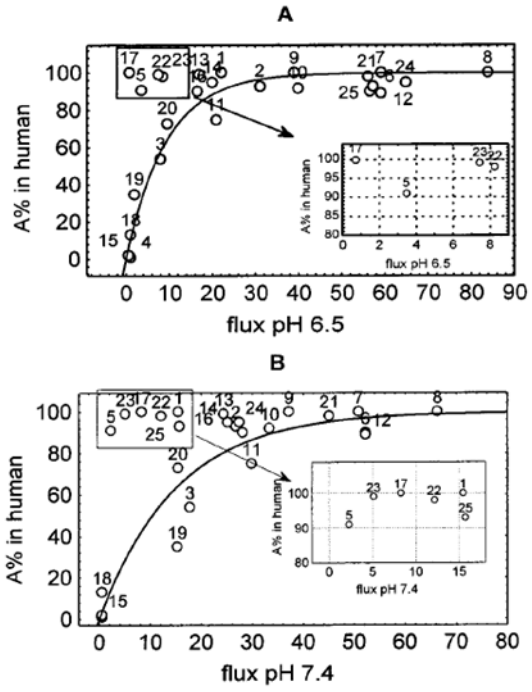

Figure 45. Absorption in humans versus PAMPA flux at pH 6.5 (a) and 7.4 (b) [58].

The relation found was an hyperbolic curve. With this relation identify the highly absorbed drugs is simpler than the other methods.

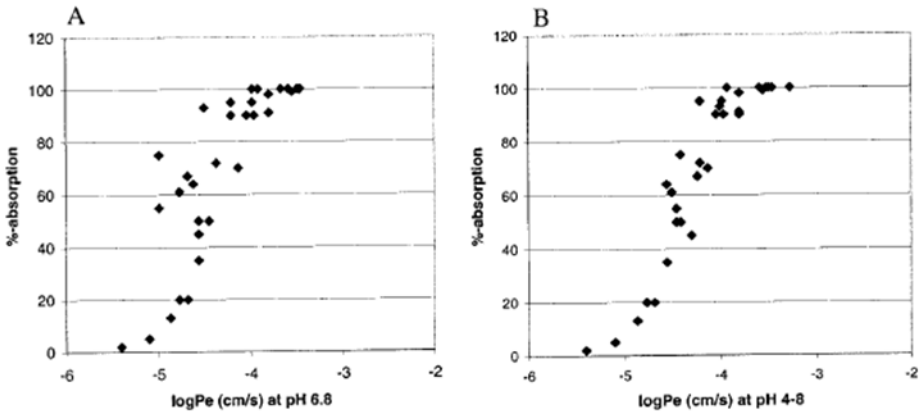

Figure 46. (A) GI-tract absorption of 32 drugs versus hexadecane membrane (HDM) log P_e at pH 6.8. (B) GI-tract absorption of 32 drugs versus hexadecane membrane log P_e at pH range 4-8 [60].

A good correlation was observed between percent absorption and HDM log P_e measured at pH 6.8 (Figure 46-A). For a number of compounds, however, the HDM log P_e value measured at pH 6.8 leads to an underestimation of the fraction absorbed. To mimic an environment which more closely resembles the conditions encountered as the substance moves through the GI-tract, permeability measurements were repeated at different pH values, varying from pH 4 to pH 8, and the highest HDM log Pe value was taken into account for each compound (Figure 46-B).

To evaluate the effective reliability of the PAMPA measurements, a comparison between the permeability of compounds obtained with the PAMPA technique and the BCS classification was realized [61]. According to the FDA, the boundary between high and low permeability should be 90% absorption in humans. The boundary between high and low solubility is that the maximum dose number (Do = a combination of dose strength and dose solubility) over the pH range of 1–7.5 equals 1. However, to strictly classify the drugs according to the BCS, solubility measurements over pH 1–7.5 are required. Simulated gastric and intestinal fluid (SGF and SIF) were selected as dissolution media. The solubility, dose number, and permeability of 18 drug compounds measured by PAMPA are

evaluated. The solubility of these compounds was measured by High Throughput Solubility Assay (HTSA).

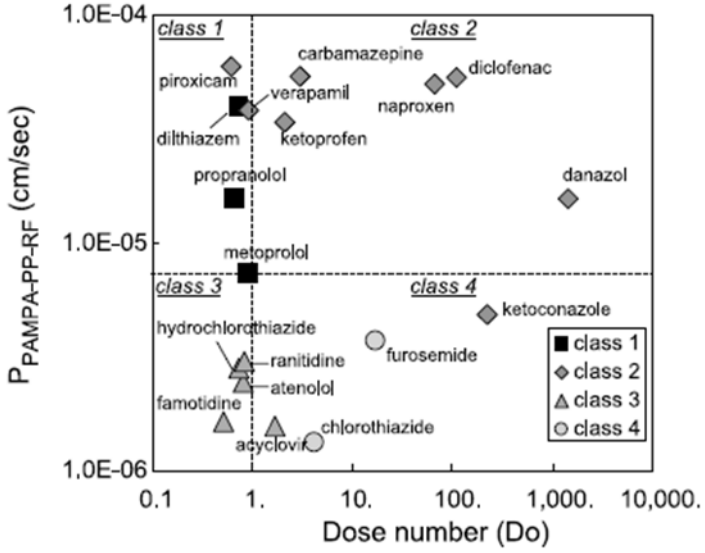

Figure 47. Plot of permeability vs. dose number (Do) obtained by PAMPA and HTSA, respectively [61].

14 of 18 compounds were correctly classified by SGF solubility, SIF solubility, and PAMPA (78% success rate) as shown in Figure 47. As previously mentioned, the compositions of the solvent coating the membrane in this system could be several. The composition of the lipidic solvent was changed during the years to improve the prediction of the permeability in PAMPA system [62]. First of all the chain length of the organic solvent was changed, then a negative charge was added to mimic the intestinal membrane, and finally the permeability coefficients were evaluated. This change in solvent composition was found to be particularly effective on permeability of charged drugs. It could been concluded that this artificial membrane-based method is a powerful method to estimate the permeability of drugs, however it could be improved and it is necessary, for advanced analysis, more studies to characterize a drug.

3.1.3 Animal perfusion studies

The rate and the extent of intestinal drug absorption *in vivo* are affected by several factors, such as dose/dissolution ratio, intestinal transit, and effective permeability across the intestinal mucosa.

Intestinal perfusion models, which measure the disappearance of the drug from the perfusion solution in the intestinal lumen, directly reflect the transport across the apical epithelial cell membrane (Figure 48).

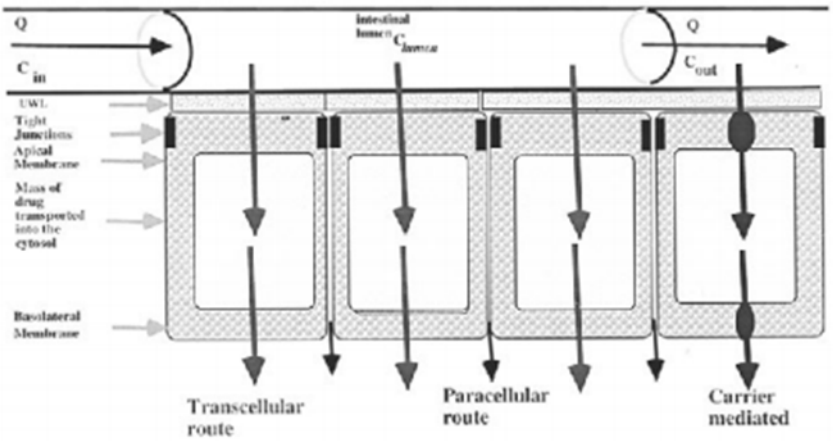

Figure 48. Schematic of the membrane transport barriers across the intestinal epithelium during a perfusion of the intestinal lumen [10].

Initial studies about new chemical entities intestinal absorption could be routinely carried out in small animal models, most commonly the rats (Figure 49).

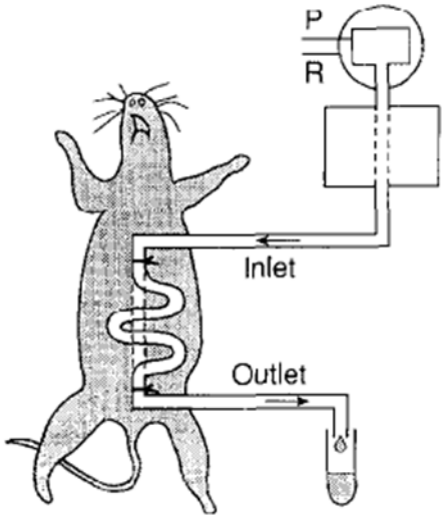

Figure 49. Schematic of an *in situ* perfusion technique [52], R = reservoir, P = pump.

The method is based on the isolation of an intestinal segment. This isolated intestinal segment (usually 6-8 cm) has an intact blood flow supply and innervation. Two polymeric cannulas are inserted through the skin and attached to the abdominal wall by ligation. Outside the animal, perfusion tubes are connected to these cannulas; inside the animal, the loop is ensured by a suture. The permeability across the intestinal segment is measured evaluating the difference between the concentration of the compound entering through the inlet and the concentration exiting from the segment. A number of *in situ* perfusion flow patterns have been used the evaluate the permeability, as shown in Figure 50.

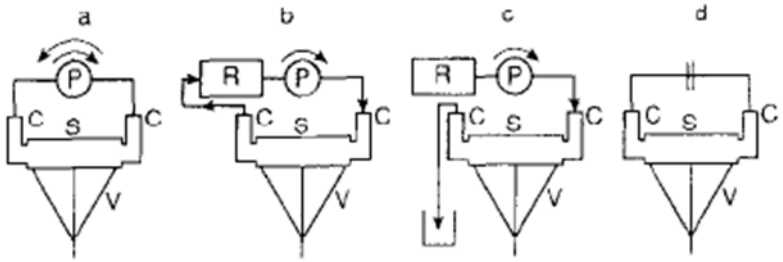

Figure 50. Different perfusion flow patterns: (a) oscillating perfusion, (b) recirculating perfusion, (c) single pass perfusion, (d) ligated intestinal loop.

In Figure 50, S is the perfused intestinal segment, V is the jejunal veins, C is the cannula, P is the pump, R is the reservoir. The oscillating perfusion is characterized by a continuous flow of the perfusate in both the directions. The recirculating perfusion is characterized by a single direction of the flow and by the presence of a reservoir. The single pass perfusion, which is the most widely used method, is characterized by a non-closed loop. Finally, the ligated intestinal loop is characterized by the absence of both the pump and the reservoir. Correlations of drug intestinal permeability obtained from rat *in situ* perfusions have been established with fraction of drug absorbed [63]. An isolated and vascularly perfused rat small intestine was used to determine the permeability values of several drug compounds.

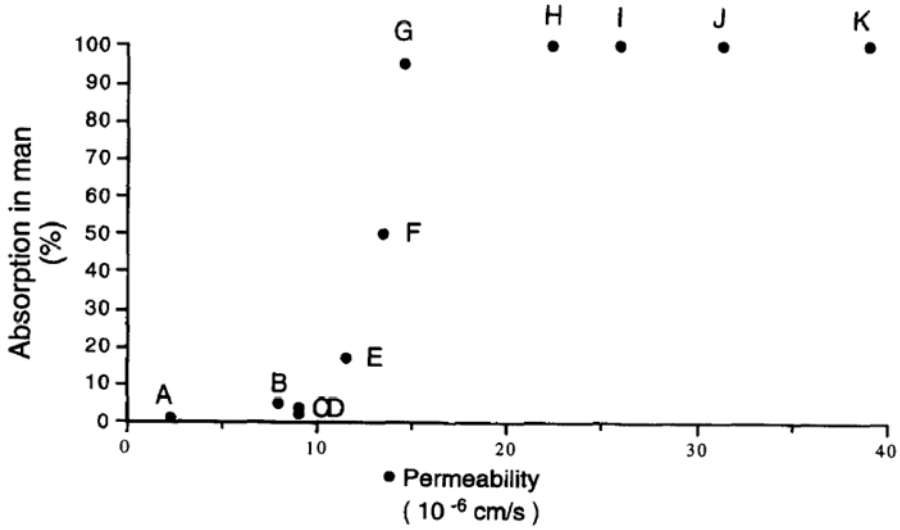

Figure 51. Correlation between oral absorption in humans and the permeability coefficients in vascularly perfused rat intestine [63].

A good correlation was obtained between the permeability values determined in this model and the proportion of an oral dose absorbed in humans. An important disadvantage of this system, as compared to rapid in vitro systems like everted rings, is the number of animals required to establish perfusion conditions that minimize within-treatment variability.

Vascularly perfused intestine

Intestinal lumenal perfusion is very useful to estimate membrane permeability. However, absorption is calculated from the difference between drug appearance in the serosal compartment and drug disappearance from the mucosal compartment. Mass balance evaluation requires sequential blood sampling, which may be difficult in small animals [52]. Vascularly perfused intestinal preparations allow these evaluations without the limitation of animal size or vascular volumes. Intestinal vascular perfusions have been performed in the rat with or without simultaneous perfusion of the intestinal lumen. The preparation involves cannulating either a pair of mesenteric vessels supplying an intestinal segment, or the superior mesenteric artery and portal vein perfusing almost the entire small intestine. The intestinal lumen is cannulated for perfusion or collection

of lumenal fluid. A catheter can also be placed in the intestinal lymph duct for lymph collection (Figure 52).

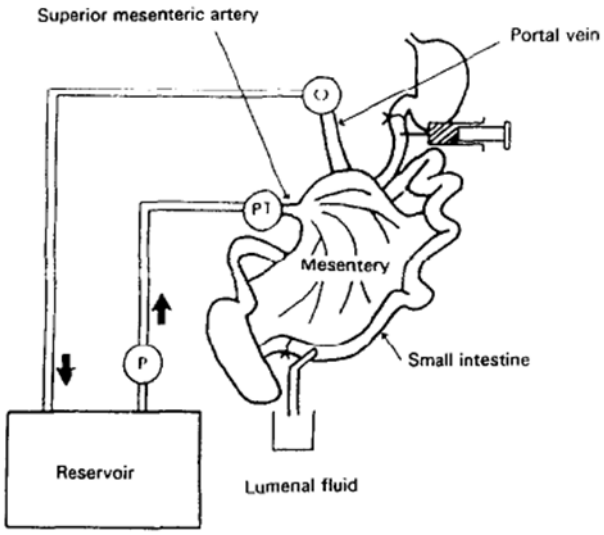

Figure 52. Schematic illustration of the vascularly perfused rat intestinal preparation and the perfusion apparatus. A pair of mesenteric vessels supplying an intestinal segment (or the superior mesenteric artery and portal vein) were cannulated [52].

In the majority of the preparations, the animal is sacrificed after the start of the perfusion, hence the intestine is the only vital organ. For this reason, it is necessary maintain the viability of the preparations for several hours and monitor the oxygen or glucose consumption, perfusate pH and pressure. Alternatively, a modification of the set-up has been made where the mesenteric vein draining a short intestinal segment is cannulated without affecting the portal flow, and the saphenous vein is catheterized to introduce blood replacing the volume collected (Figure 53).

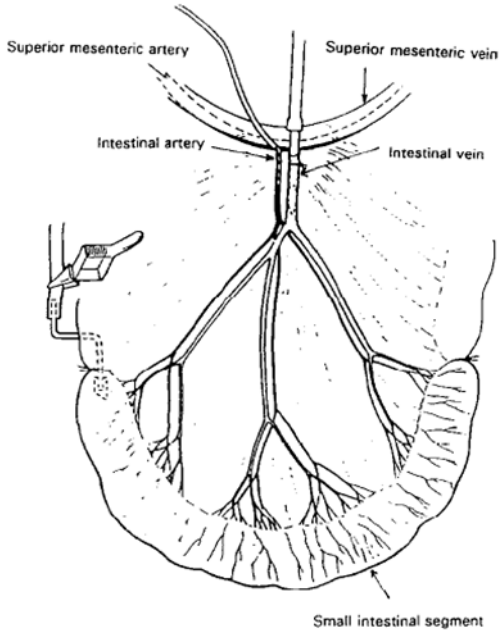

Figure 53. Schematic diagram of intestinal vascular perfusion without obstruction of mesenteric or portal blood flow [52].

A small needle can also be placed in the mesenteric artery foloptional drug input without obstructing the mesen- teric flow. In this model, arterial, neural and lymphatic supplies to the segment remain intact. In general, the vascularly perfused intestinal model is versatile: the drugs could be administered in the lumen or vascular perfusate. When administered to the intestinal lumen, drug absorption can be evaluated from a mass balance. In addition to the extent of absorption, the rate of absorption can be estimated, as well as carrier-mediated or active transport processes. Moreover, with the lymph collection, portal vs. lymphatic absorption of very lipophilic compounds can be explored. Furthermore, the preparation allows evaluation of intestinal metabolism by GI enzymes or microflora. Comparing the two perfusion methods, it could be seen that single-pass perfusions prevent build-up of metabolites or wastes, but recirculating perfusates allow accumulation of trace amounts of compound for detection. The model is advantageous because the effect of changes in experimental conditions (e.g. drug concentration, administration site, perfusate composition, flow) can be readily investigated and perfusate samplings are uncomplicated [52].

Vascularly perfused intestine-liver

In the real physiology, compounds absorbed from the intestine pass through the liver, which contains a host of metabolizing enzymes, before reaching systemic circulation. The *in situ* lumenally perfused intestinal model, coupled with systemic sampling, allows an evaluation of the amount of drugs absorbed systemically, in this way is possible to evaluate the systemic clearance, which cannot be calculated with the other methods. The main difficulty is to maintain the animal anesthetized and the preparation viable for an extended period of time. Alternatively, the vascularly perfused rat intestine-liver preparation allows a direct evaluation of the contribution of the intestine and liver in first-pass elimination. In this method, the superior mesenteric artery and the hepatic artery were cannulated for perfusate inflow, the pyloric vein was cannulated for portal sampling, and systemic sampling was done via the hepatic vein. The bile duct was also cannulated for bile collection (Figure 54).

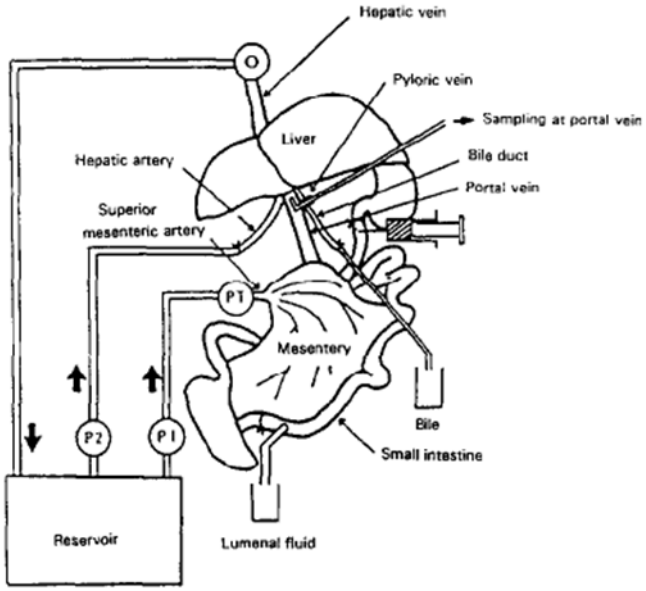

Figure 54. Schematic illustration of the vascularly perfused rat intestinal-liver preparation and the perfusion apparatus [52].

The lumenal content was removed at the end of the experiment. The vascular perfusion can be done in the single-pass mode or in the recirculating mode depending on the dose which could be added to the perfusate reservoir or injected as a bolus into the intestinal lumen. The intestine and liver were kept viable for 2 h with the vascular perfusate,

but the rest of the animal was non-vital, as the previous case. Viability of the preparations were monitored, in addition to examination of bile flow and liver enzyme level in perfusate. The vascularly perfused intestine-liver preparation is particularly useful if the goal is the simultaneously evaluation of drug absorption, intestinal extraction, and hepatic first-pass, which together determine oral bioavailability. Unlike the methods such as isolated cells or tissues, this preparation is physiologically based, with intact circulation and morphology. A disadvantage of this method is that the lack of other eliminating or non-eliminating organs which are present in the whole animal allows isolation of the individual role of the intestine or liver in first-pass. The model permits facile manipulation of experimental variables and usage of drug concentration not well tolerated *in vivo*. Sampling of perfusate or lumenal content is not limited by animal size or vascular volumes. Another drawback is that the preparation of the perfusate and the organ cannulation are time-consuming and require adept surgical skill.

3.2.4 Human perfusion studies

The most common method used to study the intestinal absorption in humans is perform standard pharmacokinetic analysis. More complex methods are intubation techniques, remote-controlled capsules, and pharmacoscintigraphy studies.However these methods are based on plasma concentration-time data, which cannot be used directly to investigate the permeability or drug dissolution *in vivo*. On the contrary, single-pass perfusion of an intestinal segment is an approaches which permits mechanistic investigations of drug absorption. The human intestinal perfusion methods have been useful to understand the phenomena which generate the *in vivo* membrane transport. This clinical method allows the research on: the first-pass effect of drugs in the liver, drug metabolism in intestinal tissue, *in vivo* dissolution of drugs, nutrient absorption, biological mechanism in case of gastrointestinal disease, and food-drug interactions [10]. An *in vivo* drug absorption technique for single-pass perfusion in human subjects, the Loc-I-Gut, has been used for the investigations [64]. This *in vivo* perfusion technique requires a 175 cm long tube an outer diameter of 5.3 mm, as shown in Figure 55. It has six inner channels and is distally provided with two elongated latex balloons.

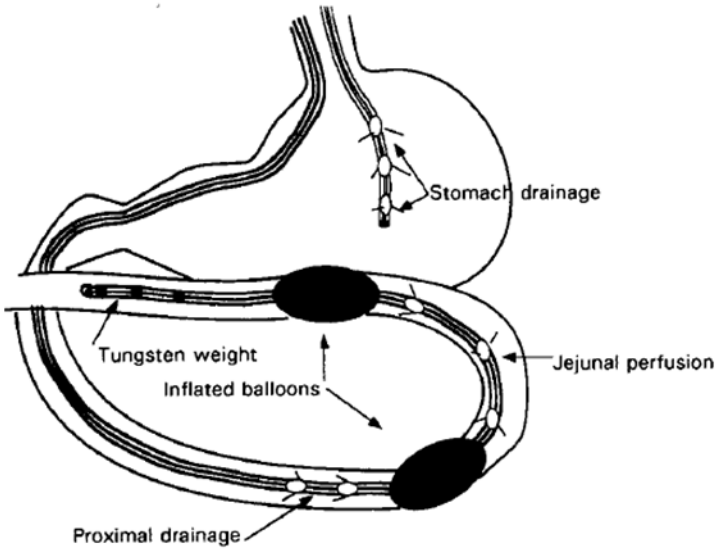

Figure 55. The multichannel tube system with double balloons enabling segmental jejunal perfusion in man [64].

Following a ten hours overnight fast, the tube is introduced orally. After the tube was positioned in the proximal jejunum, the balloons were inflated with air, making a segment of 10 cm between the two balloons in the proximal jejunum. A gastric tube was introduced orally and placed into the dependent portion of the stomach and used to aspirate the gastric content. Initially, the jejunal segment was filled manually with a saline solution, then the drug containing solution was perfused. The output fluid was collected on ice every ten minutes. During the experiment a vacuum pump was used to facilitate the aspiration of the gastric and the intestinal contents [65]. To prevent that the motility and the blood supply are altered by the presence of the balloons, the absorption of markers for the passive and transcellular absorption was evaluated. The results have shown a stability of the absorption over time and it could be concluded that the viability was not changed during the experiment [64]. Drug transport across the membrane wall of a tube is the relationship between the masses entering and leaving the tube:

$$\frac{dM}{dt} = Q \cdot (c_{in} - c_{out}) \tag{2.1}$$

where c_{in} and c_{out} are the inlet and outlet drug concentrations, respectively, and Q is the flow through the tube, usually assumed to be constant. The mass balance relationship can then be set to describe the

rate of transport of the drug across the tube membrane (absorbed mass) according to Fick's first law:

$$\frac{dM}{dt} = A \cdot P_{eff} \cdot (c_{ref}^{lumen} - c_{ref}^{blood}) \tag{2.2}$$

where A is the surface area of the membrane, P_{eff} is an effective permeability coefficient and the reference concentrations c^{lumen} and c^{blood} are on the two opposite sides of the intestinal mucosa, as shown in Figure 56.

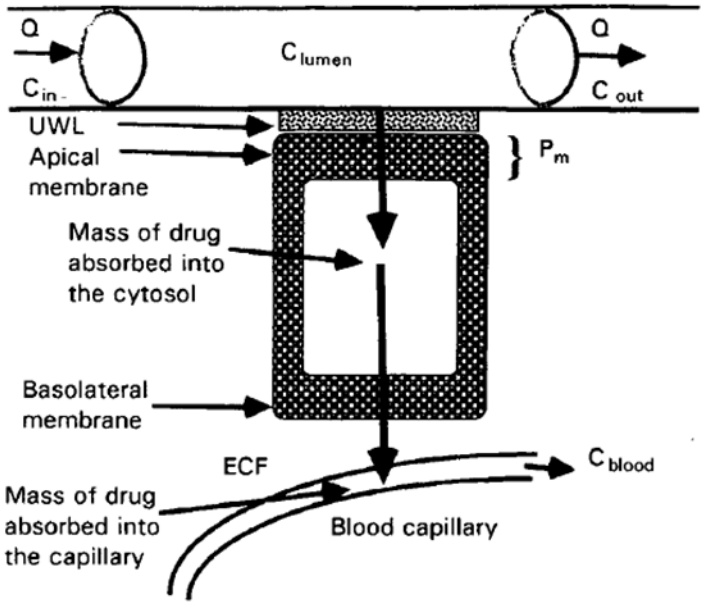

Figure 56. Schematic of the Loc-I-Gut perfusion technique [64].

The effective permeability (P_{eff}) in huamns represents both the partitioning of a drug molecule from the luminal fluid into the apical membrane and the diffusion across the lipid membrane. Hence, together with the reference drug concentration within the intestinal segment it will determine the mass-transport rate per unit area into the cytosol of the enterocyte across the apical membrane. The values of the effective permeability evaluated using various absorption models were compared and related to the extent of absorption in humans, as shown in Figure 57.

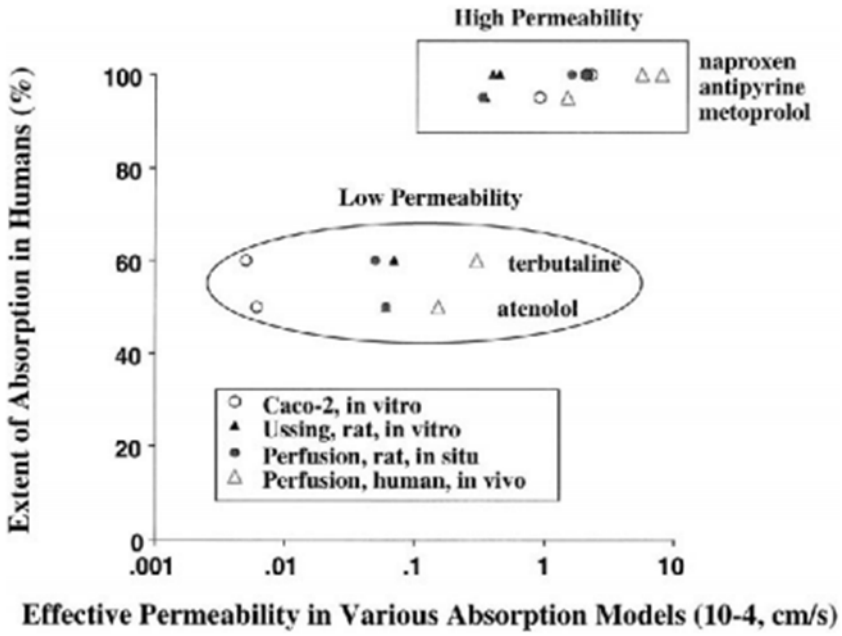

Figure 57. The effective permeability of various drugs evaluated using CaCO-2 monolayer, rat jejunal segment in Ussing chamber, the perfused rat jejunum, and the human jejunum [10].

A set of reference drug has been used to reduce the inter-laboratory variability of the permeability estimates. It could be easily seen that the values of permeability evaluated using the human jejunum are all higher than the values evaluated with other methods. As previously seen, in fact, the *in vitro* methods underestimate the permeability values. Concerning the inter-individual variability, it could be said that this is reduced for the high permeability drugs, but non-negligible for low permeability drugs.

Chapter Four

Aims

In this chapter the aims of the thesis are described.

4.1 Aims of the thesis

As described in the previous chapters, the main goal of pharmacokinetic analysis is the prediction of the drug behavior once a pharmaceutical is assumed. To reproduce the drug's fate *in vitro* or *in silico* models could be used.

Concerning the *in vitro* models, the work has the goal to design and to realize one or more devices, able to mimic the human organs involved in drug delivery. In case of oral administration, which is the most common route of administration, the organs involved are the gastrointestinal tract and the gastrointestinal circulatory system (GICS), which is assumed to be the circulatory system around the gastrointestinal tract. The main phenomena which take place in the gastrointestinal tract are dissolution and adsorption. Hence, the device will take into account the thermal, mechanical, and biochemical history of the gastrointestinal tract and the absorption across the intestinal wall which influences the distribution of the drug into the organism.

Concerning the *in silico* models, the work has the goal to propose and to validate a pharmacokinetic model able to correlate the *in vitro* dissolution profile with the *in vivo* plasma evolution, for different administration routes. This model has to take into account both the ADME phenomena (absorption, distribution, metabolism, and excretion of the drug), pharmacokinetic, and inter-individual parameters. The model has to be reliable and versatile, it has to be applicable for different administration routes and drugs. Hence, the model will take into account the main phenomena involved in the drug metabolism, the *in vitro* dissolution profile, and the dependence of the pharmacokinetic parameters on the inter-individual characteristics.

The final goal of this research is to combine the two approaches (*in vitro* and *in silico*) to model and predict the phenomena involved in the drug assumptions.

Chapter Five

Materials and methods

In this chapter the materials used for the dissolution analysis and the analytical techniques are described. Moreover, the methods used for the dissolutions, the design, and the realization of the in vitro devices are described.

5.1 Materials

5.1.1 Active molecules

Several drugs have been used in this study to evaluate the permeability and to study the release patterns.

One of the most used model drug is theophylline. It is also known as dimethylxanthine, a drug used in therapy for respiratory disease. Its structure is very similar to caffeine and it is naturally found in tea leaves or cocoa beans.

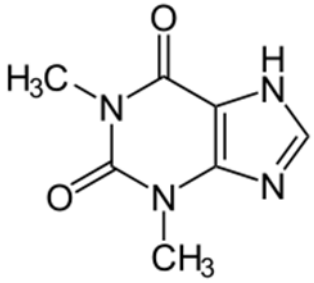

Figure 58. Theophylline structure.

The main actions of theophylline involve relaxing bronchial smooth muscles and increasing blood pressure.

When theophylline is administered intravenously, bioavailability is 100%. However, if taken orally, the absorption process could be slower, without affecting the bioavailability. Theophylline is distributed in the extracellular fluid, in the placenta, in the mother's milk and in the central nervous system. The volume of distribution is 0.5 L/kg. The protein binding is 40%. Theophylline is metabolized extensively by the liver (up to 70%) and it is excreted by the urine.

Table 2. Chemical, physical and pharmacokinetic data of theophylline.

Formula	$C_7H_8N_4O_2$
Molar mass	180.164
Melting point	270 – 274°C
Solubility	Soluble in 0.1 M HCl, 0.1 M NaOH Water solublility (1.646 g/100 ml)
CAS number	58-55-9
Bioavailability	100%
Protein binding	40%, primarily to albumin
Metabolism	hepatic to 1-methyluric acid
Half-life	5-8 hours

Diclofenac Sodium is another drug used in this work. Diclofenac is nonsteroidal anti-inflammatory drug taken to reduce inflammation and as an analgesic reducing pain in certain conditions.

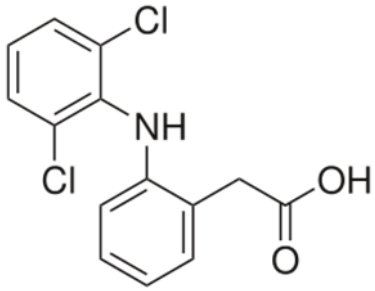

Figure 59. Diclofenac structure.

Diclofenac sodium is poorly soluble in water and acidic pH (1-3) but is rapidly soluble in alkaline pH (5-8). This drug is metabolized hepatically, in fact no active metabolite exist. The excretion is biliary, only the 1% of the drug is eliminated by urine.

Table 3. Chemical, physical and pharmacokinetic data of diclofenac sodium.

Formula	$C_{14}H_{11}C_{l2}NNaO_2$
Molar mass	318.13 g/mol
Solubility	Poorly soluble in water and acidic pH (1-3)
CAS number	15307-86-5
Melting point	275-277°C
Bioavailability	100%
Protein binding	More than 99%
Metabolism	biliary
Half-life	1.2 – 2 hr

Diclofenac is available as a generic drug in a number of formulations.

In this work, two pharmaceutical formulations containing diclofenac were used: Diclofenac EG® extended release tablets (EG S.p.a. – Milan) and Diclofenac DOC Generici (DOC Generici S.r.l.) were used to evaluate the release pattern of extended release formulations and Voltaren® 50 mg soluble gastro-resistant tablet (Novartis Farma S.p.a.) was used to evaluate the release patter of gastro-resistant formulations.

To study the permeabilities of several drugs and active molecules, propranolol was one of them. Propranolol is a non-selective beta blocker ant it is used to treat hypertension, anxiety or panic.

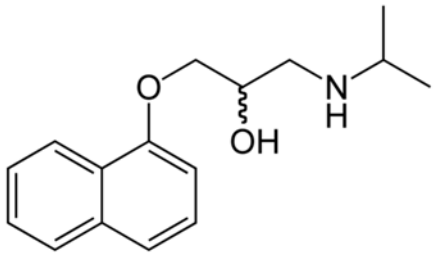

Figure 60. Propranolol structure.

Propranolol is rapidly and completely absorbed, with peak plasma levels achieved approximately 1–3 hours after ingestion. Co-administration with food appears to enhance bioavailability. Despite complete absorption, propranolol has a variable bioavailability due to

extensive first-pass metabolism. Hepatic impairment will therefore increase its bioavailability. Propranolol is a highly lipophilic drug achieving high concentrations in the brain. The duration of action of a single oral dose is longer than the half-life and may be up to 12 hours, if the single dose is high enough (e.g., 80 mg). Effective plasma concentrations are between 10–100 ng/mL. Toxic levels are associated with plasma concentrations above 2000 ng/ml. It is excreted by kidneys.

Table 4. Chemical, physical and pharmacokinetic data of propranolol.

Formula	$C_{16}H_{21}NO_2$
Molar mass	259.34 g/mol
Solubility	H_2O: 50 mg/mL
CAS number	525-66-6
Melting point	163-165 °C
Bioavailability	26%
Metabolism	Hepatic
Half-life	4–5 hours

During the permeability studies two active molecules with higher molecular size than the molecules previously described were tested. The first one was the Vitamin B12.

Vitamin B12 is a water-soluble vitamin with a key role in the normal functioning of the brain and nervous system, and for the formation of blood. It is normally involved in the metabolism of every cell of the human body, especially affecting DNA synthesis and regulation, but also fatty acid synthesis and energy production. The vitamin is the largest and most structurally complicated vitamin and can be produced industrially only through bacterial fermentation-synthesis.

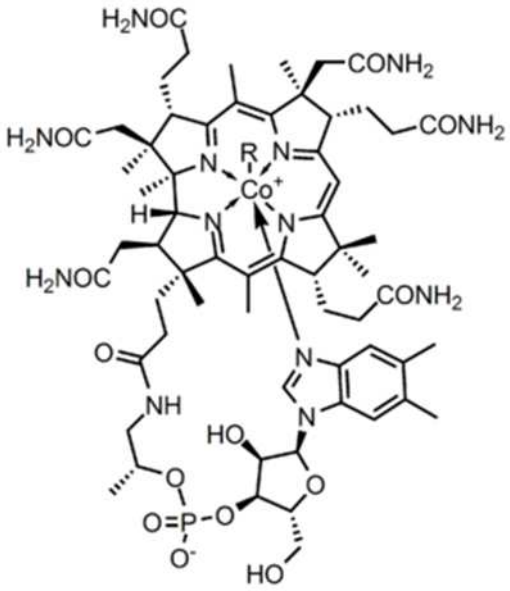

Figure 61. Vitamin B12 structure.

The human physiology of vitamin B12 is complex. Protein-bound vitamin B12 must be released from the proteins by the action of digestive proteases in both the stomach and small intestine. Gastric acid releases the vitamin from food particles; therefore antacid and acid-blocking medications (especially proton-pump inhibitors) may inhibit absorption of B12. In addition some elderly people produce less stomach acid as they age thereby increasing their probability of B12 deficiencies. Absorption of food vitamin B12 requires an intact and functioning stomach, exocrine pancreas, intrinsic factor, and small bowel. Problems with any one of these organs makes a vitamin B12 deficiency possible. Individuals who lack intrinsic factor have a decreased ability to absorb B12. The total amount of vitamin B12 stored in body is about 2–5 mg in adults. Around 50% of this is stored in the liver. Approximately 0.1% of this is lost per day by secretions into the gut, as not all these secretions are reabsorbed. Bile is the main form of B12 excretion; however, most of the B12 secreted in the bile is recycled via enterohepatic circulation. Due to the extremely efficient enterohepatic circulation of B12, the liver can store several years' worth of vitamin B12; therefore, nutritional deficiency of this vitamin is rare. How fast B12 levels change depends on the balance between how much B12 is obtained from the diet, how much is secreted and how much is absorbed. B12 deficiency may arise in a year if initial stores are low and genetic factors unfavorable, or may

not appear for decades. In infants, B12 deficiency can appear much more quickly.

Table 5. Chemical, physical and pharmacokinetic data of vitamin B12.

Formula	$C_{63}H_{88}CoN_{14}O_{14}P$
Molar mass	1355.37 g/mol
CAS number	68-19-9
Bioavailability	Readily absorbed in distal half of the ileum
Protein binding	Very high to specific transcobalamins plasma proteins. Binding of hydroxocobalamin is slightly higher than cyanocobalamin.
Metabolism	hepatic
Half-life	Approximately 6 days (400 days in the liver)
Excretion	renal

The other active molecule used in the permeability studies was the Bovine Serum Albumin (BSA).

Bovine serum albumin is a serum albumin protein derived from cows. It is often used as a protein concentration standard. "Fraction V" refers to albumin being the fifth fraction of the original Edwin Cohn purification methodology that made use of differential solubility characteristics of plasma proteins. By manipulating solvent concentrations, pH, salt levels, and temperature, Cohn was able to pull out successive "fractions" of blood plasma. The process was first commercialized with human albumin for medical use and later adopted for production of BSA.

Figure 62. Bovine Serum Albumin structure.

The full-length BSA precursor protein is 607 amino acids in length. An N-terminal 18-residue signal peptide is cut off from the precursor protein upon secretion, hence the initial protein product contains 589 amino acid residues. An additional 4 amino acids is cleaved to yield the mature BSA protein that contains 583 amino acids.

Table 6. Chemical and physical data of BSA.

Molar mass	66463 g/mol
Number of amino acid residues	583
isoelectric point in water at 25 °C	4.7
Dimensions	140x40x40 $Å^3$

5.1.2 Polymers

To ensure the gradual release of drug from a pharmaceutical form, tablets of polymer in which the drug was dispersed were prepared. In this work, substantially, two kind of polymers were used: Hydroxypropyl methylcellulose (HPMC) and a new polymer developed in this research group. HPMC (Methocel K15M Premium Grade) was a purchased from Colorcon (UK). Hydroxypropyl methylcellulose (HPMC), is a semisynthetic, inert, viscoelastic polymer used as an ophthalmic lubricant, as well as an excipient and controlled-delivery component in oral medicaments, found in a variety of commercial products.

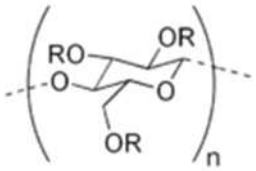

Figure 63. HPMC chemical structure.

Hypromellose is a solid, and is a slightly off-white to beige powder in appearance and may be formed into granules. The compound forms colloids when dissolved in water. Although non-toxic, it is combustible and can react vigorously with oxidising agents.

It, unlike methylcellulose, exhibits a thermal gelation property in an aqueous solution. That is, when the solution heats up to a critical temperature, the solution congeals into a non-flowable but semi-flexible mass. Typically, this critical (congealing) temperature is

inversely related to both the solution concentration of HPMC and the concentration of the methoxy group within the HPMC molecule (which in turn depends on both the degree of substitution of the methoxy group and the molar substitution). That is, the higher the concentration of the methoxy group, the lower the critical temperature. The inflexibility/viscosity of the resulting mass, however, is directly related to the concentration of the methoxy group (the higher the concentration, the more viscous or less flexible the resulting mass is). In this work an HPMC K15 M, with an intermediate viscosity.

The polymer synthetized by this research group [66] is composed by two copolymers: poly methyl methacrylate (MMA) and poly acetic acid (AA). The poly(MMA–AA) copolymers were obtained by a free radical polymerization method. In particular, the polymerization was carried out in bulk, using AMVN as initiator. The initiator was added to various volumetric ratios of MMA/AA monomers and thoroughly mixed by sonication (VibraCellTM Ultrasonic Processor, Sonics, Newtown, CT) for 3 min. The reaction mixture was poured into glass tubes, sealed, and placed vertically in a water bath which provided a uniform and accurate temperature control. The tubes were then taken out from the bath and broken under slight clamp pressure. The samples were removed from the broken glass tubes and placed in an oven in which the temperature was slowly raised up to 70°C, followed by overnight cooling. The samples were crushed and stored at room temperature. The important feature of the novel synthesized poly(MMA–AA) was the linear relationship holding between dissolution pH and volumetric percentage content of MMA.

5.1.3 Dissolution media

Chemicals used for the dissolution media were: Hydrocloric acid (HCl, CAS 7647-01-0), 37% w/w solution, density 1200 $kg \cdot m^{-3}$, MM_A = 36.5 $kg \cdot kmol^{-1}$; Sodium hydroxide (NaOH, CAS 1310-73-2), pure solid, MM_B = 40.0 $kg \cdot kmol^{-1}$; Sodium phosphate dodecahydrate ($Na_3PO_4 \cdot 12H_2O$, reagent S, CAS 10101-89-0), pure solid, MM_S = 380.12 $kg \cdot kmol^{-1}$.

5.1.4 Membranes

The synthetic membrane used during the permeability studies was a cellulose acetate membrane (purchased from Sartorius AG) with a pore size of 0.2 µm and thickness of 130 µm.

In the device simulating the transport across the intestinal walls, an hollow filter was used to reproduce the mass transport. The filter (Phylther LF17SD) used has an high surface area. The fibres were made of Polyphenylene (PPE). The characteristics of the filter are reported in the following table:

Table 7. Characteristics of the hollow fiber filter.

Surface [m^2]	1.7
Fiber wall thickness [µm]	35
Fiber inside diameter [µm]	200
Filling volume - acceptor [mL]	109
Pressure drop - acceptor [mmHg]	<25
Pressure drop - donor [mmHg]	<50
Total lenght [mm]	305
Outside diameter [mm]	55
Weight [g]	194

5.2 Methods

5.2.1 Tablet preparation

The mixture of the powders necessary to made the tablets was obtained by mixing the powders of drug and polymer in a mortar. The cylindrical matrices (0.35 g, 13 mm diameter, 2.0 mm thickness) were prepared by compressing the powder in a tabletting machine (Specac PN3000), equipped with flat-faced punches, diameter 13 mm, with a compression force of 50 kN (by a Carver Press) kept for 5 min.

5.2.2 Dissolution methods

Conventionally, the dissolution for orally administrated drugs is studied following the US Pharmacopoeia rules, as described in the USP chapter 711. In this chapter the methodologies to perform the

dissolution of different kind of drug formulation (immediate or delayed release) in different USP accepted apparatuses are specified. For the enteric coated dosage forms, USP defines two different procedures for testing the release, both of them comprising two steps: an acid stage and a neutral stage. The temperature is kept constant during all the dissolution test on 37°C, the physiological temperature. The pH is initially maintained on 1.0, to simulate the gastric environment and then it is quickly raised up to 6.8 to simulate the intestinal environment after 2 hours.

The pH 1 was obtained mixing 6.25 mL of HCl (37% w/w) with distilled water (to volume 750 mL). The solution was kept stirred at 100 rpm and at a temperature of 37°C in a USP Apparatus II. The tablet was immersed in the dissolution medium and, to evaluate the release pattern, 1 mL of the medium was withdrawn and the concentration of the drug released was evaluated by an HPLC or UV methods. After two hours the solution was neutralized by adding 250 mL of a solution composed by distilled water in which 16 g of a salt (Sodium Phosphate Tribasic Dodecahydrate) were dissolved. The tests were carried on until the complete dissolution of the tablet.

In spite of the USP recommendations, it was demonstrated that the pH in the stomach increases during the ingestion of food, depending on the pH and the buffer capacity of the food, and subsequently decreases due to acid secretions. Thus, the pH in the stomach is not 1.0 but, just before the meal, the pH is about 4.8, and it starts to decrease after the meal [67] (physiological pH evolution is shown in Figure 70). Its exact value after two hours is variable individually and it depends on the meal nature and quantity, in general it is in the range 1 - 2. For this reason, the dissolutions of the tablets were performed also in a medium following the real pH history in the gastrointestinal tract. The buffer to start the controlled pH test (pH 4.8) was prepared (V = 0.5 L) by mixing hydrocloridric acid and sodium phosphate dodecahydrate at concentrations C_A = 0.1 mol/L and C_S = 0.05 mol/L. This buffer was obtained mixing 9.5 g of phosphate and 4.2 mL of acid and adding distilled water to volume. The solutions to be used to control the pH were obtained as follows: the acid solution (HCl) was composed by 28 mL of the cloridric acid diluted to 0.5 L with distilled water; the basic solution (NaOH) was composed by 13 g of the base dissolved in 0.5 L of distilled water. The sudden increase in pH expected after two hours in the controlled pH test was accelerated by adding 1.4 g NaOH/25

mL distilled water, as an aid to the dosage of basic solution commanded by the pump.

5.2.3 Transport phenomena studies

Franz cell

To carry out the permeability measurement, a Franz cell, which is commonly used in preclinical and *in vitro* studies to evaluate the permeation of drugs, has been used [68]. The Franz cell is characterized by the presence of two different volumes: the upper one, the donor compartment, which could be filled of a medium rich in drug content, measuring 3 ml, and the lowest one, the acceptor compartment, which could be filled of a medium poor in drug content and kept stirred, measuring 7 ml.

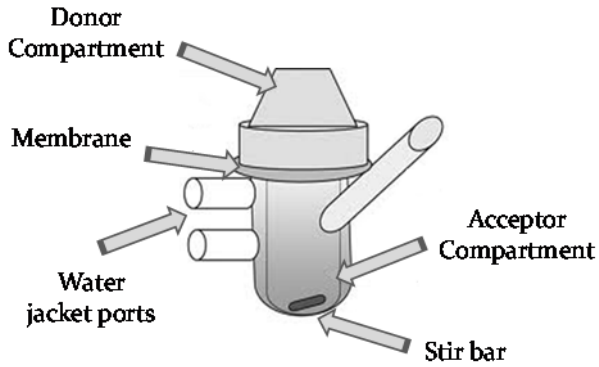

Figure 64. Schematic of a Franz cell.

The volumes of the cell are separated by a membrane of area A_s and the drug contained in the donor compartment needs to pass across the membrane to reach the acceptor compartment. The Franz cell used has the following dimensions:

Table 8. Franz cell dimensions.

Donor volume [mL]	3	V_D
Acceptor volume [mL]	7	V_A
Exchange surface [cm^2]	0.785	A_S

All the experiments are carried on at the same pH in both the compartments. The media consisted of a buffer solution at pH 6.8

which was obtained mixing 750 ml of a distilled water/HCl solution (6.25 ml HCl of 37% wt purity) and 250 ml of a solution obtained dissolving 16 g of sodium phosphate tribasic dodecahydrate in distilled water. During all the experiments, the Franz cell was immersed in a stirred bath with controlled temperature at 37°C. With the entering of this water in the jacket ports of the cell, the constant temperature is ensured.

To evaluate the permeability across the membrane, a buffer solution at a certain concentration of the selected active molecule is inserted in the donor compartment, while the acceptor compartment is filled of buffer solution free of drug. Then, the Franz cell is immersed in the stirred bath until a predetermined time. At the end of the run, the concentration of the active molecule is evaluated both in the donor compartment and in the acceptor one by an UV spectrometer Lambda 25 PerkinElmer. For each solution, the concentration of the molecule is evaluated at its specific absorption wavelength (shown in Table 9).

Table 9. Active molecules and their wavelengths studied with the Franz cell.

Molecule	Wavelength [nm]
Theophylline	275
Diclofenac	275
Propranolol	289
Vitamin B12	361
BSA	280

The experiments are carried on for different times to obtain the concentration evolution both in the donor and in the acceptor compartment. Once obtained the permeability values using the cell, it could be possible to correlate the *in vitro* values with the *in vivo* ones. Using the relation between *in vitro* and *in vivo* permeability it could be possible build a device with a higher exchange area than the Franz cell and, as a consequence, with an higher throughput capacity.

Mass exchanger

In fact, defining J_{RI} the flux across the real intestine walls, in the real intestine the mass balance equations become:

$$J_{RI} \cdot A_{RI} = A_{RI} \cdot P_{invivo} \cdot (c_D - c_A) \qquad (4.5)$$

In which A_{RI} and $P_{in\text{-}vivo}$ are the exchange area and the permeability in the real intestine, respectively. So, to obtain the same mass evolution in the real intestine and in the *in vitro* system, the following equation must be respected:

$$A_{RI} \cdot P_{invivo} = A_s \cdot P_{invitro} \tag{4.6}$$

In which A_S and $P_{in\text{-}vitro}$ are the exchange area and the permeability in the *in vitro* device, respectively.

A mass exchanger was designed to realize the exchange between two fluids, one simulating the intestinal content and the other simulating the circulatory system around the gastrointestinal tract content with the aim to realize a mass exchanger with a continuous flow (despite the Franz cell which was a batch device). The two sides of the exchanger were intended to be separated by the synthetic membrane used in the permeability studies. After the design of this apparatus, fluid-dynamic considerations were made to choose the flow parameters which made possible the comparison with the real physiology. This analysis was developed using a commercial software based on the Finite Elements Method (Comsol Multiphysics®).

Hollow fibers device

Because of the reasons shown in the paragraph 7.2, the mass exchanger designed was not useful to simulate the intestinal absorption. Focused only on the transport across the intestinal wall, a device consisting of an hollow fibre filter was used as mass exchanger. The proposed device is provided by a recirculating system, as described in Figure 65.

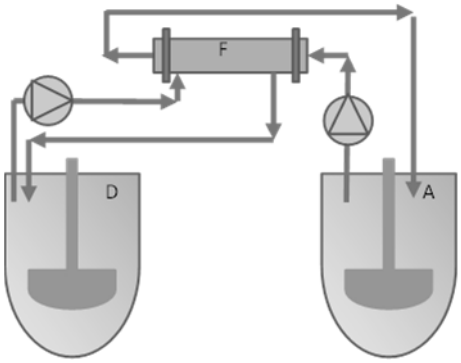

Figure 65. Schematic of the exchange system: A=Acceptor compartment, D=Donor compartment, F=Filter.

To simulate the whole gastrointestinal tract, the filter was connected with a traditional USP apparatus II. In this way, during the first two hours of the experiment, in which the pharmaceutical form orally assumed is retained in the stomach in the real physiology, the dissolution takes place in the conventional USP apparatus II vessels (thermostated and stirred vessels) without mass exchange. After the two hours, the transit from the stomach to the small intestine is simulated switching on the mass exchange. Two fluids flow in the filter, the first one (donor), simulating the intestinal content, is rich in drug and, passing across the fibres gives the drug to the second fluid (acceptor), simulating the circulatory system near the gastrointestinal tract. In the vessel containing the first fluid the drug formulation is dissolving following its release kinetic. On the other side, the second fluid is poor in drug content (initially the drug concentration is zero) and takes the drug from the first fluid. Using this system, simultaneously the release patterns obtained both with the conventional dissolution method and the novel dissolution method were analysed and compared.

5.2.4 Analytical methods

The spectra collected during the dissolution tests were used to quantify the amount of released active molecules. Since very low concentrations are expected during the release test, especially at the first stage, the common approach, based on the simple evaluation of absorbance at a fixed wavelength, was considered here not accurate enough [69]. Indeed the presence of a unknown quantity of dissolving polymer causes a shift of the spectrum, in the region of interest, which cannot to be predicted. The use of a reference solution containing all the components but the absorbing one (the drug) is not possible, since the dissolving tablets release unknown amount of the polymer together with unknown amount of the drug. In a previous work [70], a method based on the fitting of all the spectrum by a sum of Gaussian curves has been proposed, to separate the influence on the absorption spectra of the theophylline and of another polymer (Cellulose Acetate Phthalate). To clarify the method described above, an example of the spectra of theophylline could be reported. In the range between 240 and 300 nm, and an exponential decay function was used as the baseline (the dashed curve in Figure 66) for the theophylline peak; the results of spectra subtraction (raw data minus the baseline) was fitted by a single Gaussian curve (the dotted curve in Figure 66). The

parameter to be related to the drug concentration was thus the height of the fitted Gaussian curve.

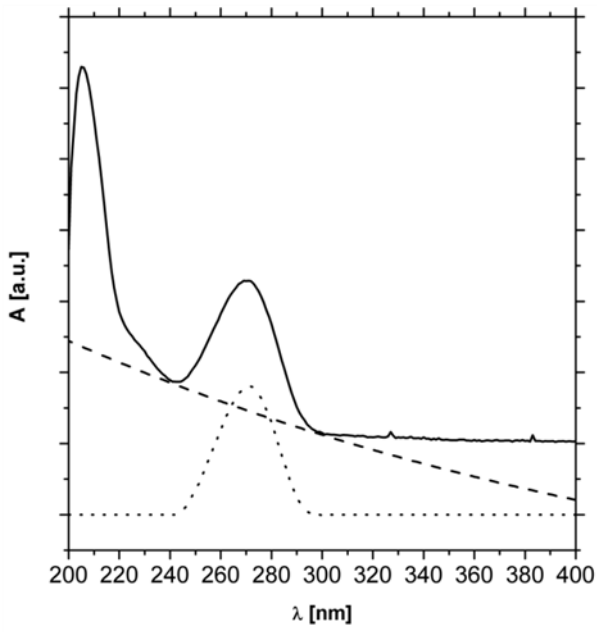

Figure 66. Example of spectra collected and subtracted.

To overcome the drawbacks related to the spectrometer technique, the release patterns were analyzed by a different analytical method: an HPLC (High Performance Liquid Chromatography) was used. By the use of this technique, measurement more reliable and accurate could be obtained, moreover, the measurement are more automated than the other technique. In spite of that, the HPLC method is destructive for the sample analyzed and requires periodic withdrawn from the dissolution medium.

Every drug analyzed requires its own HPLC method, they are summarized in the following tables, and, in both the cases the column used was a Macherey-Nagel HPLC column EC 150 mm/4.6 mm NUCLEODUR 100-5 C18 ec.

Table 10. HPLC method to detect theophylline.

Drug	Theophylline	
Injection volume	5 µL	
Eluent	Time [min]	Acetonitrile – Acetic acid 0.2% wt
	0	3% - 97%
	6	4% - 96%
	12	6% - 94%
Flow rate	2 mL/min	
Temperature	25°C	
Wavelength	275 nm	
Elution time	10 min	

Once defined the method necessary to obtain reliable and clear peaks, a tuning was approach to identify the proportion between the concentration of the molecule of interest and the area of the HPLC peak. Different solutions of theophylline at known concentration were made and they were analyzed. A typical chromatogram was shown:

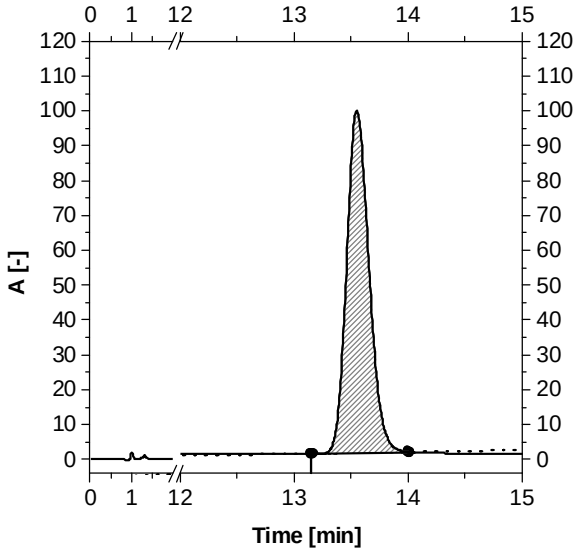

Figure 67. Typical chromatogram of a theophylline solution in pH 6.8 phosphate buffer. The dotted curve is the baseline of the peak.

Once obtained the chromatogram for each concentration value, the integration limits were identified (●) and the area between the signal and the baseline was calculated by integration. All the solutions were analyzed with this method and the results are shown in Figure 68.

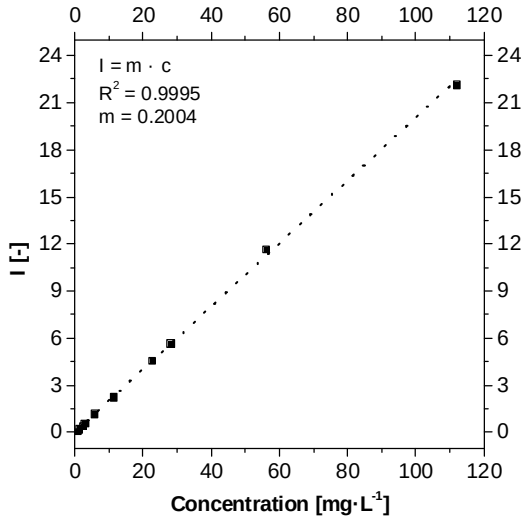

Figure 68. Relation between the concentration and the integral values for a theophylline solution in pH 6.8 phosphate buffer.

The relation between the concentration of the solution and the area under the signal was found to be linear and the slope of the straight line represents the proportionality factor. Once determined this relation, to determine the concentration of theophylline of a solution, it could be enough to evaluate the ratio between the value of the integral and the proportionality factor.

Concerning the analysis of the diclofenac:

Table 11. HPLC method to detect diclofenac.

Drug	Diclofenac
Injection volume	5 µL
Eluent	Acetonitrile 48% Acetic acid in water (0.2% wt/wt) 52%
Flow rate	2 mL/min
Temperature	30°C
Wavelength	280 nm
Elution time	6 min

Once again the chromatograms obtained for various solutions at different concentrations were collected and the area under the signals was evaluated according to the method previously described. The relation between the concentration of diclofenac in a solution and the area under the HPLC signal is reported in Figure 69.

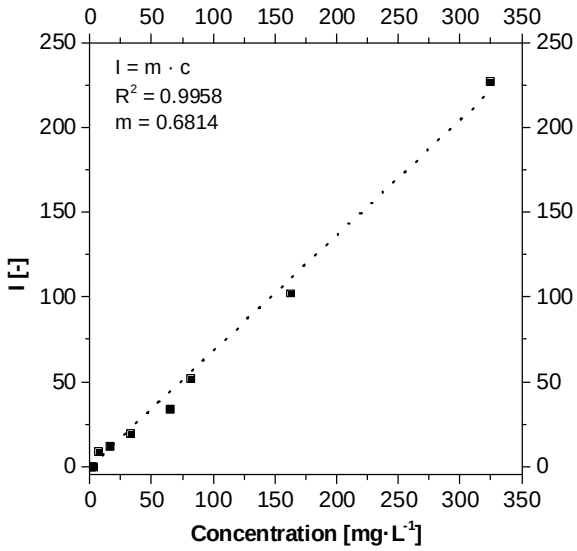

Figure 69. Relation between the concentration and the integral values for a diclofenac solution in pH 6.8 phosphate buffer.

As in the previous case, the concentration of a solution of diclofenac could be evaluated using the proportionality factor.

Obviously, the relation between the concentration of a molecule in a solution and the area under the signal curve is affected by a lot of variables. The medium in which the molecule is dissolved is particularly relevant but, of course, also the method of analysis and the HPLC column. For this reason the tunings for the various molecules have been repeated several times during the work and the value of the proportionality factor could be slightly variable.

Chapter Six

In vitro models: chemical history

In this chapter a novel apparatus which simulates the thermal and chemical (pH) history of the gastrointestinal tract is described. The release pattern of several pharmaceutical forms are evaluated with this device and compared with that obtained with conventional methods.

6.1 pH and temperature control

The main features which have to be controlled to simulate the human gastrointestinal tract are the chemical and the thermal history. With this purpose, a new device which is able to measure and to control simultaneously the pH and the temperature was designed and built [71]. Focused on the realization of a system able to reproduce a given pH evolution (as in the gastrointestinal tract), an USP apparatus II for the dissolution was used. The use of the conventional device is useful to control easily the temperature, because the vessels of the apparatus are thermostated and controlled. Then, the problem of the reading and the control of the pH in the medium was faced. The probe used to measure the pH in the vessel was a glass probe for general purposes (purchased by Crison, code number 50 14). To read the probe output signal (+/- 15 mV) a pre-amplifier has been used to amplify the voltage which has to be the input of the Data AcQuisition system. The pre-amplifier was powered by lithium batteries with an estimated life of 5 years when used with high input impedance instruments (purchased by Omega, code number PHAMP-1). The electronics are entirely encapsulated in an epoxy filled stainless steel enclosure. The input and output connections are industry standard BNC. The signal passing through the amplifier arrives at the DAQ (purchased by National Instruments USB-6008). This multifunction data acquisition is connected (via USB) to a computer. To acquire and control the pH in the medium, a program has been developed using the labVIEW environment, developed by the National Instruments. LabVIEW is a graphical programming environment to develop measure, tests, and control system using graphical icons. The input of the program are the values of pH read by the probe inserted in the dissolution medium. After a proper calibration, the signals coming from the probe are converted into electrical signals by the use of a data acquisition and are read by the program for a given time range. Then, the mean value are reported by the software. The real pH evolution taken by literature [67] was imposed as set point of the software. The set point of the software was shown in Figure 70. In fact, the pH immediately after the meal have a value of about 4.8 and starts to decrease after the food ingestion. The acidic secretions of the stomach decrease the pH values gradually. After two hours, which is the average residence time in the stomach, the bolus enters in the small intestine, this change in environment is reflected in the pH range raise up to a value of 6.8.

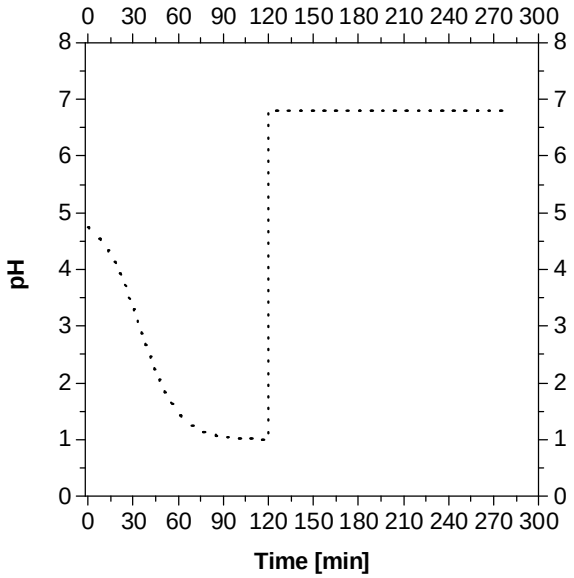

Figure 70. pH history in the gastrointestinal tract. During the first two hours the pH decreases from a value of 4.8 to 1.0, then the environment was neutralized.

Once the set point is arranged, the pH of the dissolution medium is changed by adding a basic or acid solution. To add the solutions, two pumps (one for the acidic and the other for the basic solution) were purchased by RS Components (gear motor RS code 255-9649; peristaltic pump head RS code 330-812). These pumps were activated by the program on the basis of the difference between the pH main values read by the probe and the set point value. If the pH in the dissolution medium is less than the set point value, the pump containing the basic solution is activated to increase the pH. On the other hand, if the pH value in the dissolution medium is higher than the set point value, the pump containing the acidic solution is activated to reduce the pH. In this way, the set point pH curve could be reproduced. A typical result is shown in Figure 71.

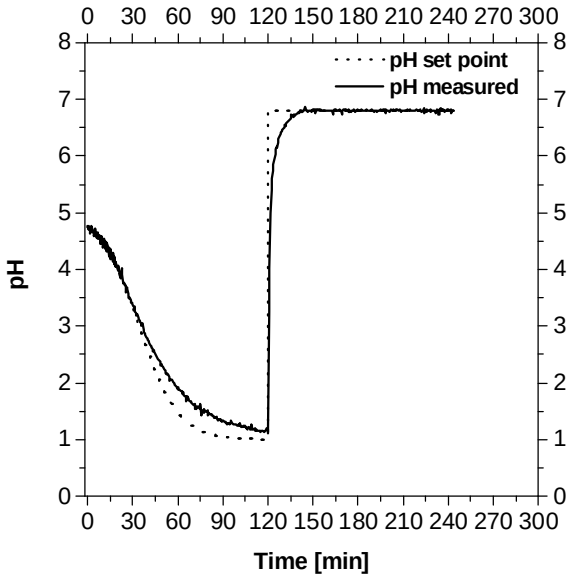

Figure 71. pH set point evolution in the gastrointestinal tract and pH reproduced with the new device.

Despite the experiments were carried on in the USP device, the program was intended also for controlling the temperature. The logic of the program is very similar for both the pH and the temperature control. In the case in which the release is not evaluated in the USP apparatus but in a separated device, also the temperature has to be controlled. In this case, the device simulating the stomach or the intestine is placed in a closed chamber together with a fan. A thermocouple (purchased by Omega, code TT-T-40-SLE-25) is placed in a chamber and the temperature is measured. The signal is read by the DAQ and compared with the set point value (which is constant at the value of 37°C, the physiological temperature). If the measured temperature is lower than the set point, a controlled fan heater is switched on and the temperature increases in the chamber, if the measured value is higher than the set point, the heater is maintained switched off and the temperature decreases because of the heat loss.

6.2 Results and discussions

6.2.1 Conventional release patterns

In order to test the influence of the pH profile in the gastrointestinal tract on the release pattern, dissolution tests were carried out firstly on a homemade tablet composed of a mixture of HPMC and theophylline (75/25% wt/wt). This system was chosen because its simplicity, in fact it was composed only by the polymer (which ensures the delayed release) and the drug, without the adding of additives or excipients. As described previously, the conventional dissolution tests provide a two-steps dissolution method, in which in the first stage the medium is kept at pH 1 and in the second stage the medium is kept at pH 6.8. The obtained release pattern is shown in Figure 72.

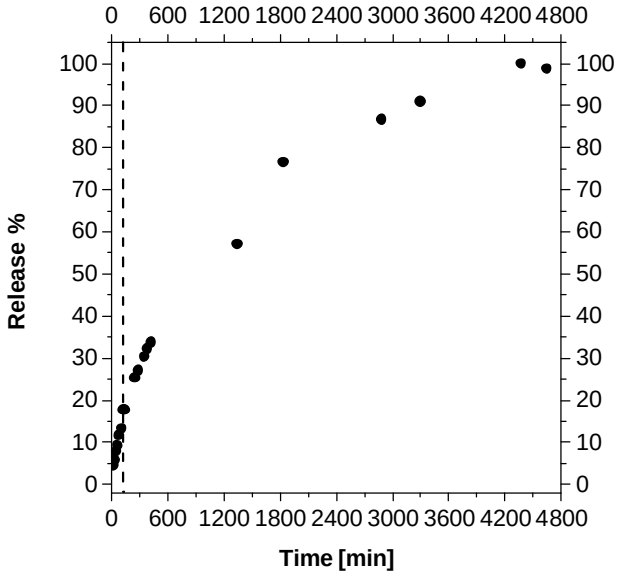

Figure 72. Release pattern of HPMC/theophylline tablet obtained following the conventional method. The dashed vertical line represents the time of neutralization (120 min).

As could be seen, this system ensured a delayed release of the drug and it was complete only after three days of dissolution. Once the dissolution method was defined, a more complex system containing additives was tested. This system was a commercial tablet of diclofenac intended for the extended release. The dissolution method

followed was the same described previously. The release profile is shown in Figure 73.

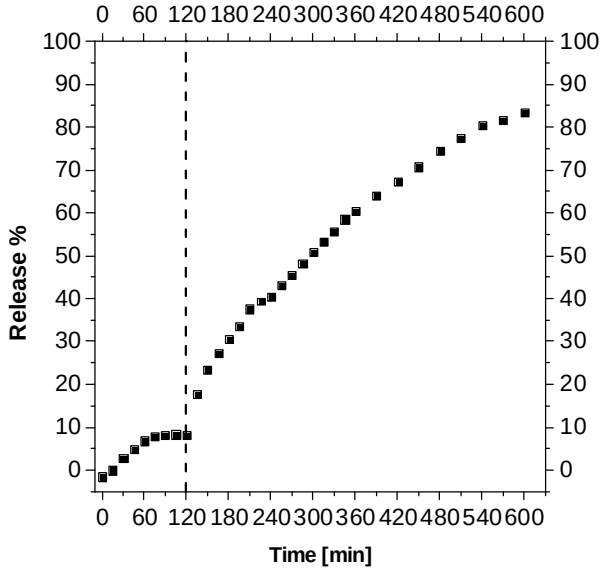

Figure 73. Release pattern of a commercial diclofenac tablet (EG). The dashed vertical line represents the time of neutralization (120 min).

As a result of the dissolution test, it could be seen that the drug amount released in the first stage of the test is low (up to 10%) then the drug in the tablet is gradually released in the following hours. If the purpose of these tablets is to vehicle the drug only in the intestinal tract and to resist to the acidic environment of the stomach, they carry out their own task with adequate accuracy. Obviously, the perfect release pattern would be that having a zero release in the first two hours and a constant release in the following hours. It could be realized with a polymer highly sensible to the changing of pH environment. A new co-polymer formulation developed in our labs [66] has been demonstrated to have high enteric features and to have the capability of changing the pH at which its dissolution occurs simply varying the relative percentage of the two co-polymers. Once characterized this polymer, tablets made of diclofenac sodium (25% w/w) and this polymer were subjected to the analysis of release pattern obtained with the conventional method. The results are shown in Figure 74.

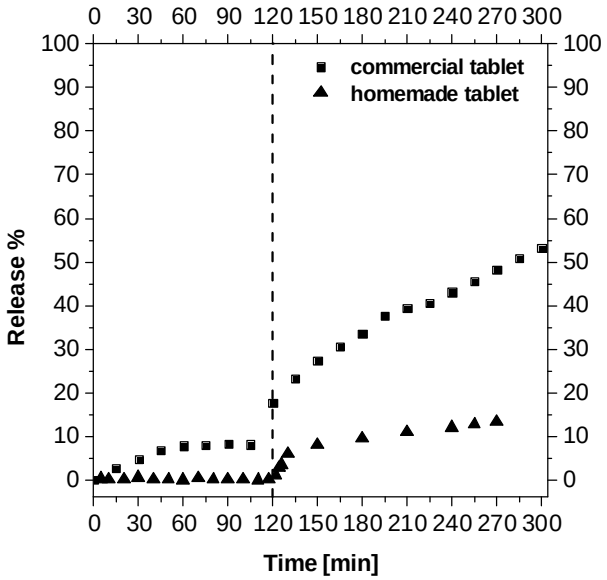

Figure 74. Comparison between the release patterns of diclofenac in a matrix of an enteric co-polymer synthetized in our labs (triangles) and in a commercial tablet (squares). The dashed vertical line represents the time of neutralization (120 min).

As could be seen, the two release patterns are very different. In the first stage the amount of drug released from the tablet made with the new polymer is completely negligible, than there is a rapid increase (into few minutes after the neutralization of the pH) in the drug dissolved in the system. This is due to the fact that the polymer starts to dissolve and then the drug is quickly release in the dissolution medium. After this stage, the system continues to release the drug with an almost constant kinetic. Conversely, the commercial tablet shows an amount of drug released higher in the first stage and a faster release kinetic. This means that the tablets made of the new polymer are not only suitable for the enteric release but even shows better features than the characteristics of existing tablets.

6.2.2 Novel release patterns

Once the release pattern of the simple homemade tablet of HPMC/ theophylline was analyzed following the conventional USP dissolution method has been analyzed, the release from the same tablet submitted to a pH history has been evaluated.

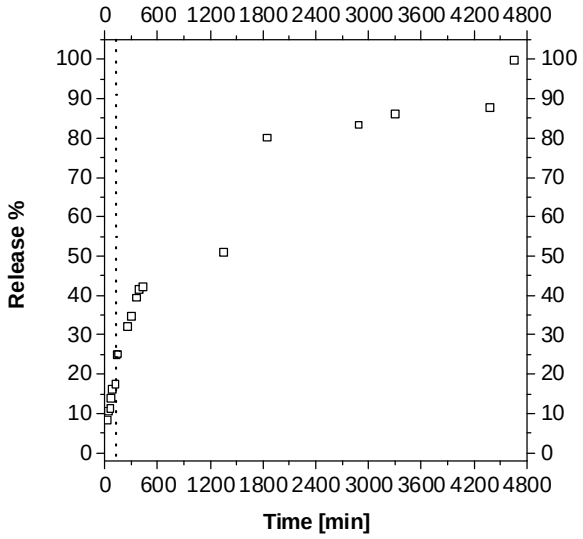

Figure 75. Release pattern of a HPMC/theophylline tablet following the real pH history. The dashed vertical line represents the time of neutralization (120 min).

Using the real pH history the release is expected to be higher than the release obtained with the conventional dissolution pattern because the higher pH in the initial stage of the dissolution damages the surface of the tablet. Comparing the two dissolution patterns:

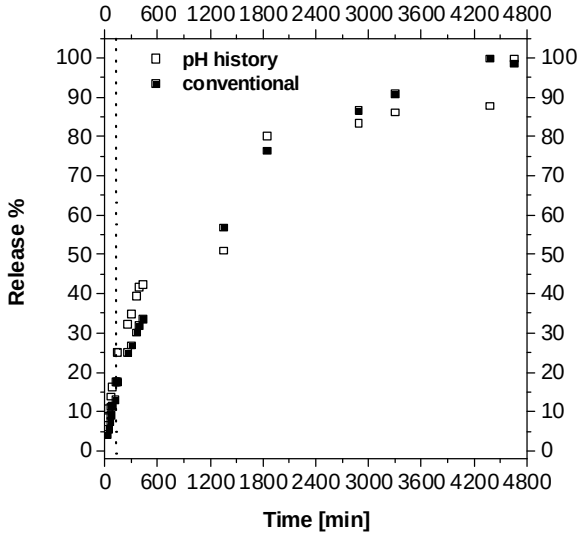

Figure 76. Release patterns of HPMC/theophylline tablets using conventional (■) and new (□) dissolution method.

In fact, the release is slightly higher, particularly in the first stage, in the case in which the real pH evolution is followed than the case in which the conventional method is followed. This behavior is could be easily seen by the following figure (a zoom of the Figure 76):

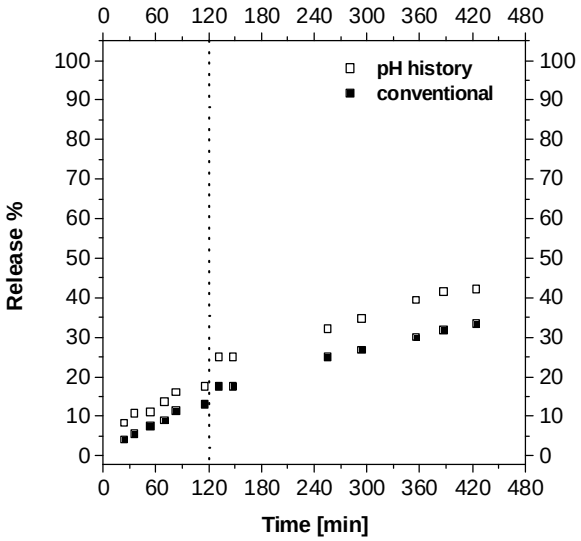

Figure 77. Release patterns of HPMC/theophylline tablets using conventional (■) and new (□) dissolution methods, first stage of dissolution. The dashed vertical line represents the time of neutralization (120 min).

The expected behavior of the release patterns was confirmed by the results.

As described before, also the release pattern of the commercial tablet of diclofenac (delayed release) obtained with the pH history was evaluated and compared with the conventional one.

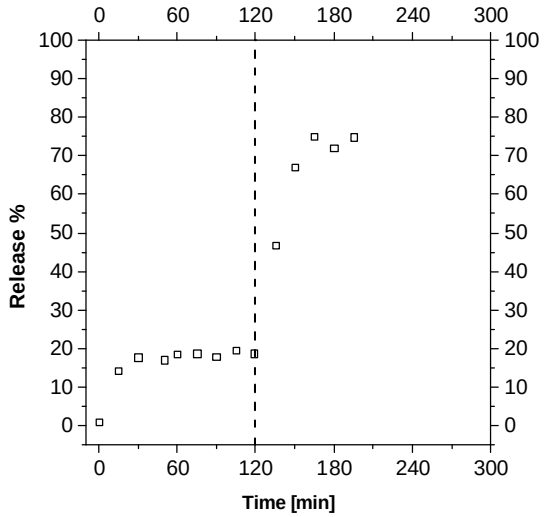

Figure 78. Release pattern of a commercial diclofenac tablet (EG) submitted to a pH history.

In the first stage of dissolution, the drug released is about 20% of the total amount. This is a side effect which is undesired because the drug is not active in the stomach, especially for drugs targeted to release in the intestinal environment. Comparing the two patterns:

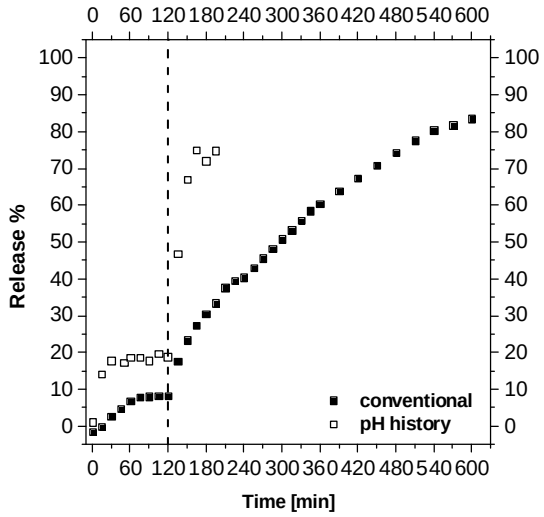

Figure 79. Release pattern of a commercial diclofenac tablet (EG) according with the conventional dissolution method (USP) and with the new device.

During the first stage, the tablet subjected to the modified pH history releases an amount of drug twice than that subjected to the conventional method. During the following stage it could be seen that all the drug is released within few hours (6 hours from the beginning of the test) if the tablet is exposed to a pH evolution, instead, the release is more gradual and slower if the tablet follows the conventional dissolution pattern. This can be due to the fact that the higher pH at the beginning of the test in the new apparatus (about 4.8) probably breaks up the surface coating of the tablet and, in the following stage, it releases the drug easily. On the other hand, the tablet subjected to a conventional dissolution pattern arrives undamaged at the neutralization and starts to release only in the second part of the test. Its release is prolonged and continues for more than 10 hours. This comparison shows that a tablet simply subjected to the conventional dissolution method, in the real gastrointestinal environment has a completely different behavior which could be understood only using a device that better simulates the real features of the gastrointestinal tract. This behavior suggests that, to resist to the acidic gastric environment, could be useful to use a more resistant coating of the tablet or an enteric polymer. Thus, the behavior of the enteric polymer synthetized in our labs subjected both to a conventional dissolution method and the method which reproduce the real pH history in the gastrointestinal tract has been studied. The results are shown in Figure 80:

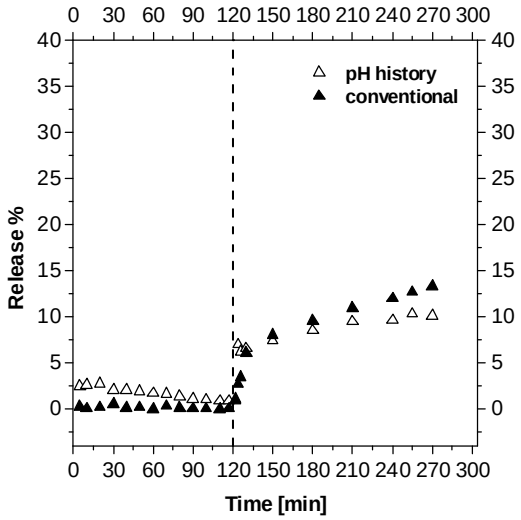

Figure 80. Comparison between the release patterns of diclofenac in a matrix of an enteric co-polymer synthetized in our labs obtained with the conventional dissolution method (▲) and with the pH history (Δ).

As could be seen, the polymer has a typical enteric behavior not only in the condition of conventional dissolution method, but even in the case in which the real pH history was reproduced. In fact, the amount of drug released in the first stage of dissolution is very close between the two cases. This fact means that even if the pH is higher in the first stage of dissolution, the polymer is not affected by the difference and remains intact and undissolved. On the contrary, when the pH is rapidly increased to an almost neutral value, the polymer starts to dissolve with the same dissolution rate for both the cases and the drug is released obtaining the same pattern. Thus, using this polymer is possible to avoid the undesired dissolution of the tablet in the gastric environment and to realize a better target delivery.

Then, the effect of the pH evolution was investigated on a different system: an enteric coated, fast release commercial tablet of diclofenac. The comparison between the two release patterns obtained with the conventional dissolution method and the modified pH history are shown in Figure 81.

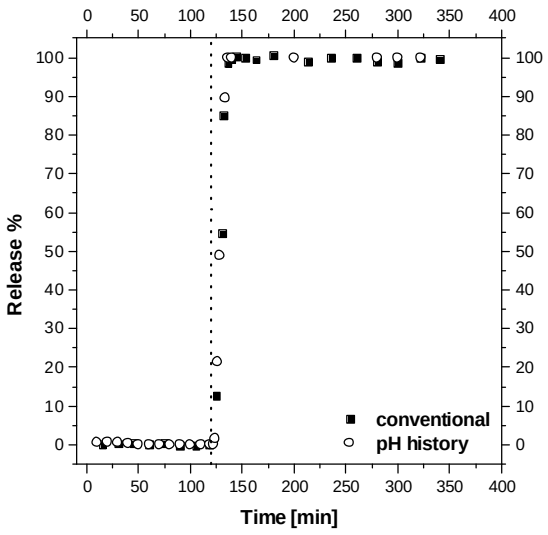

Figure 81. Release pattern of an enteric coated, fast release commercial tablet of diclofenac following the conventional USP method (black squares) or the modified release patter (empty circles). The vertical line represent the time at which the medium is neutralized.

In this case, the two release patterns are very similar. It could be noticed that in the first stage of the dissolution, the drug released is negligible, few minutes after the neutralization all the drug in the tablet is released. In fact, this pharmaceutical form is not affected by the changing in pH history and it is particularly suitable for the release targeted in the small intestine.

Chapter Seven

In vitro models: mass transport

In this chapter the reproduction of the mass transport across the intestinal walls is faced. An in vitro device able to reproduce the mass exchange is designed and realized and the release patterns of several pharmaceutical forms are studied and compared with the conventional ones.

7.1 Permeability studies

As described previously, the absorption of orally administrated drugs is largely determined by their ability to cross the gastrointestinal walls, quantified by the drug permeability. The first step to quantify the ability of an active molecule to pass across the intestinal walls is to develop a simple method to evaluate the permeability. For this reason, the method developed provides the use of a Franz cell equipped with a synthetic membrane, as described in the chapter five. Once obtained the permeability values for a set of active molecules, it could be possible to correlate the *in vitro* results with the *in vivo* permeability.

The two compartments of the Franz cell were filled one with a solution at known concentration of drug (donor compartment) and the other with a solvent drug free (acceptor compartment). The compartments were separated by a membrane. After a predetermined time, the system was opened and the concentrations of drug in both the compartments were evaluated. For each molecule the tests were run for different times, to obtain the concentration profiles, as shown in Figure 82.

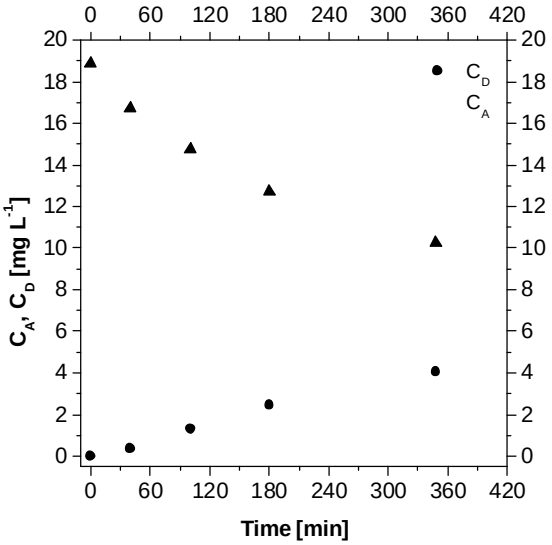

Figure 82. Thophylline concentrations profile in the donor (c_D) and in the acceptor (c_A) compartments.

As could be expected, the concentration in the donor compartment decreases starting from its the initial values (c_{D0}). On the contrary, the concentration in the acceptor compartment increases starting from

zero. The values of the concentrations versus time are reported in the following table.

Table 12. Theophylline concentrations versus time.

Time [min]	c_A [mg·L^{-1}]	c_D [mg·L^{-1}]
0	0	18.88
40	0.35	16.73
180	2.43	12.72
101	1.31	14.73
348	4.05	10.24

Once obtained experimentally the concentrations values, the permeability value is evaluated solving the mass balances within the compartments. Since the concentration in each compartment depends on the other one, the two mass balances (one for each compartment, equation 7.1) have to be solved simultaneously. Obviously, each differential equation can be solved only coupled with its initial condition.

$$\begin{cases} \dfrac{d(c_D \cdot V_D)}{dt} = -J \cdot A_s & @\ t = 0, c_A = c_{A0} \\ \dfrac{d(c_A \cdot V_A)}{dt} = J \cdot A_s & @\ t = 0, c_D = c_{D0} \end{cases} \tag{7.1}$$

c_D and c_A are the concentrations in the donor and acceptor compartment, respectively. c_{D0} and c_{A0} are the initial concentrations in the donor and acceptor compartment, respectively (initially the acceptor compartment was drug free in all the runs). $V_D = 3 \cdot 10^{-6}$ m^3 and $V_A = 7 \cdot 10^{-6}$ m^3 are the volumes of the donor and the acceptor compartment. $A_s = 7.85 \cdot 10^{-5}$ cm^2 is the exchange area between the compartments. J is the flux across the membrane and it could be expressed as a permeability (P) function:

$$J = P \cdot (c_D - c_A) \tag{7.2}$$

Defining δ as the difference between the donor and the acceptor drug concentration ($\delta = c_D - c_A$), it could be obtained:

$$\ln \frac{\delta}{\delta_0} = -\frac{P}{\gamma} \cdot t \tag{7.3}$$

In which γ is a geometrical parameter (m):

$$\gamma = \frac{1}{A_s} \cdot \left(\frac{1}{V_D} + \frac{1}{V_A} \right)^{-1} \tag{7.4}$$

The obtained values of ln (δ/δ_0) are plotted in a semi-log scale in which the slope represents the opposite of ratio between the value of P and γ.

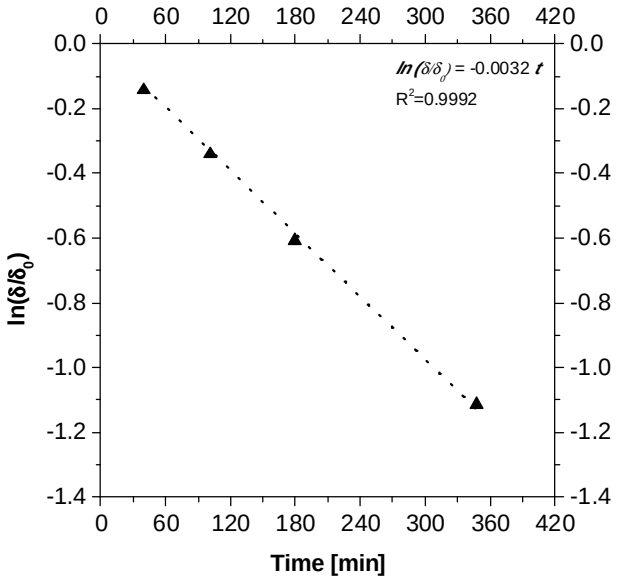

Figure 83. Logarithm of the concentration differences versus time for theophylline. The dotted line represent the linear fitting of the experimental data.

The slope was found to be -0.0032, which means a permeability value of $14.1 \cdot 10^{-7}$ m/s. Once obtained the permeability value it could be possible to solve the mass balance to predict the concentration values at every time. The continuous profiles of concentration could be easily obtained:

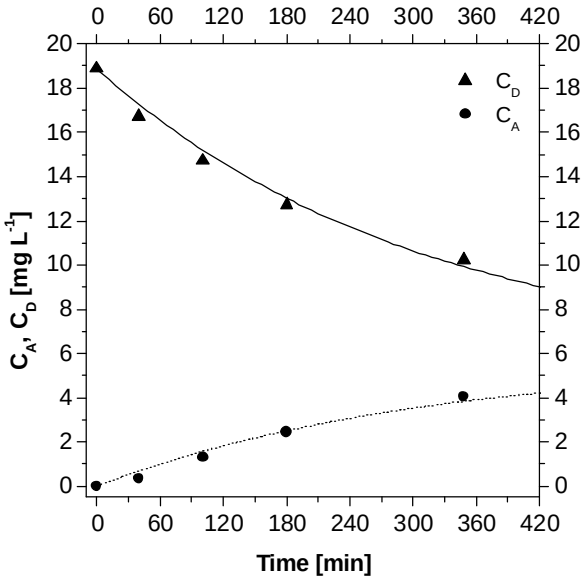

Figure 84. Predicted concentration profiles compared with the experimental value.

As could be seen, the agreement between the experimental data and the model curve is remarkable.

The same experimental protocol was applied for all the molecules analyzed.

Concerning the diclofenac, the concentrations values are reported in the following table:

Table 13. Diclofenac concentrations versus time.

Time [min]	c_A [mg·L^{-1}]	c_D [mg·L^{-1}]
0	0	20.24
30	0.53	19.74
72	0.77	18.71
81	1.18	18.26
108	1.80	17.16
150	1.97	16.00

Evaluating the logarithm of the concentration differences, it could be obtained:

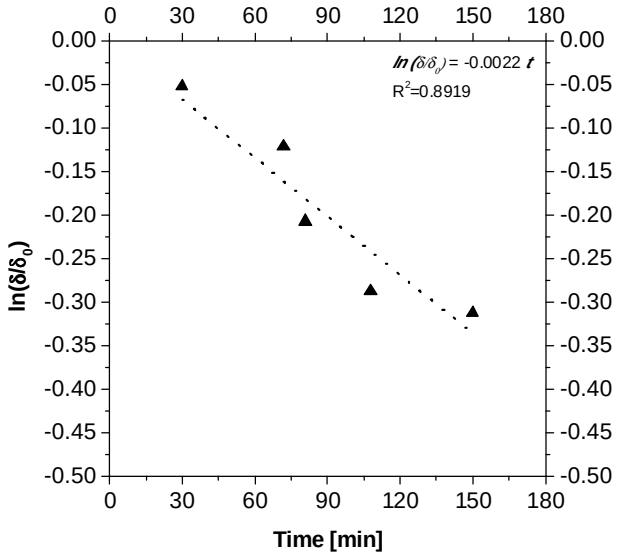

Figure 85. Logarithm of the concentration differences versus time for diclofenac. The dotted line represent the linear fitting of the experimental data.

The slope was found to be -0.0022, which means a permeability value of $9.99 \cdot 10^{-7}$ m/s. The permeability of diclofenac across the membrane is lower than the theophylline one. Thus, evaluating the model curve and comparing them with the experimental concentrations:

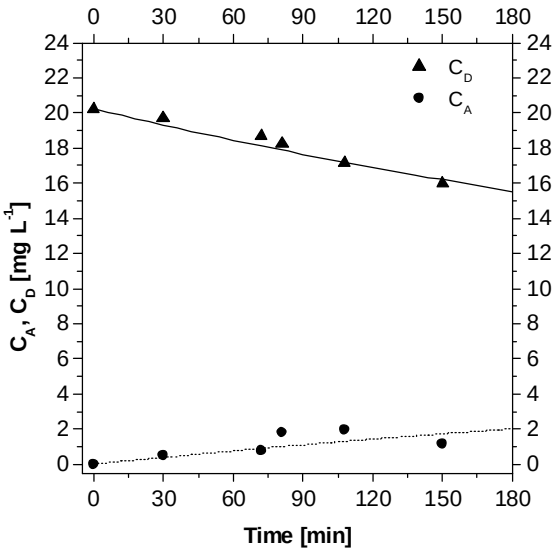

Figure 86. Diclofenac concentrations profile in the donor (c_D) and in the acceptor (c_A) compartments. The lines in figure are the model curve.

Concerning the propranolol, the concentrations values are reported in the following table:

Table 14. Propranolol concentrations versus time.

Time [min]	c_A [mg·L^{-1}]	c_D [mg·L^{-1}]
0	0	20.13
31	0.61	19.87
49	1.20	20.27
76	1.11	17.75
100	1.51	17.42
181	2.53	17.07

Evaluating the logarithm of the concentration differences, it could be obtained:

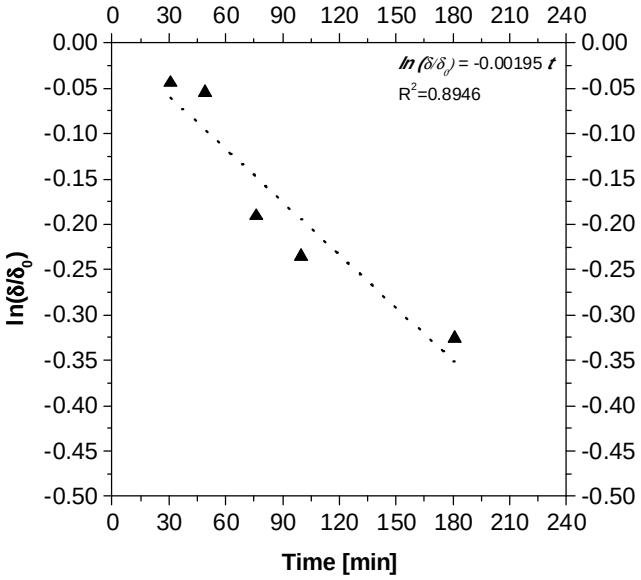

Figure 87. Logarithm of the concentration differences versus time for propranolol. The dotted line represent the linear fitting of the experimental data.

The slope was found to be -0.00195, which means a permeability value of $8.7 \cdot 10^{-7}$ m/s. Thus, evaluating the model curve and comparing them with the experimental concentrations:

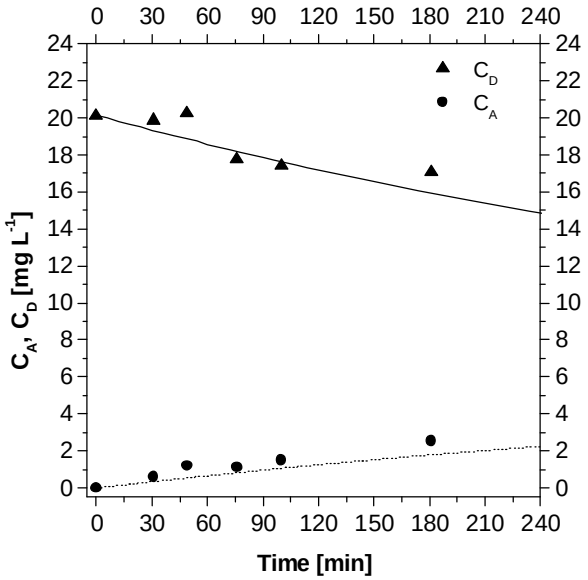

Figure 88. Propranolol concentrations profile in the donor (c_D) and in the acceptor (c_A) compartments. The lines in figure are the model curve.

Concerning the vitamin B12, the concentrations values are reported in the following table:

Table 15. Vitamin B12 concentrations versus time.

Time [min]	c_A [mg·L^{-1}]	c_D [mg·L^{-1}]
0	0	49.79
51	0.71	47.51
67	1.46	45.86
120	1.32	42.19
225	3.50	38.78

Evaluating the logarithm of the concentration differences, it could be obtained:

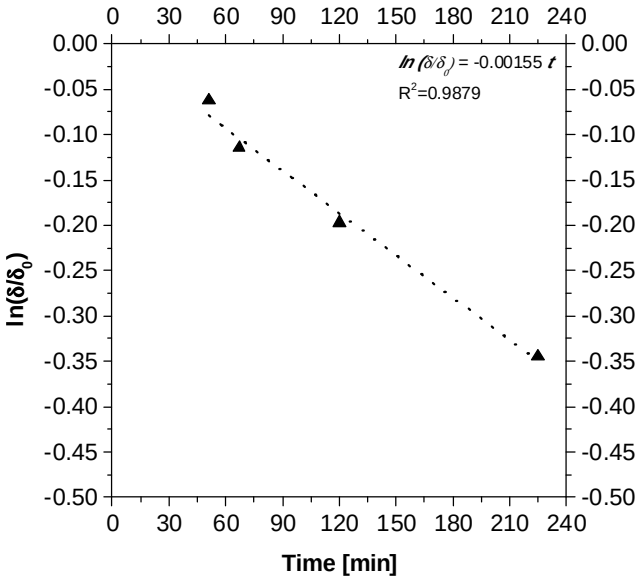

Figure 89. Logarithm of the concentration differences versus time for vitamin B12. The dotted line represent the linear fitting of the experimental data.

The slope was found to be -0.001554, which means a permeability value of $6.9 \cdot 10^{-7}$ m/s. Thus, evaluating the model curve and comparing them with the experimental concentrations:

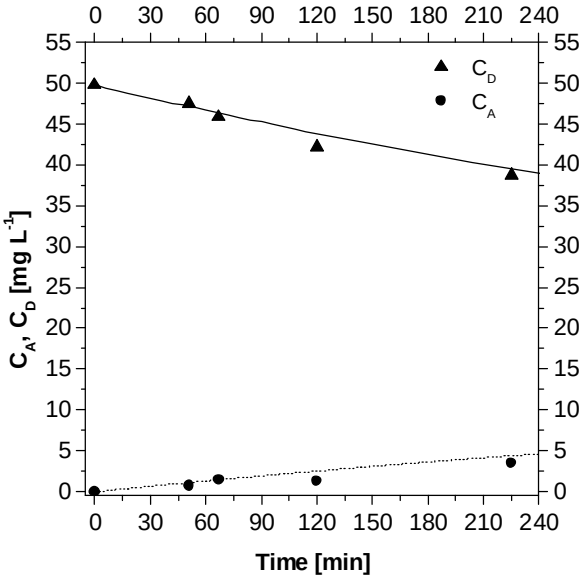

Figure 90. Vitamin B12 concentrations profile in the donor (c_D) and in the acceptor (c_A) compartments. The lines in figure are the model curve.

Finally, the concentration profiles of BSA were evaluated:

Table 16. BSA concentrations versus time.

Time [min]	c_A [mg·L^{-1}]	c_D [mg·L^{-1}]
0	0	950.58
25	7.78	935.82
43	27.42	939.56
75	56.61	941.16
180	47.04	846.78

Evaluating the logarithm of the concentration differences, it could be obtained:

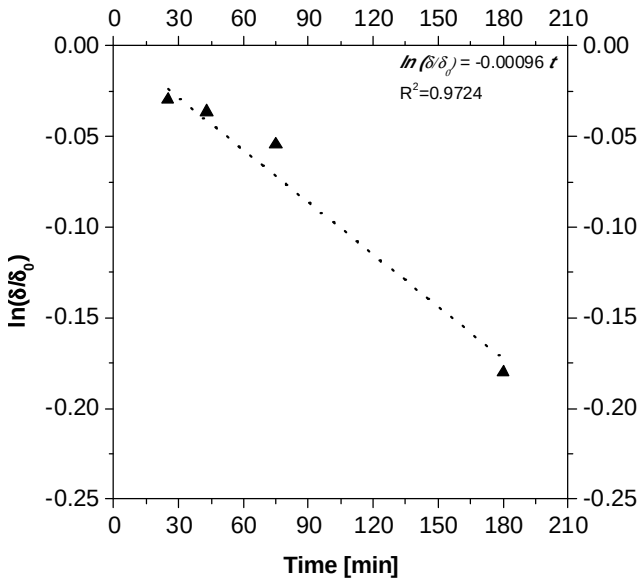

Figure 91. Logarithm of the concentration differences versus time for BSA. The dotted line represent the linear fitting of the experimental data.

The slope was found to be -0.00096, which means a permeability value of $4.3 \cdot 10^{-7}$ m/s. Thus, evaluating the model curve and comparing them with the experimental concentrations:

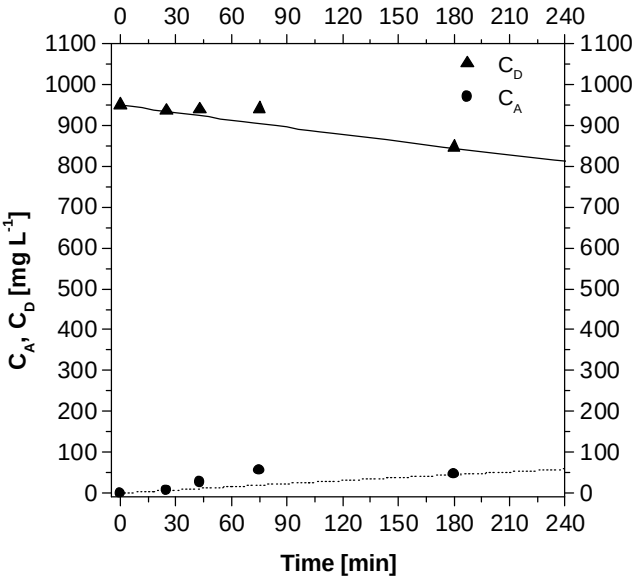

Figure 92. BSA concentrations profile in the donor (c_D) and in the acceptor (c_A) compartments. The lines in figure are the model curve.

Once the permeability values were evaluated for all the molecules analyzed, it could be possible to compare the *in vitro* permeability with the *in vivo* ones (taken by literature), the results are reported in the following table, together with the mass weight, the stokes radius, and the octanol/water partition coefficient.

Table 17. *In vitro* and *in vivo* permeability of several molecules.

	Mw [g·mol^{-1}]	r_S [nm]	pKa	Log Kow	Permeability *in vivo* [m/s]	Permeability *in vitro* [m/s]
BSA	66776	3.48 [72]	6.7 [73]	-	-	$4.3 \cdot 10^{-7}$
B12	1355.4	0.84 [74]	7.5 [75]	3.57 [76]	-	$6.9 \cdot 10^{-7}$
Propranolol	259.34	0.37 [77]	9.1 [77]	3.09 [78]	$3.01 \cdot 10^{-7}$ [79]	$8.7 \cdot 10^{-7}$
Diclofenac	296.15	0.43 [80]	4.0 [81]	1.90 [82]	$4 \cdot 10^{-7}$ [60]	$10.0 \cdot 10^{-7}$
Theophylline	180.16	0.37 [74]	8.4 [83]	-0.028 [84]	$5.2 \cdot 10^{-7}$ [85]	$14.1 \cdot 10^{-7}$

As could be expected, the permeability of a molecule across a synthetic membrane depends on the size of the molecule, but it is not

the only factor which influences the permeability value. In fact, it is important also to evaluate the octanol/water coefficient to determine the affinity of the molecule to aqueous solution (used in these experiments). Moreover, it could be noticed that in the table the *in vivo* permeability for B12 and BSA lacks. This is due to the fact that in the intestinal wall these molecules are transported actively, thus, the passage is not only due to a diffusion across the membrane as the other molecules. This means that an immediate comparison with the real value is not possible, however, the study of this compound has been very useful to understand the effect of the molecular size on the transport. Indeed, if the permeability *in vivo* and the stokes radius are related with the *in vitro* permeability, it could be obtained:

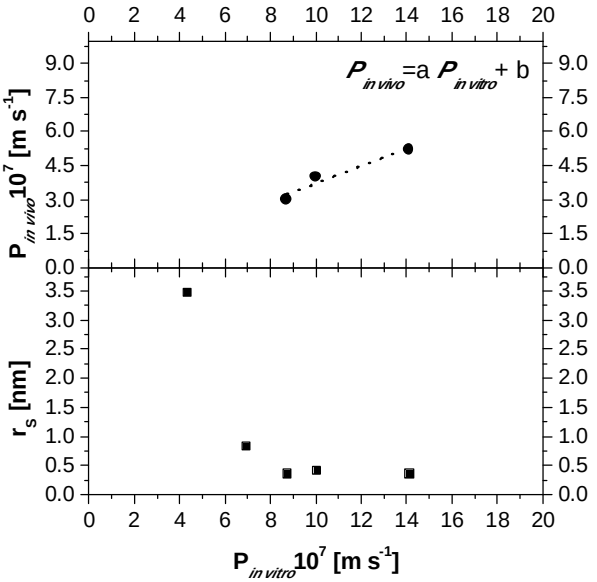

Figure 93. Comparison between *in vivo* and measured permeability (the upper graph) and dependence of *in vitro* permeability from the stokes radius of the molecules. a = -0.067; b = 0.378; R2 = 0.891.

In the Figure 93 (the upper graph) the *in vivo* and *in vitro* values of permeability are compared. It could be seen that the relation between the values is almost linear. Because of the porosity of the artificial membrane is far from that of the intestinal wall, some molecules which are allowed to pass through the intestinal wall are retained on the membrane, this is the reason why the intercept of this relation is not zero. Moreover, in the Figure 93 (the lower graph) it could be

possible to see the dependence of the permeability on the radius of the molecule. Effectively, the permeability increases with the decrease of the radius but this trend is negligible when the size of the molecule is lower, probably because the other factors (as the octanol/water partition coefficient) become more relevant.

7.2 Design of an exchange system

Therefore, by the simple method developed, it could be possible to evaluate the *in vitro* permeability of some drugs and to correlate these values to the *in vivo* ones. In fact, defining J_{RI} the flux across the real intestine walls, in the real intestine the mass balance equations become:

$$A_{RI} \cdot J_{RI} = A_{RI} \cdot P_{in\ vivo} \cdot \delta \tag{7.5}$$

In which A_{RI} and $P_{in\ vivo}$ are the exchange area and the permeability in the real intestine, respectively. So, to obtain the same mass evolution in the real intestine and in the *in vitro* system, the following equation must be respected:

$$A_{RI} \cdot P_{in\ vivo} = A_s \cdot P_{in\ vitro} \tag{7.6}$$

Using the relation between *in vitro* and *in vivo* permeability found in this work, it could be noticed that to simulate the *in vivo* permeability, a device with the following exchange area should be built:

$$A_s = A_{RI} \cdot \frac{P_{in\ vivo}}{P_{in\ vitro}} = A_{RI} \cdot \frac{a \cdot P_{in\ vitro} + b}{P_{in\ vitro}} \tag{7.7}$$

As a result, it could be possible build a device with a higher exchange area than the conventional devices and, as a consequence, with an higher throughput capacity.

With this aim a mass exchanger was designed with the goal to use the artificial membrane which was characterized in the Franz cell.

The mass exchanger is symmetric and composed from two parts. Between the two parts the artificial membrane is inserted. The membrane is supported by two guide.

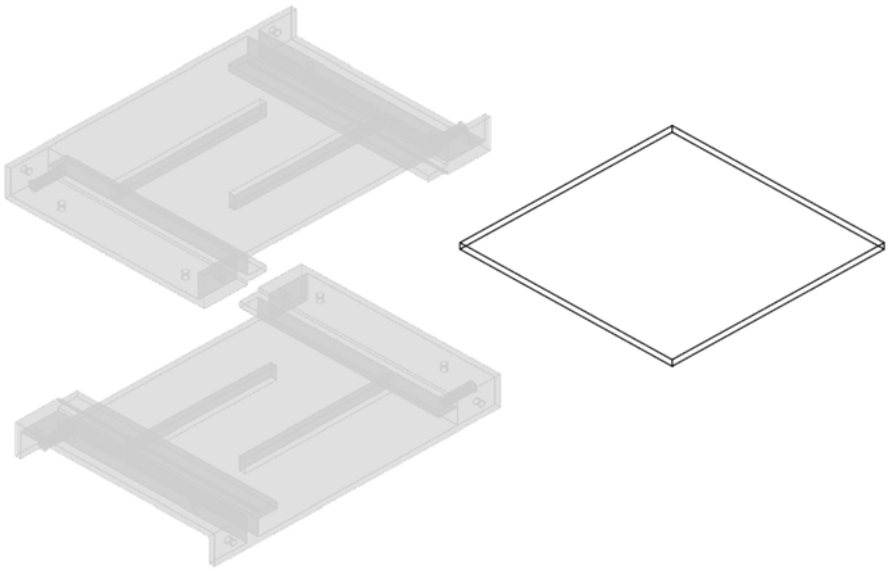

Figure 94. The two parts of the mass exchanger in which the artificial membrane is inserted.

Two different fluids flow in the exchanger, one simulating the intestinal content and the other simulating the blood in contact with the intestinal walls. Therefore, the second fluid is used to simulate the gastrointestinal circulatory system (GICS). Simplifying the real human physiology, it is assumed that the whole GICS could be simplified in the blood contained into the portal vein. According with this approximation, the flow of the second fluid was the flow of the portal vein and the drug contained in the intestinal medium have to pass across the membrane to reach the portal vein. The two fluids are disposed in counter current to maximize the driving force. To rise the exchange area between the fluids and the membrane, two baffles are inserted in the exchanger: in this way, the flow pattern of the fluids changes, as shown in Figure 95.

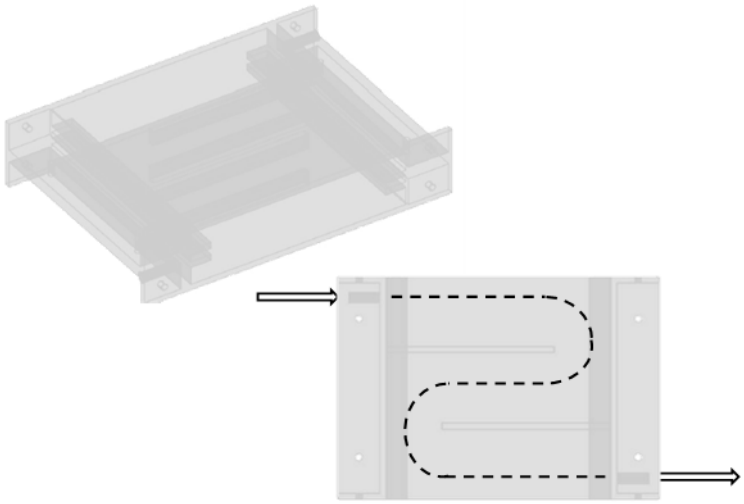

Figure 95. The assembled mass exchanger and the flow pattern.

With this arrangement, the contact area is increased without relevant increasing of the pressure drop. The exchanger is also equipped with four cylindrical entrances for the flows of the two fluid. It could be seen, moreover, that the device is equipped with perforated bases which allow the easy removal of a coverage. This settings make simpler and easier the assemblage and the cleaning of the device. The mass exchanger was completely constructed in PolyMethylMethAcrylate (PMMA), which is a transparent material and allows to see inside the device. Obviously, different membranes could be used to simulate intestinal absorption.

To simulate the fluid dynamic condition into the mass exchanger, a software (Comsol Multiphysics®) was used. This software is based on a finite elements analysis. First of all, the geometry of the mass exchanger was implemented into the software:

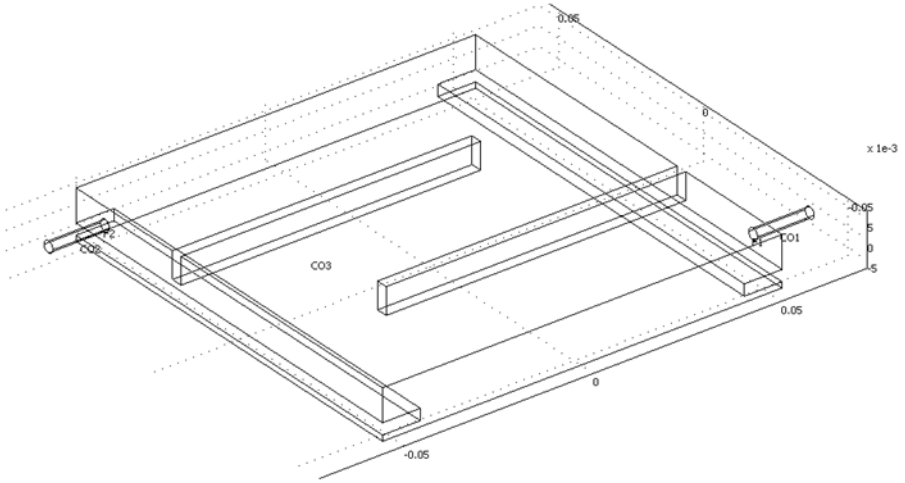

Figure 96. Geometry of the mass exchanger implemented in Comsol.

Secondly, to solve the differential equations which drive the flux into the exchanger, the geometry was divided into triangle mesh, a grid which define the shape of the 3D object.

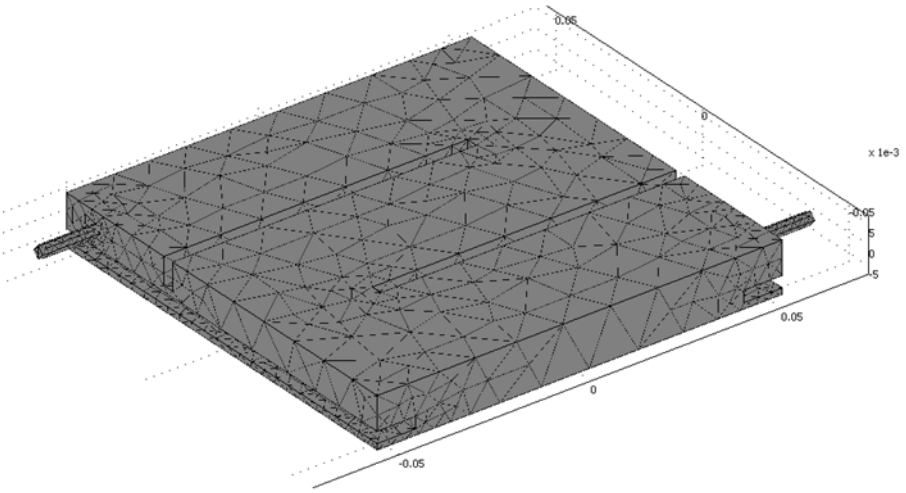

Figure 97. Mesh used for the fluid dynamic simulation.

Once imposed the laminar flow (which is realized both in the intestinal and in the portal vein flow), the physical characteristics of the fluids were implemented.

Concerning the blood side, the viscosity (μ) and density (ρ) of the fluid were considered constant. The blood viscosity depends on the hematocrit (the percentage of blood occupied by the red blood cells)

which can varies between the individuals. The relation between viscosity and hematocrit is [86]:

$$\mu = \mu_0 \cdot \left(1 + \frac{5}{2} \cdot \Phi_H + 7.35 \cdot \Phi_H^2 \right) \tag{7.8}$$

Where μ_0 is a constant value and Φ_H is the average hematocrit. The used physical characteristic are reported in Table 18:

Table 18. Physical characteristic of the blood in the portal vein.

Quantity	Value	Units
μ_0	$1.25 \cdot 10^{-3}$	Pa·s
Φ_H	0.45	-
μ	$4.5 \cdot 10^{-3}$	Pa·s
ρ	1060	$kg \cdot m^3$

The geometrical and fluid dynamic characteristics of the portal vein implemented are:

Table 19. Physical and fluid dynamic characteristics of the portal vein [87], [88].

Quantity	Value	Units	Description
D	12	mm	Diameter
L	80	mm	Length
Q	1268	$mL \cdot min^{-1}$	Volumetric flow rate
v	0.187	$m \cdot s^{-1}$	Average velocity
Re	528	-	Reynolds number

Then, the boundary conditions were defined. The condition of no slip at wall was imposed for all the surface, but the inlet, in which the velocity was imposed and the outlet, in which the condition of atmospheric pressure was imposed. The velocity field obtained into the exchanger was:

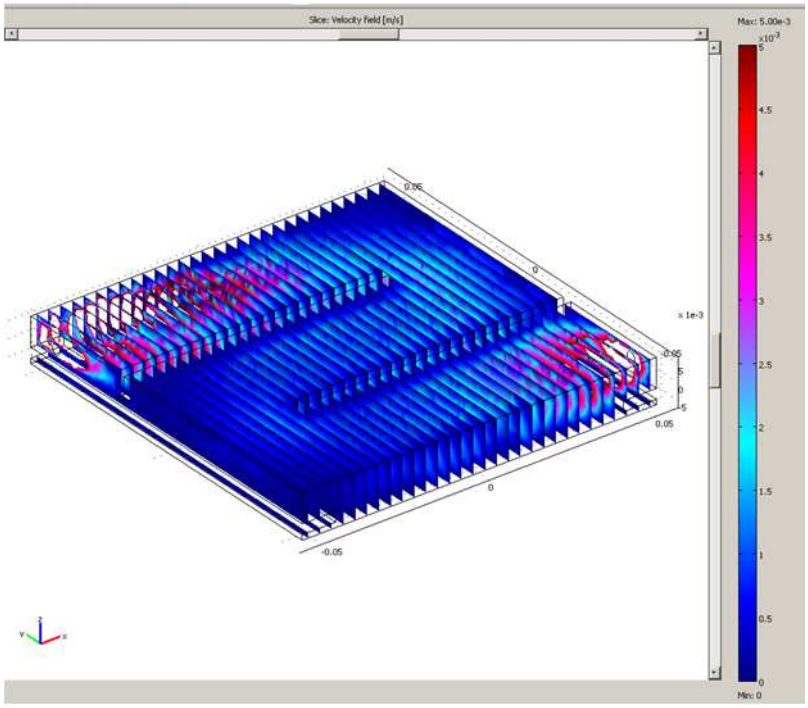

Figure 98. Velocity field into the mass exchanger (blood side).

It could be seen that the maximum velocity is realized in the inlet section of the exchanger and high values are reached in the outlet section. Therefore, the Figure 98 represents the velocity field into the exchanger if the same volumetric rate of the portal vein is realized in the *in vitro* model.

Concerning the intestinal content side, the viscosity (μ_i) and density (ρ_i) of the fluid were considered constant. Really, the viscosity of the intestinal content increases proportionally with the solid content.

Moreover, the viscosity of the intestinal content has a non-Newtonian behavior, so the viscosity decrease with the increase of the shear rate. The viscosity value reported in Table 20 and is evaluated at a shear rate of 50 s^{-1} [89].

Table 20. Physical characteristics of the intestinal content.

Quantity	Value	Units
μ_i	$1.5 \cdot 10^{-3}$	Pa·s
Shear rate	50	s^{-1}
ρ	1000	$kg \cdot m^3$

The geometrical and fluid dynamic characteristics of the small intestine implemented are:

Table 21. Physical and fluid dynamic characteristics of the small intestine.

Quantity	Value	Units	Description
D_i	5	cm	Diameter
L_i	6.25	m	Length
Q_i	60.8	$mL \cdot min^{-1}$	Volumetric flow rate
v_i	3.1	$cm \cdot min^{-1}$	Average velocity
Re_i	17.3	-	Reynolds number

Then, the boundary conditions were defined. The condition of no slip at wall was imposed for all the surface, but the inlet, in which the velocity was imposed and the outlet, in which the condition of atmospheric pressure was imposed. The velocity field obtained into the exchanger was:

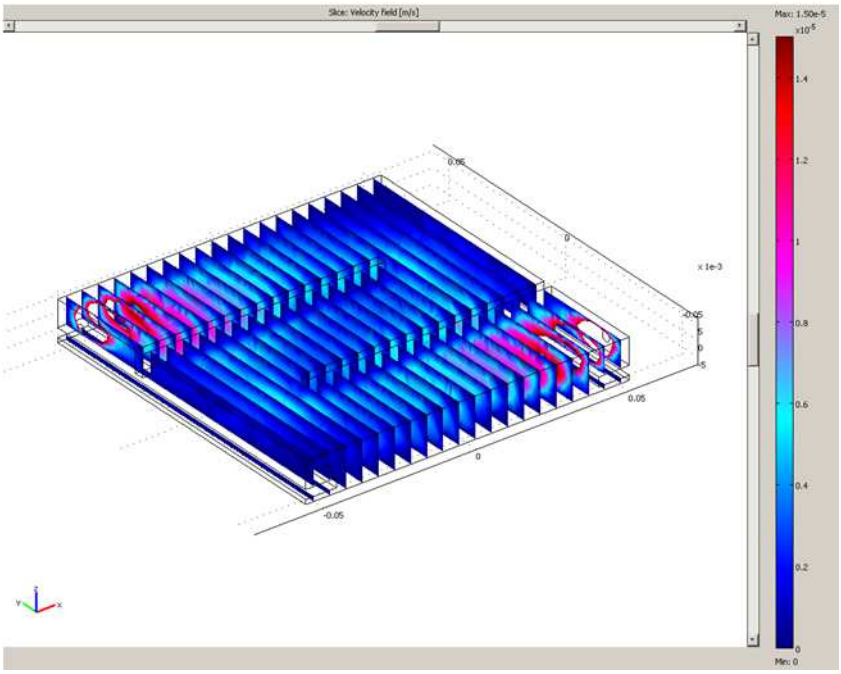

Figure 99. Velocity field into the mass exchanger (intestinal side).

As in the blood side, it could be seen that the maximum velocity is realized in the inlet section of the exchanger and high values are reached in the outlet section.

After the design of the mass exchanger, it was tried to realize the device. Starting from a slab made of PMMA, pieces were cut carefully to obtain each portion of the exchanger. Once obtained all the portions, they were glued each other to obtain the final device. The membrane was then carefully introduced between the two sides of the exchanger and the flow into the exchanger switched on. Because of the high flow rate the membrane was subjected to high stresses and it reveals itself not adequate for the purpose. Moreover, the assembly of the pieces of the device does not guarantee the hydraulic seal necessary, despite several kind of seals were applied to avoid this drawback. Furthermore, after the fluid dynamic calculations, it has been noticed that the mean velocity which is realized inside the exchanger is less than the real one of several order of magnitude. It means that the velocity field simulated is very far from the real one and this affects significantly the mass transport. On the contrary, it is not possible to design a mass exchanger with a lower volume because the exchanger area will be too small for the purposes.

Thus, an high throughput device has to be selected for this purpose and a commercial filter (described in the paragraph 5.1.4) was selected. It contains hollow fibers which guarantee an high exchange surface and the mandatory mechanical resistance.

7.3 Realization of the *in vitro* device

A device consisting of an hollow fibre filter connected with a traditional USP apparatus II has been used [90]. The filter used has the advantage of an high surface area (about 1.7 m^2), but it could be noticed that the intestinal surface area is still about two order of magnitude higher than the filter's one. However, the proposed device has to mimic the behavior of the intestinal segment instantaneously involved in the bolus transit. Then, for this purpose, the area could be enough if only the exchange area around the bolus is taken into account for the mass transport. Two fluids flow in the filter, the first one (donor), simulating the intestinal content, is rich in drug content and, passing across the fibres gives the drug to the second fluid (acceptor), simulating the circulatory system near the gastrointestinal tract. In the vessel containing the first fluid a drug formulation is

dissolving following the release kinetic characteristic of the tablet. The flow rates passing into the two sides of the filter were the same from the two compartments but they were varied to analyse the changing of transport coefficients. The proposed device is provided by a recirculating system, as described in the paragraph 5.2.3, Figure 65.

7.4 Results and discussions

Similarly to the case of Franz cell, even in this case the first step of the work consisted in characterizing the exchange membrane. The permeability values of two drugs studied (theophylline and diclofenac) were evaluated at different values of flow rate circulating in the filter. First of all, a simple system consisting of a known amount of drug dissolved in the donor vessel was analysed.

7.4.1 Experimental setup and transport parameters evaluation

The experimental system could be modelled by a simple compartmental approach, depicted in Figure 100.

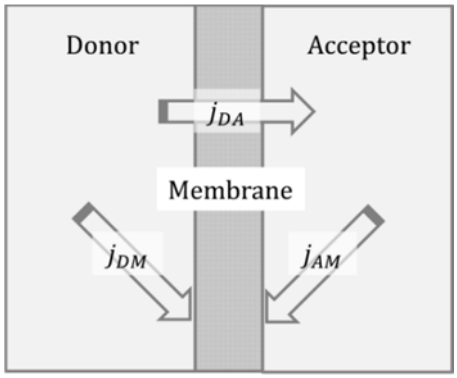

Figure 100. Sketch of the model: the donor, acceptor and membrane compartments are shown with their fluxes.

The two sides are the donor compartment and the acceptor compartment. The two compartments are separated by the filter membrane, which constitutes another compartment itself. The fluxes of drug which take place are indicated by arrows in the graph. In these experiments the two fluids were disposed in counter-current and the donor fluid flowed in straight direction and the acceptor one in lateral direction. The drug balances within the three compartments can be written as:

$$\frac{dm_D}{dt} = \frac{d(V_D \cdot c_D)}{dt} = -S \cdot (j_{DA} + j_{DM}) + G \tag{7.9}$$

In the equation (7.9) the mass balance within the donor compartment is reported.

Where c_D is the concentration in the donor compartment, V_D is the fluid volume in the donor compartment, S is the exchange area of the filter, and j are the fluxes. G is the generation term (mass of drug liberated in the donor compartment for unit of time – it is zero in the simplest case of study), which could be due to the release from a tablet. The two mass fluxes, one from the donor to the acceptor compartment, and from the donor to the membrane compartment are written as:

$$j_{DA} = P \cdot (c_D - c_A) = P \cdot \left(\frac{m_D}{V_D} - \frac{m_A}{V_A} \right) \tag{7.10}$$

$$j_{DM} = K \cdot \left(c_D - K_P \cdot \frac{m_M}{V_M} \right) \tag{7.11}$$

Where c_A is the concentration in the acceptor compartment, V_A is the fluid volume in the donor compartment. In the fluxes expressions, P is the permeability of the drug, K an overall transport coefficient from the donor or from the acceptor toward, K_P the partition coefficient of the drug between the liquid compartments and the membrane, and V_M is the volume of the membrane.

The mass balance on the acceptor compartment can be written as:

$$\frac{dm_A}{dt} = \frac{d(V_A \cdot c_A)}{dt} = S \cdot (j_{DA} - j_{AM}) \tag{7.12}$$

And the flux from the acceptor to the membrane compartment:

$$j_{AM} = K \cdot \left(c_A - K_P \cdot \frac{m_M}{V_M} \right) \tag{7.13}$$

In which m_M and V_M are the drug mass and the fluid volume in the membrane compartment respectively.

Finally, the mass balance on the last compartment (membrane) can be written:

$$\frac{dm_M}{dt} = S \cdot (j_{DM} + j_{AM}) \tag{7.14}$$

Once the model (the equations and their initials) has been defined, it describes the *in vitro* results obtained with the device used for the mass transport. Obviously, it could describe several configurations and systems depending on the pharmaceutical form and device arrangements.

On the basis of the observed results, the best optimization strategy was to make the parameter K_P/V_M independent from the acceptor flow rate, and to make the transport coefficients, P and K, directly dependent from the mass flow rate, i.e. $P = a_1\dot{V}_A, K = a_2\dot{V}_A$, in which $\dot{V}_A$ is the acceptor flow rate. The optimization gave the following results: $K_P/V_M = 1.81$ 1/L, $a_1 = 1.92 \cdot 10^{-4}$ L/(mL·m^2), and $a_2 = 7.05 \cdot 10^{-4}$ L/(mL·m^2).

The first type of experiments are performed working with a known amount of theophylline dissolved in the donor compartment, and the tests are carried out varying flow rate between 10 and 30 mL/min. During the mass exchange, some of the drug is embedded into the membrane, its value is easily obtainable from a mass balance. The concentration evolutions obtained are shown in Figure 101.

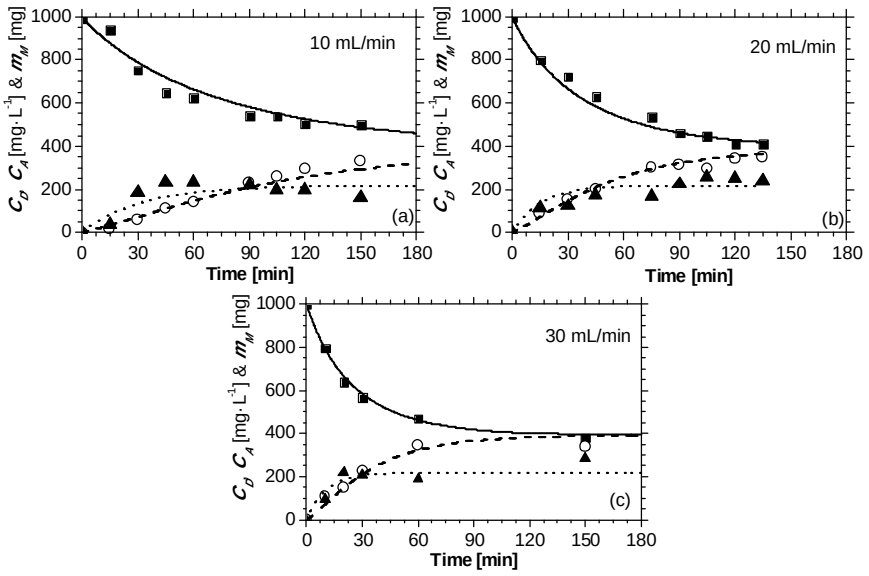

Figure 101. Theophylline concentration evolutions in donor and acceptor compartments varying the flow rate. Donor: full squares; Acceptor: open circles; Mass entrapped in the membrane: full triangles. The lines are the model simulations (continuous = donor, dashed = acceptor, dotted = mass in the membrane).

Comparing the three graphs it could be concluded that the amount of drug which is embedded in the membrane is non-dependent on the flow rate (being the process thermodynamically dictated), and the kinetics of the transport phenomena increases as the flow rate increases. Similarly, the higher the flow rate, the shorter the working time to produce the membrane saturation.

7.4.2 Conventional release pattern

Once the exchange system has been characterized, the release pattern of simple tablets made of HPMC and theophylline (75/25% w/w) are evaluated both following the conventional dissolution method (with the pH step) and the new dissolution method (with the pH variable). Obviously, the system with the filter is activated only two hours after the beginning of test because the transport is active only in the intestine. The result of a typical test following the conventional pH history is shown in Figure 102, where the reference dissolution does not take into account the exchange system.

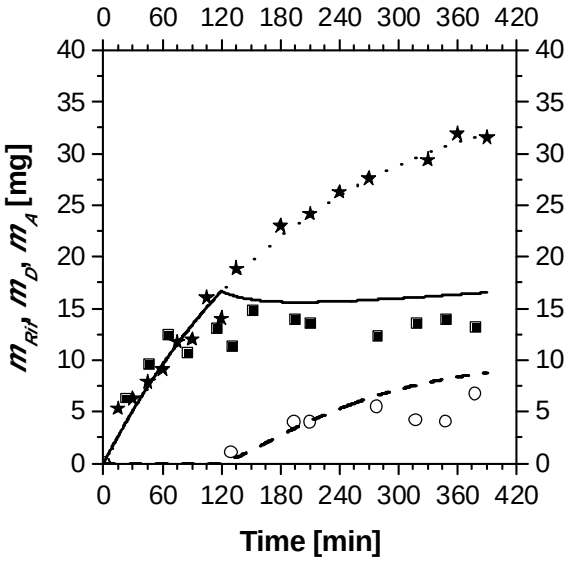

Figure 102. Evolutions of theophylline masses for conventional dissolution test (full stars), in the donor vessel (full squares) and in the acceptor vessel (open circles). Flow rate = 20 mL/min.

The concentration in the donor compartment (which mimics the gastro intestinal tract) does not increase further, after the first two hours. On the other side, the concentration in the acceptor compartment (which mimics the gastro intestinal circulatory system), increases starting from zero, as soon as the mass transfer was allowed (in the intestine). Once analyzed these results, a flow rate of 20 mL/min (the intermediate one) is chosen for further experiments. Concerning the modeling, in these experiments the generation term is the derivative of the evolution observed in the reference, and the initial concentrations are all zero. In Figure 102 also the model calculations are reported as curves. Even if the prediction is not very accurate, the agreement between model and data is satisfactory, since no further optimization parameter was used at this stage. This confirms once more that the main phenomena have been correctly identified and quantified.

7.4.3 Effect of the flow direction

Once developed the experimental set up and method and understood the main transport phenomena involved in the process, different configurations of the experimental set up are evaluate to understand their effect on the drug exchange (i.e. flow co-current and counter-

current, donor fluid flow in lateral or straight direction). For example, concerning the tablet of HPMC/theophylline, the effect of the direction of the donor fluid flow (lateral or straight direction) on the exchange process.

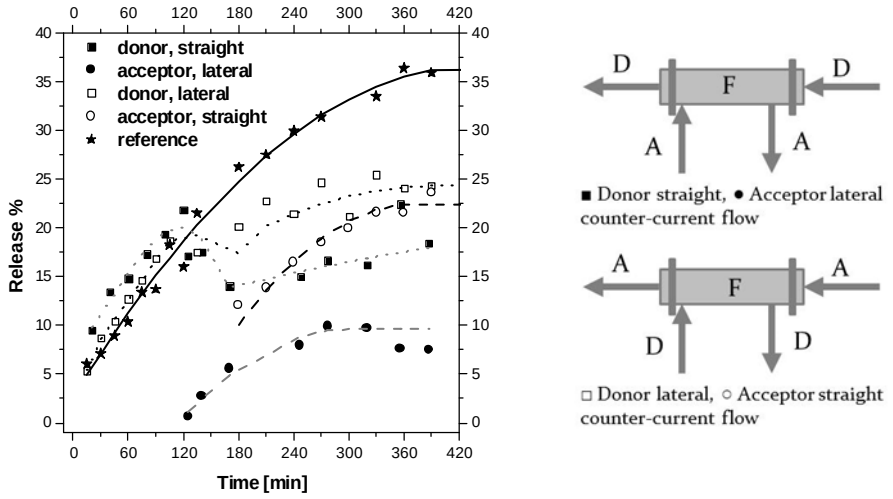

Figure 103. Release patterns of a theophylline tablet in the case in which the acceptor solution has a straight flow (closed symbols) or a lateral flow (open symbols) through the filter. The reference curve is the release pattern without the exchange system. In this graph also line guides are reported (grey = lateral direction of the fluid rich in drug content; black = straight direction of the fluid rich in drug content). On the right the two different layouts are shown.

The experimental data are significantly scattered in this case, and there are differences in the release pattern depending on the flow direction. It could be noticed that the sum of the drug amount found in the donor compartment and in the acceptor compartment should be the total amount of drug in the system. Hence, in the ideal case, the sum of the two amounts should be equal to the drug released during the reference experiment. Instead, it could be noticed that in one case (closed symbols) the sum of drug found in the compartments is lower than the drug found in the reference case. This difference is due to the amount of drug which remains embedded in the filter membrane. In the other case (open symbols) is about the same or slightly higher. Probably, this difference is due to analytical or experimental procedure. Anyway, the filter is normally intended for the lateral flow of the fluid rich in drug content and the lateral flow of the fluid poor in drug content. Hence, it is decided to assume as reference for the

other experiments the lateral flow of the donor solution and the straight flow of the acceptor solution.

7.4.4 Effect of the reciprocal flow direction

The same work described above has been done also concerning the diclofenac behavior. Once the transport parameters have been calculated for a simple system at constant concentration of diclofenac, test which provide for the use of a tablet was pointed out. For these tests, commercial tablets of diclofenac, surface coated, containing 100 mg of drug, are used. Once established the flow rate at which evaluate the exchange (20 mL/min) and the direction of the flow, the influence of the reciprocal direction of flow of the two fluids is evaluated. Hence, the release patterns are evaluated depending on the disposition in co-current or counter-current of the flow direction. The results are shown in Figure 104.

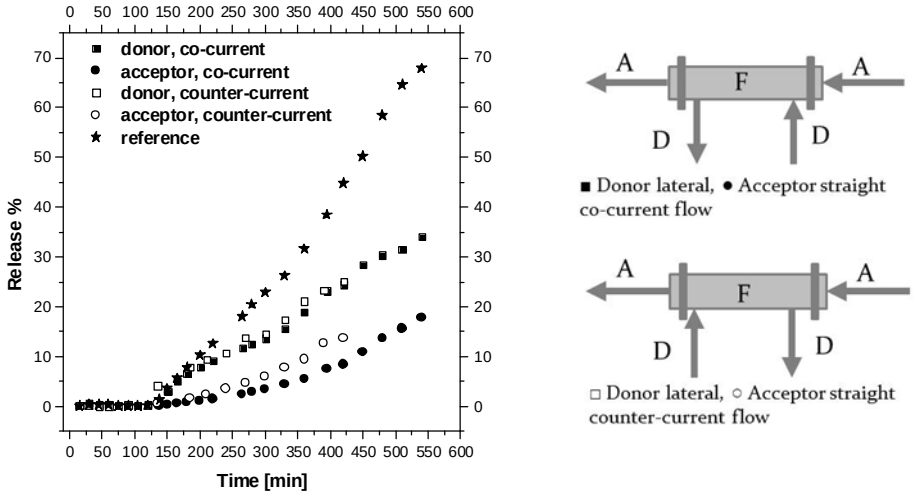

Figure 104. Comparison between the release patterns of a diclofenac commercial tablet (DOC) using a co-current or a counter-current flow following the conventional USP method. On the right the two different layouts are shown.

From the Figure 104 it could be seen that the release profile is not particularly affected by the reciprocal direction of the flow. Hence, it is assumed to use the co-current flow direction to prevent difference in pressure drops which can cause flow mixing or preferential paths.

7.4.5 Effect of pH history

The effects both of the mass exchange and the pH real evolution on the release pattern were analyzed together to obtain the complete simulation of the system. The results on a commercial, controlled release tablet of diclofenac are shown in the Figure 106.

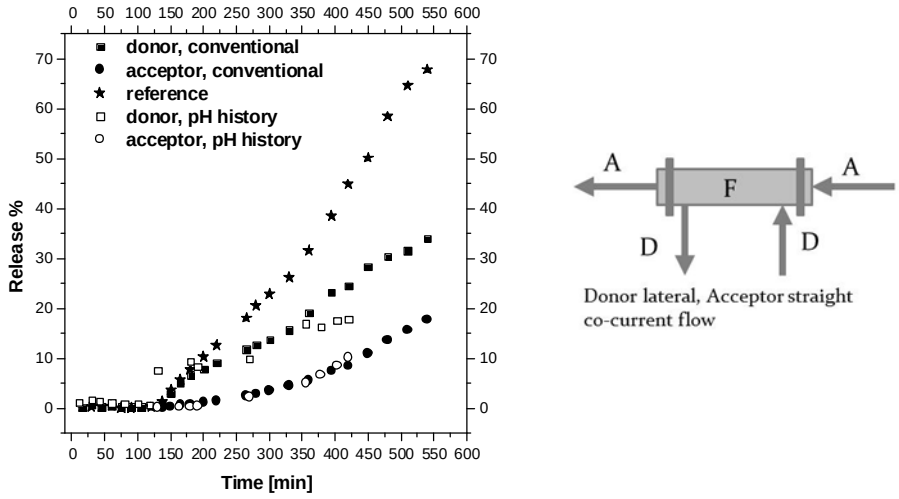

Figure 105. Diclofenac release profile (DOC) in the donor and acceptor compartment following the conventional dissolution method and the pH evolution modified. The reference is the release profile using the conventional method without mass exchange. On the right the layout of the experimental device is shown.

As could be seen from the figure, the influence of a different pH evolution on the release pattern is higher in the first stage of dissolution (in fact the drug amount released is higher than those released in the conventional case), but it loses relevance in the following steps. It is important to note that, when the pH is rapidly increased from 2.0 to 6.8 after 120 minutes, in the case of the use of the new apparatus, the increase in the amount of drug released is immediate, in the conventional case it is more gradual. It is due probably to the fact that the coating of the tablet was damaged in the first two hours of dissolution in the new apparatus, behavior which is not found if a conventional method is followed. Concerning the evaluation of the mass exchange in the two cases, it could be noticed that the amount of drug which is transferred between the two compartment is approximately the same but, obviously, the

concentration of drug in the intestinal side is very different in the case in which the exchange is considered and the standard case.

7.4.6 Release profile of an enteric fast release tablet

The last pharmaceutical system analyzed was a commercial enteric fast release diclofenac tablet. Also in this case the effect of the flow rate on the mass exchange for the conventional USP method is studied. The results are shown in Figure 106.

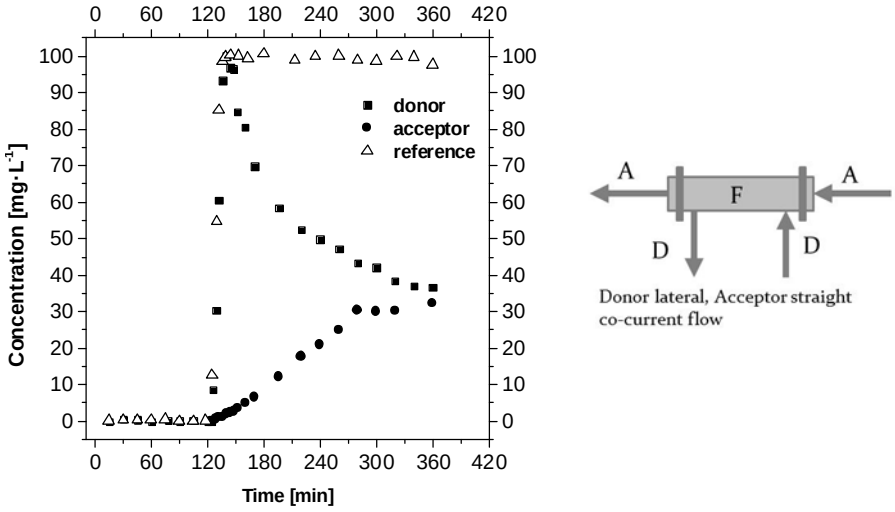

Figure 106. Release patterns for enteric fast release diclofenac (co-current flow). On the right the layout of the experimental device is shown.

For this system the release pattern is completely different. In fact, during the first two hours of dissolution, the tablet does not release the drug. Reversely, when the pH of the dissolution medium is neutralized, the drug is completely released in few minutes (reference in Figure 106). In the case in which the mass exchange is activated, it could be seen the evolution of the donor and acceptor concentrations. After four hours the system could be considered at steady state. Once again, the sum of the drug amount found in the donor and in the acceptor compartment is lower than the amount in the reference condition, this is due to the fact that part of the drug is embedded in the filter.

Chapter Eight

In vitro models: mechanical history

In this chapter the reproduction of the peristaltic waves along the stomach is faced. An in vitro device able to reproduce the contractions is designed and realized. The release patterns of tablets are evaluated using this device and compared with that obtained with the conventional one.

8.1 Design of the gastric motility

With the aim to realize a device which could reproduce more realistically the mechanics of the stomach, an apparatus which realize the peristaltic waves was developed.

First of all, the element representing the stomach has to be chosen. To allow the contractions along the stomach, the material has to be compressible and elastic; of course the material has to be chemically inert and it has to not interact with the substances inside the stomach. Concerning the shape of the element, the real J-shape of the stomach is hard to be reproduced but it is necessary at least reproduce the difference in diameter between the top and the bottom of the stomach. Thus, the chosen element has to be larger at the top, which represents the fundus of the real stomach, and narrower at the bottom, which represents the antral part of the stomach, ending at the pylorus. The total volume has to be about 1 liter.

Concerning the peristaltic waves, the position of the contractions has a key role in the reproduction of the mechanical behavior of the stomach. As described previously, the contractions start only in the antral part of the stomach, whereas they are negligible in the upper part, which is only a reservoir for foods. The frequency of the contraction is three waves per minute and their strength is variable. In fact the strength of the contraction depends on the position: it is lower in the body of the stomach and it increases approaching the pylorus. The maximum strength is at the pyloric position.

All these features have to be taken into account in the realization of the *in vitro* device.

8.2 Realization of the *in vitro* device

To simulate the stomach a lattice bag, elastic, and with a volume of 1 liter was chosen. To ensure the right position of the peristaltic waves, a guide for the contraction elements was equipped on the simulated stomach, as shown in Figure 107.

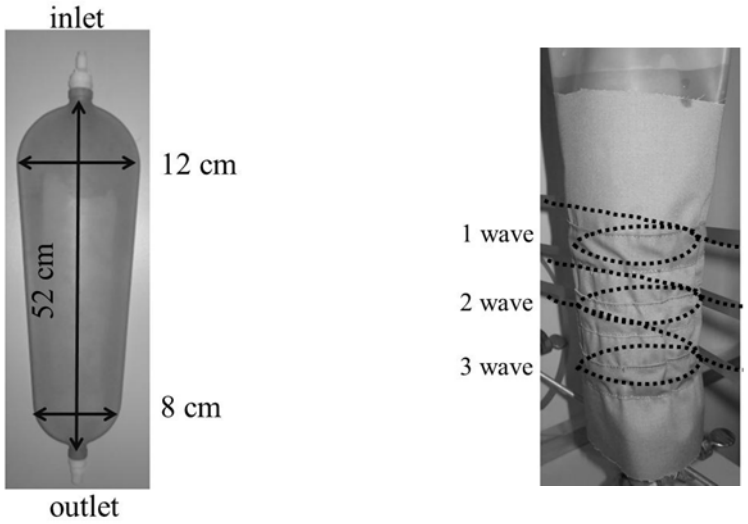

Figure 107. Lattice bag used for the simulation of the stomach on the left, the guide with the contraction elements on the right.

Once identified the apparatus simulating the stomach and the other parts involved in the building of the *in vitro* device, they have been assembled and the final result is schematized in Figure 108.

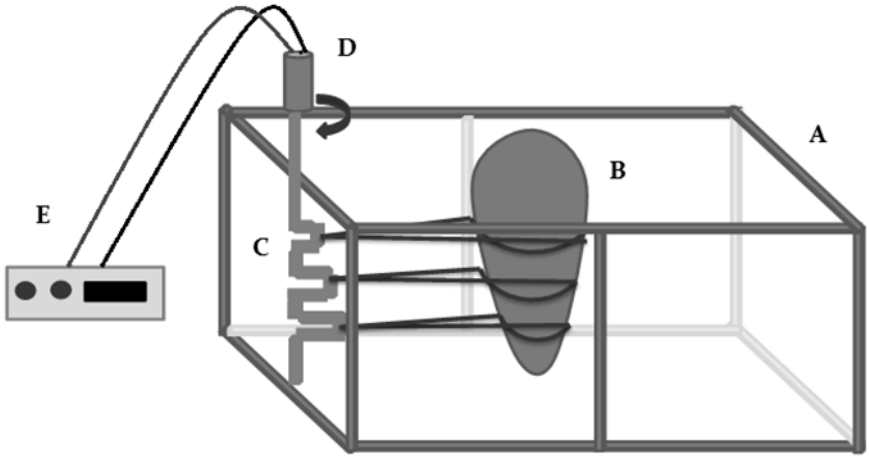

Figure 108. Schematic of the apparatus which simulates the peristaltic waves in the stomach.

The device is composed of an external structure (A) which has the role to support all the components. The main component of the device is the lattice bag (B) described previously. This bag is connected to a camshaft (C) which has the role to generate the peristaltic waves. In

fact, with the rotation of the cams, the connections shrink the bag which, locally, reduces its volume (obviously the total volume remains the same, so there is also the upper zone (the fundus) which expands). The peristaltic waves are been considered acting only in the lower part of the stomach (the antrum) for the reasons discussed above. The fact that the pyloric wave is the strongest is the reason why the cam at the bottom of the shaft is longer than the others: in that way, when it is subjected to the rotation, it causes a stronger pressure on the bag than the other contractions. Only three waves have been considered to reproduce the ratio of three contraction at minute which is realized in the reality. Each cam is rotated of 120° respect to the previous one to ensure the right pattern of the waves. The shaft could be putted in rotation by a gear motor (D). The speed rotation could easily regulated by the voltage alimentation (E) of the motor which could be set at the desired value.

8.3 Results and discussions

Once the device has been built, it was tested evaluating the release pattern of a commercial tablet of diclofenac (extended release). During the tests a conventional pH pattern was performed, which means that in the artificial stomach the pH is constant and equal to 1. Obviously the test runs only for two hours (the mean residence time in the stomach), after that the release medium was neutralized and moved on the conventional USP device to continue the release test simulating the intestinal environment.

8.3.1 Release pattern in the artificial stomach

Once the tablet was inserted into the artificial stomach, it falls at the bottom of the artificial stomach. To analyze the concentration of the drug inside the stomach (and the release), samples of stomach content were withdrawn from the bottom by a valve. Since it is expected that the concentration will be not constant because the contractions do not ensure perfect mixing, to evaluate the mixing power of the realized system samples of the content were withdrawn also from the top of the artificial stomach. In this way is possible to compare the concentration of drug between the top and the bottom of the artificial stomach. It is clear that if the device ensures perfect mixing, it could expected a release profile very similar to the conventional one, with the concentrations equal at the top and the bottom and very low for all the

2 hours of the test. On the contrary, if this system does not ensure perfect mixing, a different concentration is expect between the top and the bottom. In particularly, because of the position of the tablet, it could be expected that the concentration is higher at the bottom and lower at the top. The typical release pattern obtained is shown in Figure 109.

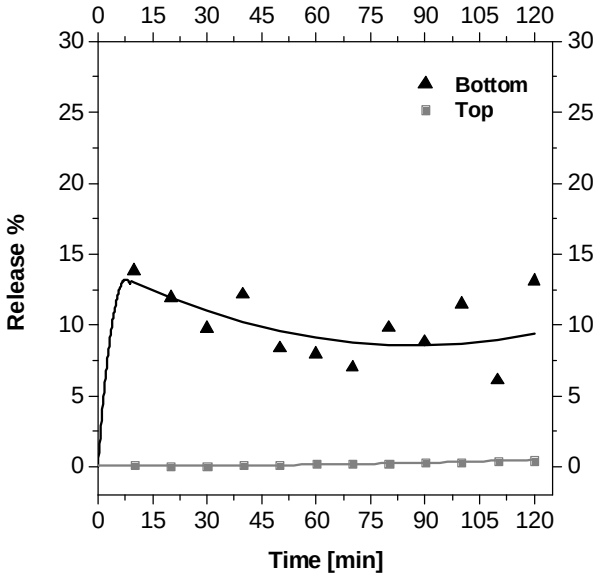

Figure 109. Release pattern of a commercial extended release tablet of diclofenac in the *in vitro* device simulating the mechanics of the stomach. The % release is evaluated on the basis on the drug content in the tablet.

As could be seen from the figure, the values of concentration at the top is lower than the values at the bottom, it means that the hypothesis of not perfect mixing were confirmed. In the graph also the eye guides are reported. At the beginning of the run the concentration at the bottom rapidly increases starting from zero and release an high amount of drug in the first 10 minutes. After that it could be seen that the concentration decreases at the bottom, this behavior is probably due to the fact that the drug released is diluted (both for the effect of mixing and the diffusion) in the dissolution medium. Then, at the bottom, the drug concentration continues to increase mainly for the effect of the dissolution of the tablet. Concerning the concentration behavior at the top of the artificial stomach, it could be seen that the concentration starts from zero and slowly increases during the run and its value is very low.

After the two hours, the content of the artificial stomach was quantitatively moved in the USP apparatus II to simulate the passage in the intestinal environment. The pH of the dissolution medium was neutralized to a value of 6.8. The obtained release pattern is shown in Figure 110.

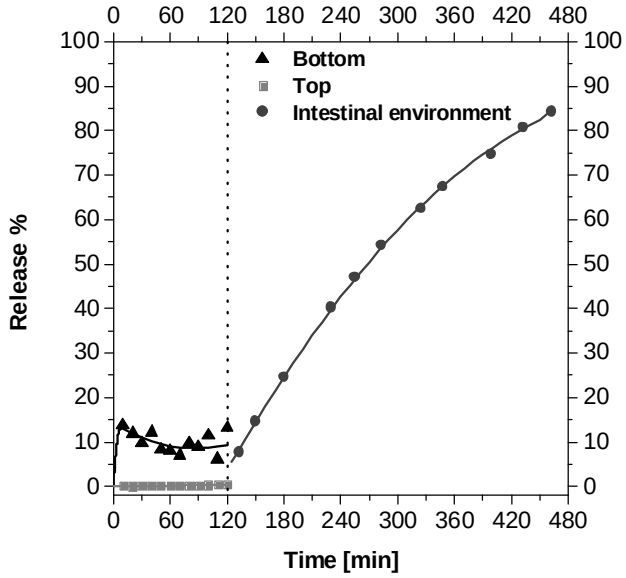

Figure 110. Release pattern of a commercial extended release tablet of diclofenac in the *in vitro* device simulating the mechanics of the stomach and the intestinal environment. The % release is evaluated on the basis on the drug content in the tablet.

In Figure 110 the dotted vertical line represents the time at which the dissolution medium was moved in the USP apparatus mixed with a velocity of 100 rpm. As could be seen the release continues for the following five hours starting from a concentration value which is intermediate between the concentration released at the bottom of the artificial stomach and the concentration released at the top of the artificial stomach. This is due to the fact that the conventional apparatus realizes a perfect mixing and the drug released at the bottom and at the top of the artificial stomach is immediately uniformed.

Comparing the release pattern obtained with the pattern obtained following a conventional method it is obtained:

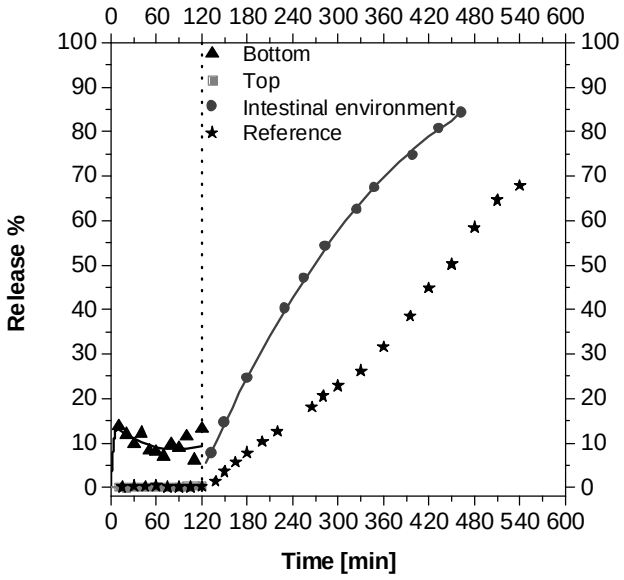

Figure 111. Comparison between the release pattern of a commercial extended release tablet of diclofenac in the *in vitro* device simulating the mechanics of the stomach and the intestinal environment and in the conventional apparatus. The % release is evaluated on the basis on the drug content in the tablet.

Compared with the release pattern obtained following the conventional method, the release is higher in the first stage of dissolution, at the bottom of the artificial stomach. This behavior is due to the fact that the poor mixing generate a large layer of dissolution medium in which the drug does not diffuse. In the second stage of dissolution the release obtained by the *in vitro* device is higher than the conventional one. This is due to the fact that the tablet is affected by higher stresses on the surface respect to the tablet used in the conventional method. In fact, the compression of the artificial stomach tend toward damage the tablet because of the shear close to the tablet. On the contrary, when a tablet is inserted in the conventional apparatus, often it falls on the bottom of the vessel and the shear caused by the paddle does not affect the surface of the tablet. The damaging of the surface coating is particularly relevant in the second stage of dissolution. In fact, when the pH in the dissolution medium is neutralized, the drug contained in the polymer matrix is released and, if the coating is damaged yet, this release is faster or immediate after the neutralization. Instead, in the conventional method, the effect of the pH firstly has to disintegrate the coating of

the tablet and then has to facilitate the release. Of course, the release rate is particularly influenced by this aspect.

8.3.2 Effect of the frequency of the contractions

Once evaluated the effect of a different type of mixing in the stomach respect to the conventional one, the effect of the increasing of the frequency of the contractions was taken into account. Thus, the frequencies of the contractions was increased varying the alimentation voltage of the gear motor controlling the shaft rotation speed. The release obtained at the bottom of the artificial stomach is shown in Figure 112.

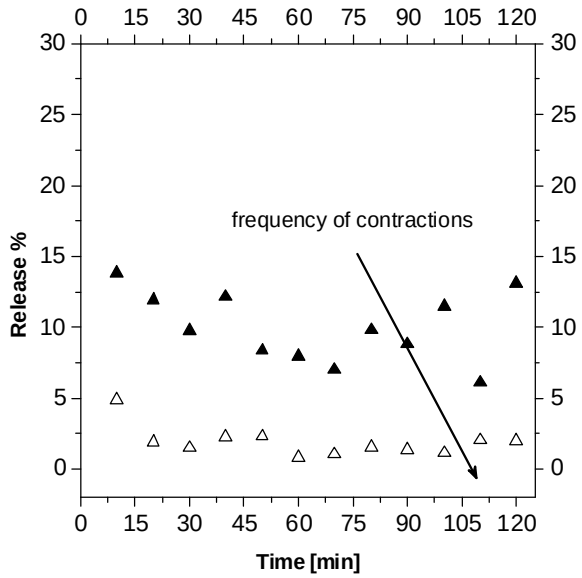

Figure 112. Release at the bottom of the artificial stomach varying the frequency of the contractions. The % release is evaluated on the basis on the drug content in the tablet.

As could be seen, the release at the bottom of the artificial stomach is lower increasing the frequency of the contractions. This is due to the fact that an higher mixing effect occurs and the concentration inside the bag is more homogeneous then the previous case. In fact, increasing the mixing, the amount of drug released is diluted in all the volume of dissolution medium, resulting in a whole lower concentration, and thus a lower release. After the two hours, as in the previous case, the passage in the intestinal environment was

reproduced and the release pattern was analyzed. Comparing the release patterns obtained varying the frequency of contractions and the conventional one:

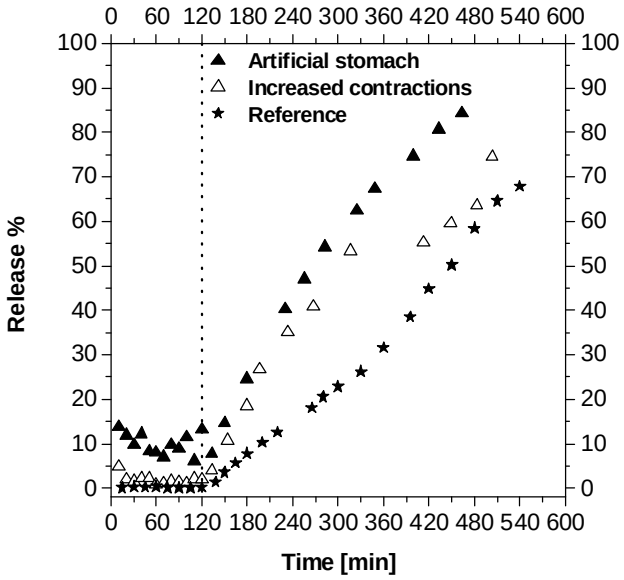

Figure 113. Complete release pattern varying the frequency of the contractions compared with the conventional release. The % release is evaluated on the basis on the drug content in the tablet.

As the previous case, the release pattern in the second stage in higher than the conventional one because the damaging of the tablet affects the release rate facilitating the drug dissolution.

Chapter Nine

In silico pharmacokinetics

In this chapter the physiologically based pharmacokinetic model developed is described. The influence of the dissolution method and of the inter-individual parameters on the model parameters is evaluated.

9.1 Physiologically based pharmacokinetic model

The prediction of the drug concentration in the blood, tissue, and organs is the goal of the *in silico* pharmacokinetic modeling. A physiologically based pharmacokinetic (PBPK) model previously developed [45] was refined and applied to reproduce and predict the plasmatic concentrations of drugs for several cases of study.

First of all, the model used could be schematized in the following compartments:

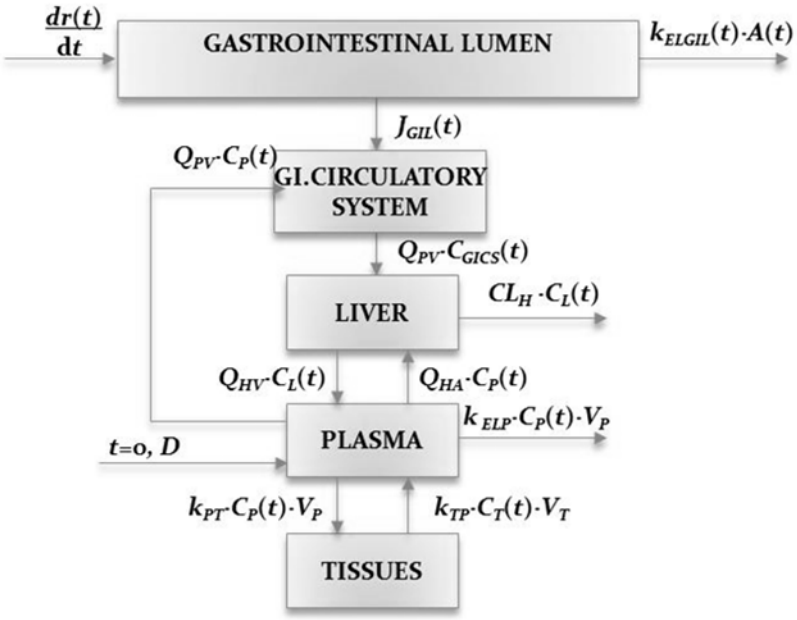

Figure 114. Schematic of the *in silico* model.

Each block of the model represents an organ, a tissue, or a group of them and the blocks are interconnecting and interacting between them. The gastrointestinal lumen could be divided further in gastric lumen, small intestine lumen, and large intestine lumen, these three compartments are passed through in series if the pharmaceutical form is administered orally. Thus, the model is composed by seven compartments: gastric lumen, small intestine lumen, large intestine lumen, circulatory system around the gastrointestinal lumen, liver, plasma, and tissue. The liver compartment takes into account the metabolization due to the hepatic functions of the body, the plasma compartment takes into account the behavior of the largely perfused tissue and organs, and the tissue compartment takes into account the

behavior of the scarcely perfused tissue and organs. The continuous arrows represent the mass flow rates between the compartments. The dashed arrows represent the drug inlets after administration by intravenous or oral route: in the case of intravenous injection (i.i.), the only dashed arrow which needs to be considered is that entering the plasma compartment, while, in the case of oral assumption (o.a.), the dashed arrows which need to be considered are those entering the gastric (from ingestion to gastric emptying), the small intestine (from gastric emptying to small intestine emptying), and the large intestine (from small intestine emptying to large intestine emptying) lumen. The PBPK model consists of the mass balance equations on the compartments and of the initial conditions which are necessary for solving them. The assumption made in doing mass balances are that the blocks can be likened to continuous stirred reactors and that the mechanism of drug transport across biological membranes (such as the gastrointestinal walls and the blood vessels walls) is the passive diffusion. The equation describing the system are:

$$\frac{dA_{GIL}(t)}{dt} = G(t)\cdot\frac{dr(t)}{dt} - J_{GIL}(t) - k_{ELGIL}(t)\cdot A_{GIL}(t) \tag{9.1}$$

$$V_{GICS}\cdot\frac{dc_{GICS}(t)}{dt} = Q_{PV}\cdot c_P(t)\cdot\frac{dr(t)}{dt} - Q_{PV}\cdot c_{GICS}(t) + \\ + J_{GL}(t) + J_{SIL}(t) + J_{LIL}(t) \tag{9.2}$$

$$V_L\frac{dc_L(t)}{dt} = Q_{PV}\cdot c_{GICS}(t) + Q_{HA}\cdot c_P(t) - (Q_{HV} + CL_H)\cdot c_L(t) \tag{9.3}$$

$$V_P\cdot\frac{dc_P(t)}{dt} = Q_{HV}\cdot c_L(t) + k_{TP}\cdot c_T(t)\cdot V_T + \\ - (Q_{HA} + Q_{PV} + k_{PT}\cdot V_P + k_{ELP}\cdot V_P)\cdot c_P(t) \tag{9.4}$$

$$V_T\cdot\frac{dc_T(t)}{dt} = k_{PT}\cdot c_P(t)\cdot V_P - k_{TP}c_T(t)\cdot V_T \tag{9.5}$$

In which the first equation represents the mass balance inside the gastrointestinal compartment, the equation (9.2) represents the mass balance inside the gastrointestinal circulatory system, the equation (9.3) represents the mass balance inside the liver compartment, the equation (9.4) represents the mass balance inside the plasma compartment, the equation (9.5) represents the mass balance inside the tissue compartment. In the following table the symbols used in the mass balances with the description and the measure units are reported.

Table 22. Description of the symbols reported in the mass balances.

Symbol	Description	Measure units
$A_{GIL}(t)$	Time evolution of the drug contents in the gastrointestinal lumen	kg
$G(t)$	time function which activates the drug release during the transit of the pharmaceutical form in the gastric lumen	-
$r(t)$	time evolution of the *in vitro* measured drug release	kg
$J_{GIL}(t)$	time evolution of the mass flow rate of the drug exchanged between the gastrointestinal lumen and the gastrointestinal circulatory system	$kg \cdot s^{-1}$
k_{ELGIL}	kinetic constant of elimination (metabolism and excretion)	s^{-1}
$A_{GIL}(t)$	time evolution of the drug contents (masses) in the gastrointestinal lumen	kg
V_{GICS}	physical volume of the gastrointestinal circulatory system	m^3
$c_{GICS}(t)$	time evolution of the drug concentration in the gastrointestinal circulatory system	$kg \cdot m^{-3}$
Q_{PV}	blood volumetric flow rates of the portal vein	$m^3 \cdot s^{-1}$
$c_P(t)$	time evolution of the drug concentration in the plasma	$kg \cdot m^{-3}$
$J_{SIL}(t)$	time evolution of the mass flow rate of the drug exchanged between the small intestine lumen and the gastrointestinal circulatory system	$kg \cdot s^{-1}$
$J_{LIL}(t)$	time evolution of the mass flow rate of the drug exchanged between the large intestine lumen and the gastrointestinal circulatory system	$kg \cdot s^{-1}$
V_L	physical volume of the liver	m^3
Q_{HA}	blood volumetric flow rates of hepatic artery	$m^3 \cdot s^{-1}$
Q_{HV}	blood volumetric flow rates of the hepatic vein	$m^3 \cdot s^{-1}$
C_{LH}	hepatic clearance	$kg \cdot m^{-3}$
$C_L(t)$	time evolution of the drug concentration in the liver	$kg \cdot m^{-3}$
V_P	distribution volume of the plasma compartment	m^3
k_{TP}	mass transfer coefficient from tissues compartment to plasma	s^{-1}
$C_T(t)$	time evolution of the drug concentration in the tissues	$kg \cdot m^{-3}$
V_T	distribution volume of the tissues compartment	m^3
k_{PT}	mass transfer coefficient from plasma to tissues	s^{-1}

This model has been developed [45] to obtain a predictive tool with a limited number of parameters. The model has been validated by comparison with experimental data from literature in several case histories: the intravenous administration of zinc sulfate in rats, the oral administration of theophylline and of diltiazem in humans.

9.2 Influence of dissolution method

9.2.1 Influence of pH history

The *in vitro* results obtained using the device able to reproduce the chemical history in the gastrointestinal tract, and in particular the pH history, were subsequently used to build an *in silico* model able to take into account the pH changes experienced by a drug once ingested [71].

As described previously, the model needs an input function to describe the drug administration kinetics, *r(t)* is the time evolution of the *in vitro* measured drug release. The derivative of the *in vitro* drug release has to be used as forcing function in the model. Then, the experimental data obtained using the *in vitro* device (see paragraph 6.2) have to be fitted to obtain continuous function which can be differentiate. Both the release kinetic obtained by the conventional method and by the novel technique have been fitted by the following equations:

$$r(t) = \begin{cases} a \cdot \left[1 - \exp\left[-b \cdot \left(t - t_o^{'}\right)\right]\right] & t \le t^* \\ c \cdot \left[1 - \exp\left[-d \cdot \left(t - t_o^{''}\right)\right]\right] & t > t^* \end{cases} \tag{9.6}$$

In which t^* represents the time in which the pharmaceutical form remains in the gastric environment (minutes), a, b, c, d, $t_o^{'}$, and $t_o^{''}$ are parameters which have to be fitted. The function parameters for both the conventional and the novel dissolution technique are reported in Table 23. The function is plotted in Figure 115.

Table 23. Function parameters for the equation fitting the release kinetic both for the conventional dissolution method ($r_{conv}(t)$) and for the novel dissolution method ($r_{mod}(t)$).

Function	Parameter	Value	Parameter	Value
$r_{conv}(t)$	a	12.03 mg	d	0.00 min^{-1}
	b	0.02 min^{-1}	$t_o^{'}$	0 min
	c	116.48 mg	$t_o^{''}$	51.28 min
$r_{mod}(t)$	a	18.61 mg	d	0.10 min^{-1}
	b	0.09 min^{-1}	$t_o^{'}$	-0.66 min
	c	74.45 mg	$t_o^{''}$	124.60 min

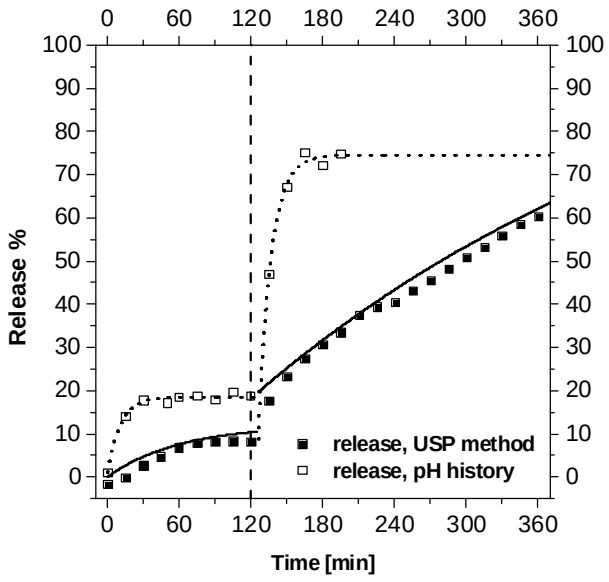

Figure 115. Fitting of the release patterns of a diclofenac tablet obtained with the conventional dissolution method (■ experimental data; continuous curve: fitting) and with the pH history (□ experimental data; dotted line: fitting).

Once identified the function describing the time evolution of the *in vitro* drug release, the input function of the model, which consists of the release profile derivative, is known. To use the *in silico* model, it is necessary to know model parameters used to describe the diclofenac

pharmacokinetics. With the purpose to evaluate these parameters, the model is used to fit an experimental plasma evolution of diclofenac after oral administration of a 50 mg dose [91]. The experimental data and the model prediction after parameters optimization are plotted in Figure 116.

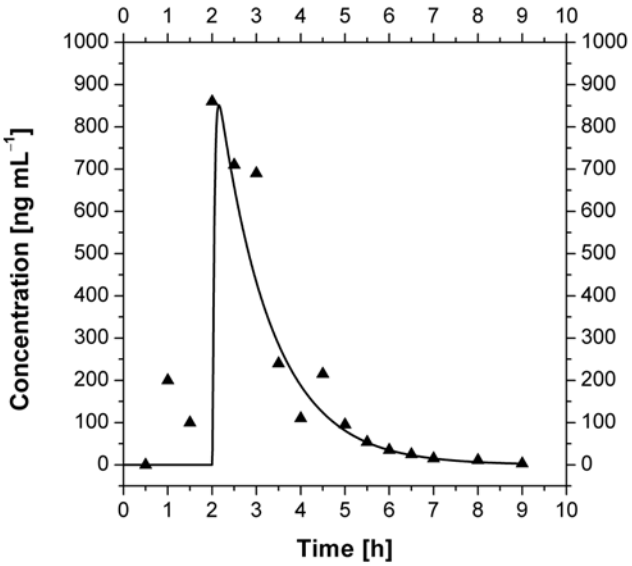

Figure 116. Plasma profile of diclofenac after oral administration of a 50 mg dose [91]. Symbols are experimental data, line is the model prediction after parameter optimization.

The model parameters used to describe the diclofenac pharmacokinetics obtained are reported in Table 24. In this case history the pharmacokinetic parameters have been considered not variable with the inter-individual parameters.

Table 24. The model parameters used to describe the diclofenac pharmacokinetics obtained.

Parameter	Value	Parameter	Value
t_{GL}	2 h	k_{AGL}	0 s^{-1}
t_{SIL}	9 h	k_{ASIL}	$4.79 \cdot 10^{-4}$ s^{-1}
V_L	$1.5 \cdot 10^{-3}$ m^3	k_{ELSIL}	$1.17 \cdot 10^{-4}$ s^{-1}
Q_{PV}	$1.63 \cdot 10^{-5}$ $m^3 \cdot s^{-1}$	k_{ELGL}	0 s^{-1}
Q_{HA}	$0.54 \cdot 10^{-5}$ $m^3 \cdot s^{-1}$	V_T	$152 \cdot 10^{-3}$ m^3
Q_{HV}	$2.17 \cdot 10^{-5}$ $m^3 \cdot s^{-1}$	V_P	0.10 m^3
C_{LH}	$1.65 \cdot 10^{-5}$ $m^3 \cdot s^{-1}$	V_{GICS}	$9.96 \cdot 10^{-6}$ m^3
R_{GICS}	6.67	V_B	$0.1 \cdot 10^{-3}$ m^3

Once obtained the parameters, the model is able to simulate the plasma concentration starting from the *in vitro* release profiles. The model results are shown in Figure 117.

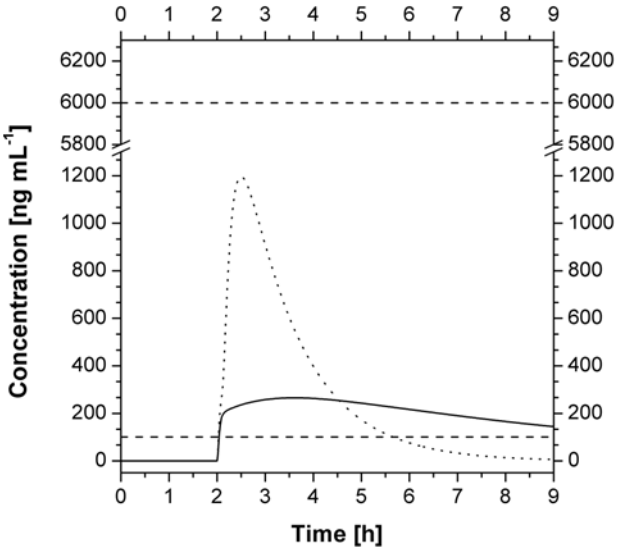

Figure 117. The plasma profiles obtainable: if the real *in vitro* release kinetics would be the one observed using the conventional dissolution method (the continuous line), and if the real *in vitro* release kinetics would be the one observed using the novel apparatus (the dotted line). The horizontal dashed lines represent the minimum effective concentration (the lower one, [92]) and the minimum toxic concentration (the higher one, [93]), therefore they identify the therapeutic window.

It should be noticed that both profiles are contained in the therapeutic window, which is represented by horizontal dashed lines in Figure 117, even if the profiles shapes are very different. Following the conventional method, an almost constant plasma profile is obtained and the drug concentration remains in the therapeutic window for a long time. Analyzing this profile, it should be concluded that the pharmaceutical dosage form is very effective for the controlled oral release and the rate of drug entering in blood is constant. In spite of these consideration, if the *in vitro* release kinetics used as input for the model consists of the dissolution profile obtained following the real pH evolution experienced by the pharmaceutical form, the simulated plasma profile is completely different. It could be noticed that the maximum concentration of the drug in the blood is six times higher and the drug remains over the minimum effective concentration for a shorter period. Thus, the differences between the dissolution profiles are reflected and amplified in the plasma concentrations.

Once more, the availability of the modified dissolution technique, together with the pharmacokinetic model, suggests that a pharmaceutical form, designed to fulfill the requirements imposed by USP testing methods, in a real system would show a completely different behavior. The dissolution under a variable pH causes a large release in the gastric environment and a fast release in the intestine, and this dissolution kinetics should cause an anticipated and higher maximum plasma concentration (with respect to that expected if the *in vitro* release kinetics would be the one observed during an USP test), and a faster exit from the therapeutic window.

9.2.2 Influence of mass transport

The results obtained using the device which simulates the mass transport across the intestinal wall were used to compare the concentration profile in the gastrointestinal tract reproduced *in vitro* with the concentration profile predicted *in silico* by the model. With reference to an enteric fast release tablet of diclofenac (paragraph 7.4.6), the gastrointestinal concentration profile was evaluated taking into account the mass transport of the drug between the intestine and the circulatory system. Of course also the reference release pattern was evaluated: the release from the tablet was evaluated following the conventional dissolution method and the mass transport was not taken into account. Thus, if the conventional release pattern is used as

forcing function by the model, the *in silico* simulation has to reproduce the gastrointestinal concentration profile. The comparison between the predicted *in silico* concentration and the reproduced *in vitro* one is shown in Figure 118.

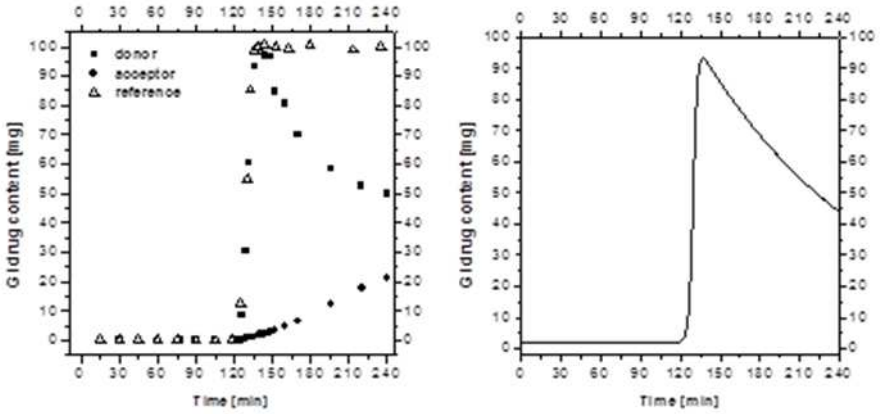

Figure 118. Comparison between the gastrointestinal concentration profile reproduced *in vitro* (on the left) and simulated *in silico* (on the right).

As could be seen, the gastrointestinal release (and then concentration) shows the same qualitatively pattern. In fact, the concentration is zero in the first two hours (in the stomach the drug is not released), increases instantaneously to the maximum within few minutes after the passage in the intestine (the tablet is completely destroyed), and starts to decrease due to the effect of exchange with the gastrointestinal circulatory system. It has to be remembered that in the model simulation the gastrointestinal circulatory system compartment is almost drug free due to the effect of the hepatic clearance, on the contrary, the acceptor compartment in the *in vitro* experiments increases its concentration while the exchange is happening. This is the reason why the two pattern could not be quantitatively the same.

9.3 Influence of inter-individual parameters

The previously developed model was improved to take into account the different metabolic responses which different subjects can have. Particularly, the model was modified to simulate the different absorption of a drug (verapamil) depending on the age and gender of the subject. Verapamil is a drug frequently used for the treatment of hypertension, angina, and arrhythmias. The model was used to fit the *in vivo* data collected by Gupta et al. [94]. In this work, the drug is

administered orally in a racemic mixture of two isomers: R-verapamil (which is almost inactive) and S-verapamil (which is the active isomer). Tablets of a controlled release gastrointestinal therapeutic system containing 180 mg of verapamil were administered to the subjects. Because of a racemic mixture of the two isomers was administered, it was considered during the modeling that the administration was of 90 mg of S-verapamil and 90 mg of R-verapamil. The experimental plasma concentration profiles were taken from young and elderly subjects, each group could be furthermore divided in male and female subjects. As described previously, the model needs for the simulation an *in vitro* dissolution kinetic. This kinetic was taken by literature, from the work of Kim et al. [95]. The released mass fraction versus time is reported in Figure 119.

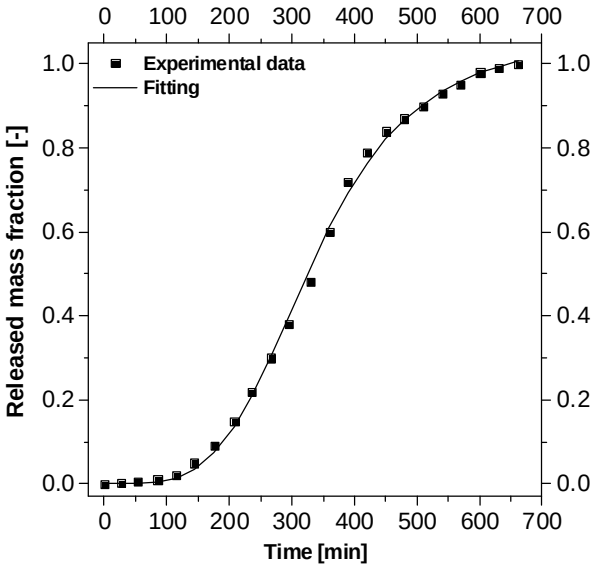

Figure 119. *In vitro* release kinetic of verapamil [95].

The experimental data have been fitted (R^2=0.998) to obtain the verapamil release kinetic *in vitro*. This function has been used in the model as forcing function.

The selected active molecule has a feature: during the metabolization, the drug is subjected to a degradation (oxidative demethylation) and it forms the molecule called norverapamil [96]. This degradation happens both in the gastrointestinal tract and in the liver. The formation of the intermediate metabolite has to be taken into account

in the model. Therefore, the equation set of the model was changed and a disappearance rate was added in the set of differential equations describing the fate of verapamil. On the other hand, a term of formation rate was added in the set of differential equation describing the fate of norverapamil. The modified set of equation was reported.

Verapamil

$$\frac{dA_{GILV}(t)}{dt} = G(t)\cdot\frac{dr(t)}{dt} - J_{GILV}(t) - k_{ELGILV}(t)\cdot A_{GILV}(t) + - r_{NGIL}\cdot M_{wV} \tag{9.7}$$

$$V_{GICS\cdot}\frac{dc_{GICSV}(t)}{dt} = Q_{PV}\cdot c_{PV}(t)\cdot\frac{dr(t)}{dt} - Q_{PV}\cdot c_{GICSV}(t) + + J_{GLV}(t) + J_{SILV}(t) + J_{LILV}(t) \tag{9.8}$$

$$V_L\frac{dc_{LV}(t)}{dt} = Q_{PV}\cdot c_{GICSV}(t) + Q_{HA}\cdot c_{PV}(t) + - (Q_{HV} + CL_H)\cdot c_{LV}(t) - r_{NL}\cdot M_{wV} \tag{9.9}$$

$$V_{P\cdot}\frac{dc_{PV}(t)}{dt} = Q_{HV}\cdot c_{LV}(t) + k_{TP\cdot}c_{TV}(t)\cdot V_T + - (Q_{HA} + Q_{PV} + k_{PT}\cdot V_P + k_{ELP}\cdot V_P)\cdot c_{PV}(t) \tag{9.10}$$

$$V_{T\cdot}\frac{dc_{TV}(t)}{dt} = k_{PT\cdot}c_{PV}(t)\cdot V_P - k_{TP}c_{TV}(t)\cdot V_T \tag{9.11}$$

In which r_{NGIL} and r_{NL} are the formation rates of norverapamil in the gastrointestinal lumen and in the liver compartment, respectively. M_{wV} is the molecular weight of verapamil. This set of equations has to be written for each molecule in the body. Of course all the equations and their initial conditions have to be resolved simultaneously.

Norverapamil

$$\frac{dA_{GILN}(t)}{dt} = G(t)\cdot\frac{dr(t)}{dt} - J_{GILN}(t) - k_{ELGILN}(t)\cdot A_{GILN}(t) + - r_{NGIL}\cdot M_{wN} \tag{9.12}$$

$$V_{GICSN\cdot}\frac{dc_{GICSN}(t)}{dt} = Q_{PV}\cdot c_{PN}(t)\cdot\frac{dr(t)}{dt} - Q_{PV}\cdot c_{GICSN}(t) + + J_{GLN}(t) + J_{SILN}(t) + J_{LILN}(t) \tag{9.13}$$

$$V_L \frac{dc_{LN}(t)}{dt} = Q_{PV} \cdot c_{GICSN}(t) + Q_{HA} \cdot c_{PN}(t) + - (Q_{HV} + CL_H) \cdot c_{LN}(t) - r_{NL} \cdot M_{wN} \quad (9.14)$$

$$V_{P.} \frac{dc_{PN}(t)}{dt} = Q_{HV} \cdot c_{LN}(t) + k_{TP.} c_{TN}(t) \cdot V_T + - (Q_{HA} + Q_{PV} + k_{PT} \cdot V_P + k_{ELP} \cdot V_P) \cdot c_{PN}(t) \quad (9.15)$$

$$V_{T.} \frac{dc_{TN}(t)}{dt} = k_{PT.} c_{PN}(t) \cdot V_P - k_{TP} c_{TN}(t) \cdot V_T \quad (9.16)$$

In which r_{NGIL} and r_{NL} are the formation rates of norverapamil in the gastrointestinal lumen and in the liver compartment, respectively. M_{wN} is the molecular weight of norverapamil.

The norverapamil formation rate has been assumed as a Michaelis-Menten kinetic. This kinetic describes the formation rate for reaction catalyzed by enzymes varying the concentration of substrate.

$$r_{iN} = \frac{V_{MAX} \cdot [S]}{k_M + [S]} \quad (9.17)$$

V_{MAX} is the maximum reaction rate which is realized when the substrate [S] saturates all the enzyme in solution. k_M is the Michaelis-Menten constant, it is the substrate concentration at which the reaction rate is the half of the maximum one. The values of these parameters are shown in [97].

Table 25. Michaelis-Menten kinetics parameters.

Compartment	V_{MAX} [mol/s·kg]	k_M [mol/m^3]	[S] [kg/m^3]
Gastrointestinal tract	$5.05 \cdot 10^{-6}$	0.041	A_{iV}/V_B
liver	$3.31 \cdot 10^{-6}$	0.03	C_{LV}

The substrate concentrations are exactly the verapamil concentrations in gastrointestinal tract and liver, it means that they are the differential equation solutions.

This set of 10 differential equations has to be written for each isomer.

9.3.1 Model simulations

The *in silico* model has been used to fit the experimental data (plasmatic concentrations of the molecules) changing the pharmacokinetic parameters. The results are reported for the four molecules (S and R-verapamil, S and R-norverapamil) and the four groups of subjects (young and elderly, male and female) and compared with the experimental data. The blue triangle are the experimental data, the continuous lines are the model simulation.

Concerning the S-isomer, the results are:

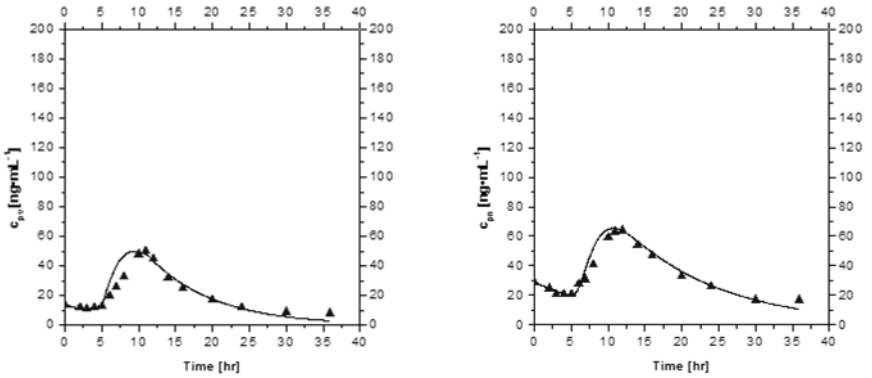

Figure 120. Plasma concentration of S-verapamil (left) and S-norverapamil (right) for elderly females (EF).

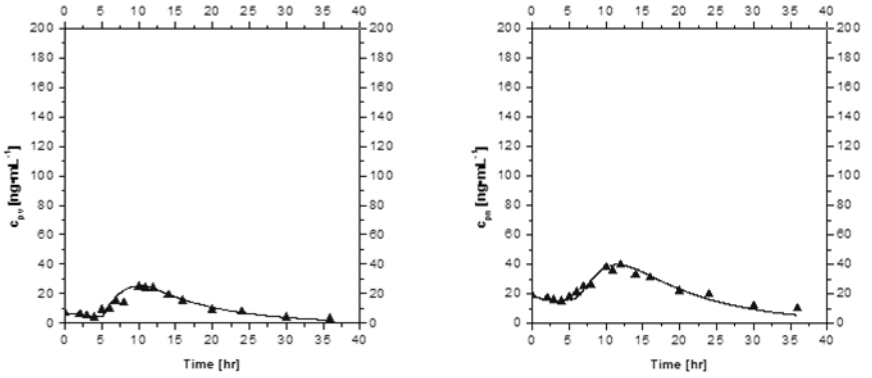

Figure 121. Plasma concentration of S-verapamil (left) and S-norverapamil (right) for elderly males (EM).

It could be seen that the plasma concentration of the S-isomer is higher in the elderly females than in the elderly males. Among of the two isomers, the concentrations are comparable. The prediction of the

model are acceptable in these cases. Little imprecisions there are in the case of S-verapamil for the elderly females.

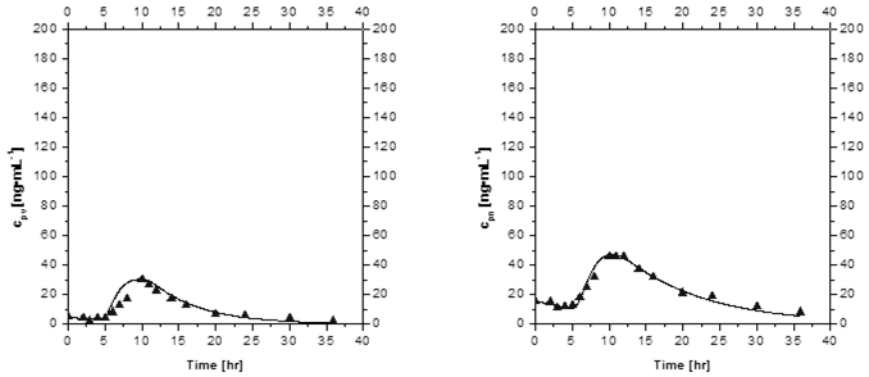

Figure 122. Plasma concentration of S-verapamil (left) and S-norverapamil (right) for young females (YF).

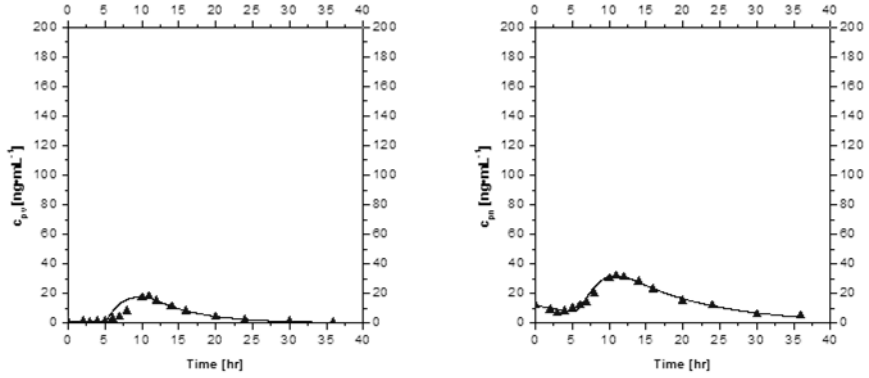

Figure 123. Plasma concentration of S-verapamil (left) and S-norverapamil (right) for young males (YM).

In these cases the concentrations of norverapamil are quite higher than those of verapamil. The model simulation fit sufficiently the experimental data.

Concerning the R-isomer, the results are:

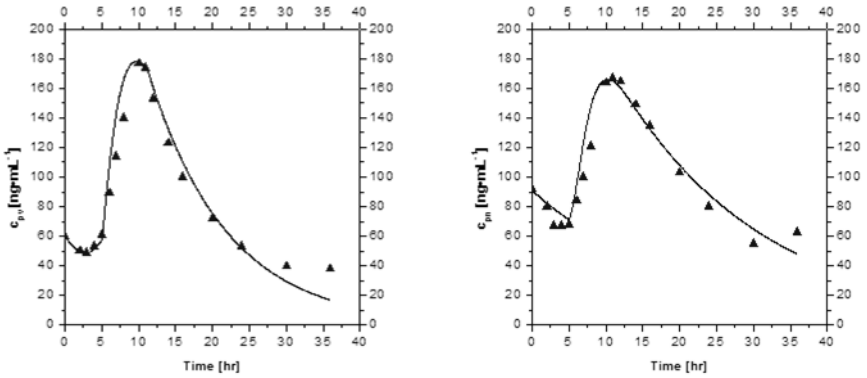

Figure 124. Plasma concentration of R-verapamil (left) and R-norverapamil (right) for elderly females (EF).

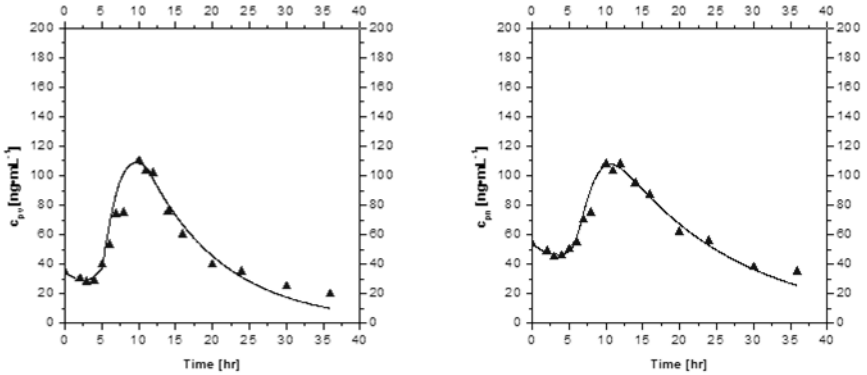

Figure 125. Plasma concentration of R-verapamil (left) and R-norverapamil (right) for elderly males (EM).

In the case of R-isomer the concentrations are higher than the case of S-isomer. The model prediction are satisfactory but the end of the curve which is not correctly predicted.

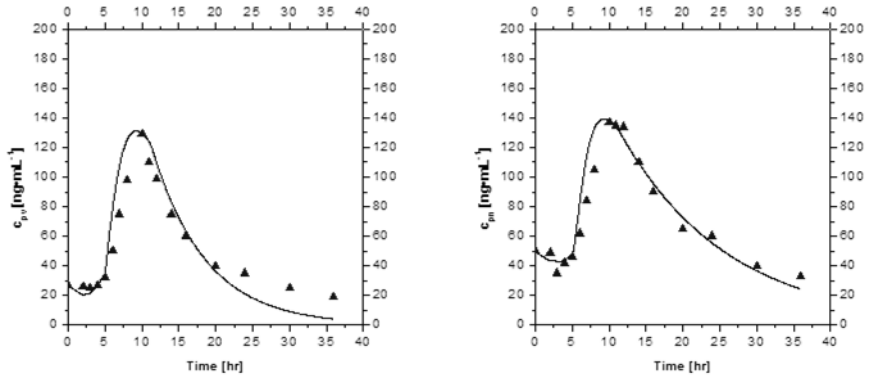

Figure 126. Plasma concentration of R-verapamil (left) and R-norverapamil (right) for young females (YF).

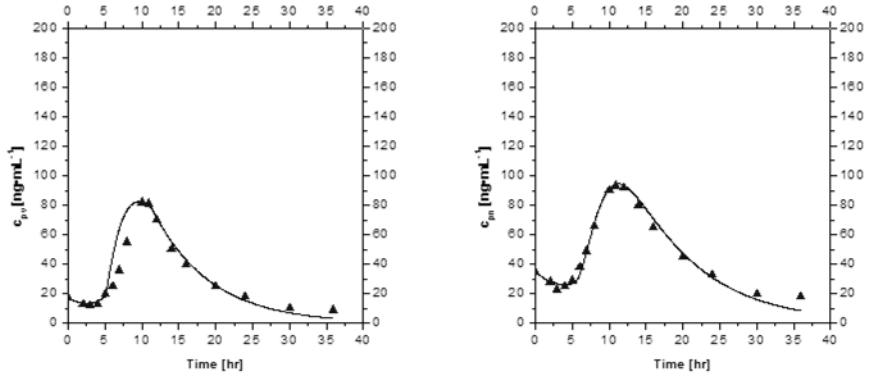

Figure 127. Plasma concentration of R-verapamil (left) and R-norverapamil (right) for young males (YM).

To test the reliability of the model and its applicability to the experimental data, the pharmacokinetic parameters of the data and those resulting from the model were compared. The results are reported in the following tables.

Table 26. Area under curve of the experimental data and of the model for verapamil and norverapamil (S-isomer). The error is reported.

		AUC_V	AUC_N	$(R_V)^2$	$(R_N)^2$
S-EF	exp	$2.64 \cdot 10^6$	$4.40 \cdot 10^6$	0.89	0.96
	mod	$2.56 \cdot 10^6$	$4.32 \cdot 10^6$		
	err	-3%	-2%		
S-YF	exp	$1.28 \cdot 10^6$	$3.05 \cdot 10^6$	0.89	0.98
	mod	$1.3 \cdot 10^6$	$2.76 \cdot 10^6$		
	err	1.56%	-9.5%		
S-EM	exp	$1.42 \cdot 10^6$	$2.97 \cdot 10^6$	0.91	0.97
	mod	$1.39 \cdot 10^6$	$2.69 \cdot 10^6$		
	err	-2%	9%		
S-YM	exp	$6.53 \cdot 10^5$	$2.03 \cdot 10^6$	0.81	0.97
	mod	$7.13 \cdot 10^5$	$1.95 \cdot 10^6$		
	err	9.2%	-3.84%		

Table 27. Pharmacokinetic parameters of the experimental data and of the model for verapamil and norverapamil (S-isomer). The error is reported.

		$t_{max,V}$	$t_{max,N}$	$C_{max,V}$	$C_{max,N}$
S-EF	exp	11	12	50	64
	mod	10	11	49.65	65.28
	err	-9%	8.3%	-0.7%	2%
S-YF	exp	10	10	30	46
	mod	6	10.42	30.11	46.85
	err	-4.0%	4.2%	0.36%	1.8%
S-EM	exp	10	12	25	40
	mod	10.48	11.63	25.26	39.85
	err	4.8%	-3.08%	1%	0.38%
S-YM	exp	11	11	18	32
	mod	10	10.98	17.43	31.94
	err	9.1%	-0.18%	3.16	0.2%

The same comparison was done per the R-isomer.

Table 28. Area under curve of the experimental data and of the model for verapamil and norverapamil (R-isomer). The error is reported.

		AUC_V	AUC_N	$(R_V)^2$	$(R_N)^2$
R-EF	exp	$1.07 \cdot 10^7$	$1.3 \cdot 10^7$	0.96	0.93
	mod	$1.02 \cdot 10^7$	$1.3 \cdot 10^7$		
	err	-4.7%			
R-YF	exp	$6.6 \cdot 10^6$	$9.4 \cdot 10^6$	0.93	0.91
	mod	$6 \cdot 10^6$	$9.12 \cdot 10^6$		
	err	-9%	-2.98%		
R-EM	exp	$6.46 \cdot 10^6$	$8.46 \cdot 10^6$	0.93	0.96
	mod	$6.21 \cdot 10^6$	$8.04 \cdot 10^6$		
	err	-3.87%	-4.96%		
R-YM	exp	$3.94 \cdot 10^6$	$6.04 \cdot 10^6$	0.89	0.99
	mod	$3.89 \cdot 10^6$	$5.58 \cdot 10^6$		
	err	-1.27%	-7.62%		

Table 29. Pharmacokinetic parameters of the experimental data and of the model for verapamil and norverapamil (R-isomer). The error is reported.

		$t_{max,V}$	$t_{max,N}$	$C_{max,V}$	$C_{max,N}$
R-EF	exp	10	11	177	167
	mod	9.72	10.26	177.94	166.01
	err	-2.8%	-6.69%	0.53%	-0.59%
R-YF	exp	10	10	129	137
	mod	9.22	9.33	129.56	138.16
	err	-7.8%	-6.75%	0.43%	0.85%
R-EM	exp	10	10	110	108
	mod	9.65	10.66	108.45	107.6
	err	-3.5%	6.66%	-1.41%	-0.37%
R-YM	exp	10	11	82	93
	mod	9.58	11.31	82.02	94.31
	err	-4.17%	2.82%	0.02%	1.41%

In all the cases the error between the experimental results and the model predictions is less than 10%. It could be concluded that the model could be used satisfactorily for the simulations of verapamil and norverapamil plasma concentrations.

9.3.2 Model parameters

As mentioned above, the model parameters are increased in number respect to the previously version of the model because the norverapamil formation kinetic has been taken into account. After the simulation of all the experimental data set, the model parameters for both the S and the R-isomer of verapamil and norverapamil were compared. Obviously, this match was done for all the class of subject: elderly males and females and young males and females. The results are shown in term of histograms.

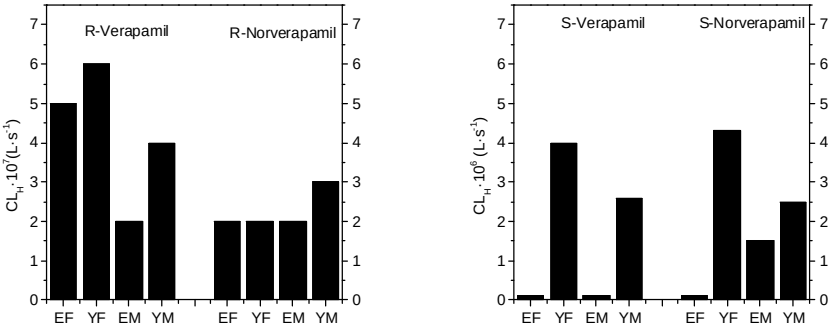

Figure 128. Hepatic clearance of verapamil and norverapamil for all the groups of subjects.

It could be seen that R-verapamil is removed from the blood easier than S-verapamil. Moreover, it is clear than the liver of young people removes the drug easier than the liver of elderly people.

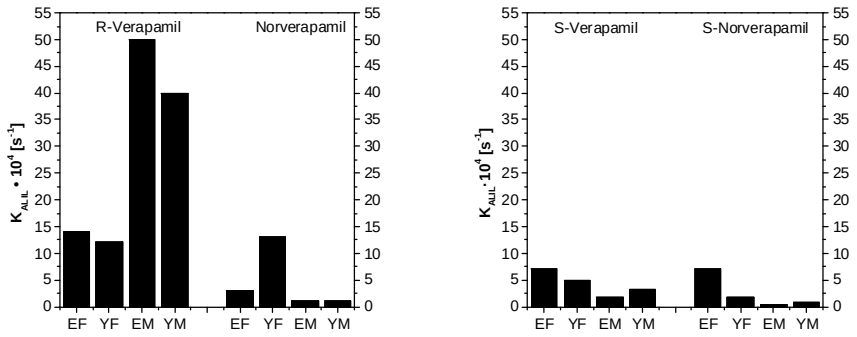

Figure 129. Absorption kinetic constant in the large intestine of verapamil and norverapamil for all the groups of subjects.

It could be seen that males absorb the drug in large intestine more than three times faster than the females. Moreover, verapamil is absorbed easier than norverapamil in almost all the cases.

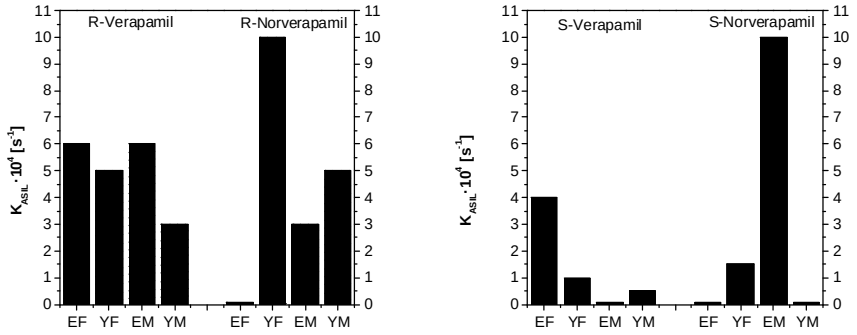

Figure 130. Absorption kinetic constant in the large intestine of verapamil and norverapamil for all the groups of subjects.

Concerning the absorption in the large intestine, the differences between males and females are not so marked as in the precedent case. In general, it could be said that the absorption kinetic of the R-isomers is faster than the S-isomers.

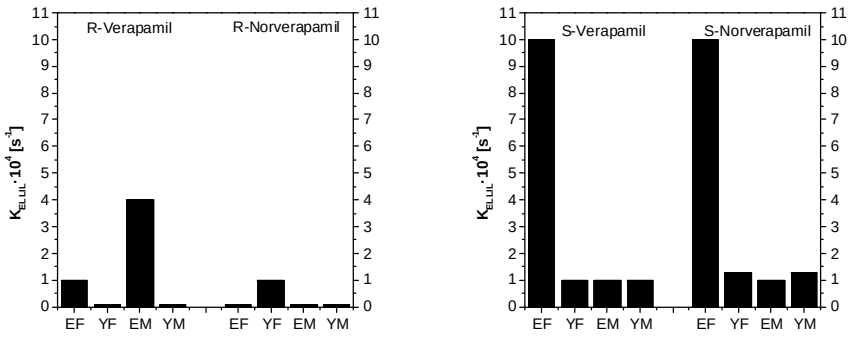

Figure 131. Elimination kinetic constant in the large intestine of verapamil and norverapamil for all the groups of subjects.

The S-isomers are eliminated faster than the R-isomers, particularly from elderly female.

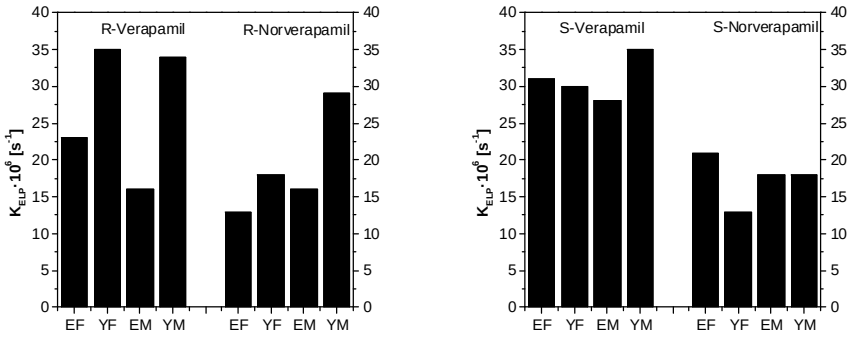

Figure 132. Elimination kinetic constant in the plasma of verapamil and norverapamil for all the groups of subjects.

The plasma elimination rate is faster for young subjects and slower for elderly subjects.

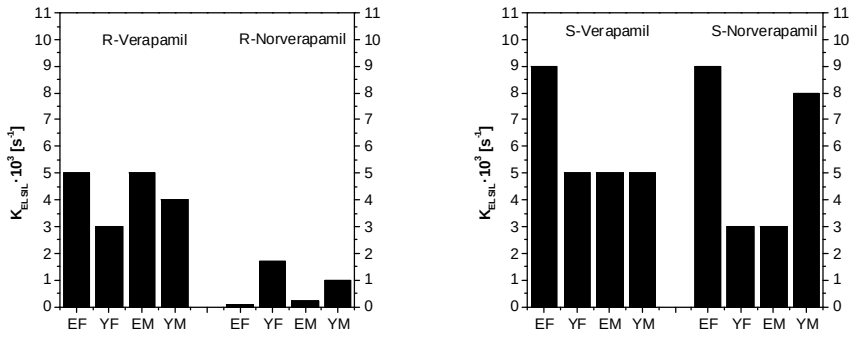

Figure 133. Elimination kinetic constant in the small intestine of verapamil and norverapamil for all the groups of subjects

The S-isomer is eliminated faster than the R-isomer. Moreover, no changes in the elimination rate could be appreciated among the different groups of subjects.

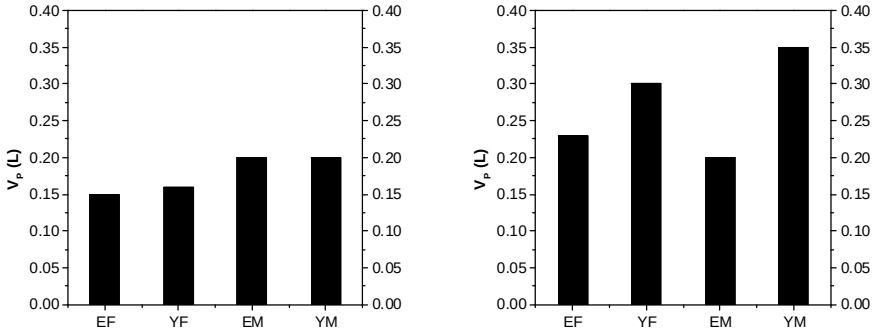

Figure 134. Plasma volume for R-isomer (left) and S-isomer (right).

The plasma volume takes into account also the percentage of the protein-bounded drug. This feature makes possible that two different plasma volumes are calculated for the R and S-isomers. It could be seen that the volume is smaller in the elderly subjects than the young ones. Moreover, males have a bigger plasma volume than females.

Chapter Ten

Conclusions

In this chapter the conclusions of the work are illustrated. The future perspectives of the research are proposed.

10.1 Conclusions

During these activities, *in vitro* and *in silico* models have been developed to model and predict the phenomena involved in the drug assumption.

Concerning the *in vitro* models, a device able to reproduce a given pH history in the gastrointestinal tract has been developed. The device is able to measure the pH of the dissolution medium and, by the use of a dedicated software, to adjust its value to follow a set point pattern. The device is completely automatized and could be used to reproduce the real pH history experienced by the drug in the gastrointestinal tract. Conventional release patterns of several pharmaceuticals have been evaluated and compared with the release pattern obtained if the real pH history is followed. The main result obtained is that the release patterns are completely different and, in particular, it was demonstrated that a pH higher in the first stage of dissolution (as the real one) could influence significantly the release pattern and undesired behavior could be obtained.

Once the chemical history has been reproduced, the mass transport across the intestinal wall has been faced. Using an hollow fibers filter in which two fluids flow, one simulating the intestinal content and the other simulating the blood flow, the drug exchange is studied. Firstly the permeability of the drug and the mass exchange rate varying the flow rate of the fluids are investigated. The release patterns of various systems considering the mass exchange and the conventional USP dissolution method are analyzed. The concentrations in both the vessels (donor and acceptor compartments) are evaluated and compared with the release pattern obtained according with the conventional method. Then, the effect of mass exchange was combined with the effect of the pH real history and the release patterns are evaluated. It has been observed that the influence of a different pH evolution on the release pattern is higher in the first stage of dissolution but it loose relevance in the following stage. When the pH is rapidly increased, in the case of the use of the new apparatus, the increase in the amount of drug release is immediate, in the conventional case it is more gradual. On the contrary, the amount of drug which is transferred between the two compartment is approximately the same between the two methods.

The final step has been consisted on the reproduction of the gastric motility. The main component of the device was the artificial stomach

connected to a camshaft which has the role to generate the peristaltic waves. In fact, with the rotation of the cams, the connections shrink the stomach which, locally, reduces its volume. By the use of this device which better reproduce the human physiology, the release patterns of commercial tablet have been evaluated and compared with the conventional one. The device built has found to be able to better reproduce the poor mixing of the stomach. Moreover, the release pattern was found to be influenced by the different mixing. In fact, the reproduced contractions damage significantly the tablet affecting the dissolution rate.

Concerning the *in silico* models, a physiologically based pharmacokinetic model has been used to simulate the fate of a drug once it has been administered. The model was composed by seven differential equations and their initial conditions, each representing the mass balance of one compartment, which has the role to describe the human body. The equations have to be solved simultaneously and describe the concentrations of a drug in each compartment. To be effective, the model needs of an *in vitro* dissolution function which describe the dissolution kinetic of a tablet and it needs a limited number of parameters. The model has been used to simulate the plasmatic concentration of diclofenac using the *in vitro* dissolution patterns obtained by the new device. Once obtained the values of the parameters by fitting the plasmatic concentration of diclofenac (taken by literature), the model is able to simulate the plasmatic concentration in the case in which the conventional dissolution pattern is followed or a pH history is experienced by the pharmaceutical form. Comparing the plasmatic concentrations obtained by the two methods, it was noted that the profiles are qualitatively and quantitatively different which means that the plasmatic concentration is very different in the reality from the expected one.

Once developed the method to reproduce the mass transport in the intestine, a conventional release pattern has been used as forcing function to compare the gastrointestinal concentration obtained *in vitro* (simulating the mass exchange) with the one predict by the model. The two patterns were very similar, meaning that the main transport phenomena have been identified and correctly reproduce by both of the two approaches.

Finally, the model was refined to take into account also the effect of the inter-individual parameters on the pharmacokinetic parameters.

The experimental data of the plasmatic concentration of a drug (S- and R-verapamil and their metabolites) were taken from literature for different groups of subjects, divided on the base on the age and gender. Because of the kinetic of drug metabolization in the gastrointestinal tract and in the liver, the equations of the model have been modified to take into account the simultaneous presence of different molecules (drug and its main metabolites) in the body. The model has been used to fit the concentration value modifying the model parameters. Then, the parameter values were compared to evaluate the effect of the gender and age.

To sum up, both the *in vitro* and the *in silico* tools have been used in conjunction to reproduce and model the phenomena involved in the drug assumptions.

10.2 Future perspectives

The future perspectives of this work are addressed to a more realistic and careful reproduction of the phenomena which take place in the human body after drug assumption.

Concerning the mass transport reproduction, after the simulation of the mass transport across the intestinal wall, even the cleaning and metabolization functions of the liver should be taken into account. This means to add another compartment in the model (simulating the liver) which continuously cleans the compartment simulating the gastrointestinal circulatory system from the drug. The model will be constituted by three different compartments that exchange drug simultaneously. Concerning the peristaltic waves reproduction, it could be useful, after the realization of the device simulating the contractions, to reproduce exactly the same strength of the waves and the same reduction in volume between the artificial stomach and the real one. Measuring the drug content in all the portions of the stomach along its length it could useful to understand the mixing mechanisms.

Once realized all the components of the reproduced human body, all the parts have to be connected between them to realize a single device able to reproduce the entire pattern from the stomach to the liver of drugs.

Concerning the *in silico* model, the model could be refined taking into account the presence of the inter-individual parameters in the model equation. It could be possible making the pharmacokinetic parameters

dependent on the inter-individual parameters (i.e. age, gender, or body mass). Despite the number of parameters will be increased, it has to be considered that the model become predictive useful for a subjective therapy.

References

1. Brink, B., J. Schlegel, and C. Code, *The pressure profile of the gastroduodenal junctional zone in dogs*. British Medical Journal, 1965. **6**(2): p. 163.
2. Kelly, K., *Gastric emptying of liquids and solids: roles of proximal and distal stomach*. The American journal of physiology, 1980. **239**(2): p. G71.
3. MCrea, E., et al., *The normal movements of the stomach*. Experimental Physiology, 1924. **14**(4): p. 379-397.
4. Sheiner, H., *Gastric emptying tests in man*. British Medical Journal, 1975. **16**(3): p. 235.
5. Barker, M., I. Cobden, and A. Axon, *Proximal stomach and antrum in stomach emptying*. British Medical Journal, 1979. **20**(4): p. 309.
6. McConnell, E., H. Fadda, and A. Basit, *Gut instincts: explorations in intestinal physiology and drug delivery*. International journal of pharmaceutics, 2008. **364**(2): p. 213-226.
7. Weitschies, W., et al., *Magnetic marker monitoring: an application of biomagnetic measurement instrumentation and principles for the determination of the gastrointestinal behavior of magnetically marked solid dosage forms*. Advanced drug delivery reviews, 2005. **57**(8): p. 1210-1222.
8. Diakidou, A., et al., *Characterization of the contents of ascending colon to which drugs are exposed after oral administration to healthy adults*. Pharmaceutical research, 2009. **26**(9): p. 2141-2151.

9. Jantratid, E., et al., *Dissolution media simulating conditions in the proximal human gastrointestinal tract: an update.* Pharmaceutical research, 2008. **25**(7): p. 1663-1676.

10. Dressman, J.B. and H. Lennernäs, *Oral drug absorption*. 2000: Marcel Dekker.

11. Grassi, M., *Understanding drug release and absorption mechanisms: A physical and mathematical approach*. 2007: CRC.

12. Amidon, G., et al., *A theoretical basis for a biopharmaceutic drug classification: the correlation of in vitro drug product dissolution and in vivo bioavailability.* Pharmaceutical research, 1995. **12**(3): p. 413-420.

13. Banakar, U., *Pharmaceutical dissolution testing.* Drugs and the pharmaceutical sciences, 1991. **49**: p. 1-426.

14. FDA, *Guidance for industry. Extended release oral dosage forms:development, avaluation, and application of in vitro/in vivo correlations. Center for Drug Evaluation and Research (CDER).* 1997.

15. XXIII, U. *The United States Pharmacopeia*. 1995.

16. Pillay, V. and R. Fassihi, *Unconventional dissolution methodologies.* Journal of Pharmaceutical Sciences, 1999. **88**(9): p. 843-851.

17. Stricker, H., *Die Arzneistoffresorption im Gastrointestinaltrakt - ln vitro-Untersuchung Lipophiler Substanzen.* Pharm Ind, 1973. **35**(1): p. 13 - 17.

18. Savalle, B., G. Miranda, and J. Pelissier, *In vitro simulation of gastric digestion of milk proteins.* Journal of Agricultural and Food Chemistry, 1989. **37**(5): p. 1336-1340.

19. M. Minekus, P.M., R. Havenaar and J. H. J. Huis in't Veld, *A Multicompartmental Dynamic Computer - controlled Model Simulating the Stomach and Small Intestine.* Alternatives to Laboratory Animals, 1995. **23**: p. 197 - 209.

20. Minekus, M. and R. Havenaar, *In vitro model of an in vivo digestive tract*. 1996, US Patent 5,525,305.

21. Minekus, M., et al., *A computer-controlled system to simulate conditions of the large intestine with peristaltic mixing, water absorption and absorption of fermentation products.* Applied Microbiology and Biotechnology, 1999. **53**(1): p. 108-114.

22. Blanquet, S., et al., *The 'biodrug' concept: an innovative approach to therapy.* Trends in biotechnology, 2001. **19**(10): p. 393-400.

23. Cardot, J., E. Beyssac, and M. Alric, *In Vitro-In Vivo Correlation: Importance of Dissolution in IVIVC.* Dissolution Technologies, 2007. **14**(1): p. 15.

24. K.Tam, Y. and K.E. Anderson, *Simulated Biological Dissolution and Absorption System.* U. S. Patent 6,022,733, 2000.

25. Wickham, M. and R. Faulks, *International Publication Number WO 2007/010238*. 2007.

26. Rozga, J. and A. Demetriou, *Artificial gut*. 2002, US Patent 6,379,619 B1.

27. Garbacz, G., et al., *Irregular absorption profiles observed from diclofenac extended release tablets can be predicted using a dissolution test apparatus that mimics in vivo physical stresses.* European Journal of Pharmaceutics and Biopharmaceutics, 2008. **70**(2): p. 421-428.

28. Garbacz, G., et al., *Comparison of dissolution profiles obtained from nifedipine extended release once a day products using different dissolution test apparatuses.* European Journal of Pharmaceutical Sciences, 2009. **38**(2): p. 147-155.

29. Garbacz, G., et al., *Investigation of the dissolution characteristics of nifedipine extended-release formulations using USP apparatus 2 and a novel dissolution apparatus.* Dissol Tech, 2009. **16**: p. 7-13.

30. BOGATAJ, M., G. COF, and A. MRHAR, *PERISTALTIC MOVEMENT SIMULATING STIRRING DEVICE FOR DISSOLUTION TESTING*. 2010, WO Patent WO/2010/014,046.

31. Schulze, K., *Imaging and modelling of digestion in the stomach and the duodenum.* Neurogastroenterology & Motility, 2006. **18**(3): p. 172-183.

32. Goldsmith, H.S. and H. Akiyama, *A comparative study of Japanese and American gastric dimensions*. Annals of surgery, 1979. **190**(6): p. 690.

33. Pal, A., et al., *Gastric flow and mixing studied using computer simulation*. Proceedings of the Royal Society of London. Series B: Biological Sciences, 2004. **271**(1557): p. 2587-2594.

34. Pal, A., J.G. Brasseur, and B. Abrahamsson, *A stomach road or "Magenstrasse" for gastric emptying*. Journal of biomechanics, 2007. **40**(6): p. 1202-1210.

35. Ferrua, M. and R. Singh, *Modeling the fluid dynamics in a human stomach to gain insight of food digestion*. Journal of food science, 2010. **75**(7): p. R151-R162.

36. Ferrua, M.J., F. Kong, and R.P. Singh, *Computational modeling of gastric digestion and the role of food material properties*. Trends in Food Science & Technology, 2011.

37. Jain, R., et al., *Kinetics of uptake, distribution, and excretion of zinc in rats*. Annals of Biomedical Engineering, 1981. **9**(4): p. 347-361.

38. Gueorguieva, I., I. Nestorov, and M. Rowland, *Reducing whole body physiologically based pharmacokinetic models using global sensitivity analysis: diazepam case study*. Journal of pharmacokinetics and pharmacodynamics, 2006. **33**(1): p. 1-27.

39. Nestorov, I., L. Aarons, and M. Rowland, *Physiologically based pharmacokinetic modeling of a homologous series of barbiturates in the rat: a sensitivity analysis*. Journal of pharmacokinetics and pharmacodynamics, 1997. **25**(4): p. 413-447.

40. Yu, L. and G. Amidon, *A compartmental absorption and transit model for estimating oral drug absorption*. International journal of pharmaceutics, 1999. **186**(2): p. 119-125.

41. Yu, L., et al., *Transport approaches to the biopharmaceutical design of oral drug delivery systems: prediction of intestinal absorption*. Advanced drug delivery reviews, 1996. **19**(3): p. 359-376.

42. Agoram, B., W. Woltosz, and M. Bolger, *Predicting the impact of physiological and biochemical processes on oral drug bioavailability.* Advanced drug delivery reviews, 2001. **50**: p. S41-S67.

43. Jamei, M., et al., *Population-based mechanistic prediction of oral drug absorption.* The AAPS journal, 2009. **11**(2): p. 225-237.

44. Jamei, M., et al., *The Simcyp® population-based ADME simulator.* 2009.

45. Di Muria, M., G. Lamberti, and G. Titomanlio, *Physiologically Based Pharmacokinetics: A Simple, All Purpose Model.* Industrial & Engineering Chemistry Research, 2010. **49**(6): p. 2969-2978.

46. Grass, G., *Simulation models to predict oral drug absorption from in vitro data.* Advanced drug delivery reviews, 1997. **23**(1-3): p. 199-219.

47. Willmann, S., et al., *A physiologic model for simulating gastrointestinal flow and drug absorption in rats.* Pharmaceutical research, 2003. **20**(11): p. 1766-1771.

48. Willmann, S., A. Edginton, and J. Dressman, *Development and validation of a physiology-based model for the prediction of oral absorption in monkeys.* Pharmaceutical research, 2007. **24**(7): p. 1275-1282.

49. Willmann, S., et al., *A physiological model for the estimation of the fraction dose absorbed in humans.* J. Med. Chem, 2004. **47**(16): p. 4022-4031.

50. Plusquellec, Y., et al., *A pharmacokinetic model for multiple sites discontinuous gastrointestinal absorption.* Medical engineering & physics, 1999. **21**(8): p. 525-532.

51. Kamlet, M.J., et al., *Linear solvation energy relationships: 36. Molecular properties governing solubilities of organic nonelectrolytes in water.* Journal of Pharmaceutical Sciences, 1986. **75**(4): p. 338-349.

52. Stewart, B.H., et al., *Discrimination between drug candidates using models for evaluation of intestinal absorption.* Advanced drug delivery reviews, 1997. **23**(1): p. 27-45.

53. Lennernäs, H., et al., *Comparison between active and passive drug transport in human intestinal epithelial (Caco-2) cells in vitro and human jejunum in vivo.* International journal of pharmaceutics, 1996. **127**(1): p. 103-107.

54. Irvine, J.D., et al., *MDCK (Madin–Darby canine kidney) cells: a tool for membrane permeability screening.* Journal of Pharmaceutical Sciences, 1999. **88**(1): p. 28-33.

55. Di, L., et al., *Development of a new permeability assay using low-efflux MDCKII cells.* Journal of Pharmaceutical Sciences, 2011. **100**(11): p. 4974-4985.

56. Tavelin, S., et al., *Prediction of the oral absorption of low-permeability drugs using small intestine-like 2/4/A1 cell monolayers.* Pharmaceutical research, 2003. **20**(3): p. 397-405.

57. Linnankoski, J., et al., *Paracellular porosity and pore size of the human intestinal epithelium in tissue and cell culture models.* Journal of Pharmaceutical Sciences, 2009. **99**(4): p. 2166-2175.

58. Kansy, M., F. Senner, and K. Gubernator, *Physicochemical high throughput screening: parallel artificial membrane permeation assay in the description of passive absorption processes.* Journal of medicinal chemistry, 1998. **41**(7): p. 1007-1010.

59. Avdeef, A., *Absorption and drug development: solubility, permeability, and charge state*. 2003, Hoboken: John Wiley & Sons, Inc.

60. Wohnsland, F. and B. Faller, *High-throughput permeability pH profile and high-throughput alkane/water log P with artificial membranes.* Journal of medicinal chemistry, 2001. **44**(6): p. 923-930.

61. Obata, K., et al., *Biopharmaceutics classification by high throughput solubility assay and PAMPA.* Drug development and industrial pharmacy, 2004. **30**(2): p. 181-185.

62. Sugano, K., et al., *High throughput prediction of oral absorption: improvement of the composition of the lipid solution used in parallel artificial membrane permeation assay.* Journal of biomolecular screening, 2001. **6**(3): p. 189-196.

63. Levet-Trafit, B., et al., *Estimation of oral drug absorption in man based on intestine permeability in rats*. Life sciences, 1996. **58**(24): p. PL359-PL363.

64. LENNERNÄS, H., et al., *A Residence-Time Distribution Analysis of the Hydrodynamics within the Intestine in Man during a Regional Single-pass Perfusion with Loc-I-Gut: In-vivo Permeability Estimation*. Journal of pharmacy and pharmacology, 1997. **49**(7): p. 682-686.

65. Takamatsu, N., et al., *Human intestinal permeability of piroxicam, propranolol, phenylalanine, and PEG 400 determined by jejunal perfusion*. Pharmaceutical research, 1997. **14**(9): p. 1127-1132.

66. Barba, A.A., et al., *Synthesis and characterization of P (MMA-AA) copolymers for targeted oral drug delivery*. Polymer bulletin, 2009. **62**(5): p. 679-688.

67. Marteau, P., et al., *Effect of the microbial lactase (EC 3.2. 1.23) activity in yoghurt on the intestinal absorption of lactose: an in vivo study in lactase-deficient humans*. British Journal of Nutrition, 1990. **64**(01): p. 71-79.

68. Cascone, S., G. Lamberti, and G. Titomanlio, *A rule of thumb in designing in-vitro systems to simulate the intestinal absorption*. Heat and Mass Transfer. **Submitted**.

69. Cascone, S., et al., *Microencapsulation effectiveness of small active molecules in biopolymer by ultrasonic atomization technique*. Drug development and industrial pharmacy, 2012(00): p. 1-8.

70. Barba, A.A., et al., *Simultaneous measurement of theophylline and cellulose acetate phthalate in phosphate buffer by UV analysis*. Canadian Journal of Analytical Sciences and Spectroscopy, 2008. **53**(6): p. 249-253.

71. Cascone, S., et al., *The influence of dissolution conditions on the drug ADME phenomena*. European Journal of Pharmaceutics and Biopharmaceutics, 2011.

72. Ikeda, S. and K. Nishinari, *Intermolecular forces in bovine serum albumin solutions exhibiting solidlike mechanical behaviors*. Biomacromolecules, 2000. **1**(4): p. 757-763.

73. SADLER, P.J. and A. TUCKER, *pH induced structural transitions of bovine serum albumin*. European Journal of Biochemistry, 1993. **212**(3): p. 811-817.

74. Matsuyama, H., M. Teramoto, and H. Urano, *Analysis of solute diffusion in poly (vinyl alcohol) hydrogel membrane*. Journal of membrane science, 1997. **126**(1): p. 151-160.

75. Smith, E.L., et al., *B12 vitamins (cobalamins). 1. Vitamins B12c and B12d*. Biochemical Journal, 1952. **52**(3): p. 389.

76. Brennan, R.A. and R.A. Sanford, *Continuous steady-state method using Tenax for delivering tetrachloroethene to chloro-respiring bacteria*. Applied and environmental microbiology, 2002. **68**(3): p. 1464.

77. Mudry, B., et al., *Quantitative structure-permeation relationship for iontophoretic transport across the skin*. Journal of Controlled Release, 2007. **122**(2): p. 165-172.

78. Sangster, J., *Octanol-water partition coefficients: fundamentals and physical chemistry*. 1997: Wiley.

79. Pade, V. and S. Stavchansky, *Link between drug absorption solubility and permeability measurements in Caco 2 cells*. Journal of Pharmaceutical Sciences, 1998. **87**(12): p. 1604-1607.

80. Vaughan, A.D., J.B. Zhang, and M.E. Byrne, *Enhancing therapeutic loading and delaying transport via molecular imprinting and living/controlled polymerization*. AIChE Journal, 2010. **56**(1): p. 268-279.

81. Lee, H.S., et al., *Simultaneous determination of aceclofenac and diclofenac in human plasma by narrowbore HPLC using column-switching*. Journal of pharmaceutical and biomedical analysis, 2000. **23**(5): p. 775-781.

82. Scheytt, T., et al., *1-Octanol/water partition coefficients of 5 pharmaceuticals from human medical care: carbamazepine, clofibric acid, diclofenac, ibuprofen, and propyphenazone*. Water, Air, & Soil Pollution, 2005. **165**(1): p. 3-11.

83. Crommlin, D., J. Modderkolk, and C. De Blaey, *The pH dependence of rectal absorption of theophylline from solutions of aminophylline in situ in rats*. International journal of pharmaceutics, 1979. **3**(6): p. 299-309.

84. Pinsuwan, S., A. Li, and S.H. Yalkowsky, *Correlation of octanol/water solubility ratios and partition coefficients.* Journal of Chemical and Engineering Data, 1995. **40**(3): p. 623-626.

85. Rinaki, E., G. Valsami, and P. Macheras, *Quantitative biopharmaceutics classification system: The central role of dose/solubility ratio.* Pharmaceutical research, 2003. **20**(12): p. 1917-1925.

86. Mauri, R., *La reologia e il flusso del sangue.*

87. Weinreb, J., et al., *Portal vein measurements by real-time sonography.* American Journal of Roentgenology, 1982. **139**(3): p. 497.

88. Bradley, S., et al., *The estimation of hepatic blood flow in man.* Journal of Clinical Investigation, 1945. **24**(6): p. 890.

89. Takahashi, T. and T. Sakata, *Viscous properties of pig cecal contents and the contribution of solid particles to viscosity.* Nutrition, 2004. **20**(4): p. 377-382.

90. Lamberti, G., et al., *In-vitro simulation of drugs intestinal absorption.* International journal of pharmaceutics, 2012.

91. Willis, J., et al., *The pharmacokinetics of diclofenac sodium following intravenous and oral administration.* European Journal of Clinical Pharmacology, 1979. **16**(6): p. 405-410.

92. Nishihata, T., et al., *Clinical investigation of sodium diclofenac sustained-release suppositories.* International journal of pharmaceutics, 1988. **42**(1): p. 251-256.

93. Winek, C.L., W.W. Wahba, and T.W. Balzer, *Drug and chemical blood-level data 2001.* Forensic science international, 2001. **122**(2): p. 107-123.

94. Gupta, S., et al., *Age and gender related changes in stereoselective pharmacokinetics and pharmacodynamics of verapamil and norverapamil.* British journal of clinical pharmacology, 1995. **40**(4): p. 325.

95. Kim, C., *Asymmetrically coated table.* 2006, Google Patents.

96. Abernethy, D.R., et al., *Stereoselective verapamil disposition and dynamics in aging during racemic verapamil administration.* Journal of Pharmacology and Experimental Therapeutics, 1993. **266**(2): p. 904.

97. Von Richter, O., et al., *Cytochrome P450 3A4 and P-glycoprotein Expression in Human Small Intestinal Enterocytes and Hepatocytes: A Comparative Analysis in Paired Tissue Specimens&ast*. Clinical Pharmacology & Therapeutics, 2004. **75**(3): p. 172-183.

Short curriculum

Sara Cascone was born on March 23rd, 1985. She gained the high school degree in 2004 and started to study Chemical Engineering at University of Salerno. She achieved the bachelor degree in Chemical Engineering, cum laude, in 2007. Then, she obtained the master degree in Chemical Engineering, summa cum laude, in November 2009 with a project dealing with microencapsulation of biopolymer by ultrasonic assisted atomization. Since November 2009 she attends the Doctorate course in "Science and technologies for chemical, pharmaceutical and food industry" (XI cycle 2009-2012), with a project dealing with *in silico* and *in vitro* models in pharmacokinetic studies. She produced 10 papers on international journals and 10 communications to international conferences.

Papers

1. **S. Cascone**, G. Lamberti, M. Cafaro, G. Titomanlio, "Measurements of water content in cellulose derivative (HPMC) based hydrogels via texture analysis", *Carbohydrate Polymers*, 92(1) 765-768 (2013).
2. G. Lamberti, **S. Cascone**, M. Iannaccone, G. Titomanlio, "In-vitro simulation of drugs intestinal absorption", *International Journal of Pharmaceutics*, 439(1-2) 165-168 (2012).
3. G. Lamberti, **S. Cascone**, G. Titomanlio, "An engineering approach to biomedical sciences: advanced testing methods and pharmacokinetic modeling", *Translational Medicine @ UniSa*, 4 (4) 34-38 (2012).
4. G. Lamberti, **S. Cascone**, G. Titomanlio, A.A. Barba, "Controlled release of drugs from hydrogel based matrices systems: experiments and modeling", *Chemical And Biochemical Engineering Quarterly*, 26(4) 321-330 (2012).

5. **S. Cascone**; Lamberti, G.; Titomanlio, G.; Barba, A.A.; d'Amore, M. Microencapsulation effectiveness of small active molecules in biopolymer by ultrasonic atomization technique, *Drug Development and Industrial Pharmacy*, 38(12) 1486-1493 (2012).

6. **S. Cascone**, F. De Santis, G. Lamberti, G. Titomanlio, "The influence of dissolution conditions on the drug ADME phenomena", *European Journal of Pharmaceutics and Biopharmaceutics*, 79 (2011) 382-391.

7. M. Grassi, G. Lamberti, **S. Cascone**, G. Grassi, "Mathematical modeling of simultaneous drug release and in vivo absorption", *International Journal of Pharmaceutics*, 418 (1) (2011) 130-141.

8. A.A Barba; M. d'Amore; **S. Cascone**; G. Lamberti; G. Titomanlio Intensification of biopolymeric microparticles production by ultrasonic assisted atomization. *Chemical Engineering and Processing: Process Intensification* 48(10), 1475-1481, 2009.

9. A.A Barba; M. d'Amore; **S. Cascone**; S. Chirico; G. Lamberti; G. Titomanlio. On the behavior of HPMC/Theophylline matrices for controlled drug delivery. *Journal of Pharmaceutical Sciences* 98(11), 4100-4110, 2009.

10. **S. Cascone**, G. Lamberti, G. Titomanlio, "A rule of thumb in designing in-vitro systems to simulate the intestinal absorption", submitted to *Heat and Mass Transfer*.

Conference proceeding

1. **Cascone S**.; Lamberti G.; Paolucci F.; Titomanlio G.; "In vitro and in silico approaches to reproduce pharmacokinetic relevant phenomena", Proceedings of *8th World Meeting on Pharmaceutics, Biopharmaceutics and Pharmaceutical Technology*, Istanbul, Turkey 19-22 March, 2012.

2. **Cascone, S.**; De Santis, F.; Lamberti, G.; Titomanlio, G.; Barba, A.A.; "Alternatives to Laboratory Animals: In Vitro and In Silico Approaches", Proceedings of *8th CESPT*, Graz, Austria, September 16th-18th 2010.

3. **Cascone S**.; Barba A.A.; d'Amore M.; Lamberti, G.; Rabbia L.; Titomanlio G.; "Microencapsulation of active molecules in biopolymers by ultrasound assisted atomization", Proceedings of *CHISA2010/ECCE 7*, Praha, Czech Republic, 28 August - 1 September, 2010.

4. Barba A.A.; d'Amore M.; **Cascone S**.; Lamberti G.; Rabbia L.; Titomanlio G.; Grassi M.; Grassi G.; "Pluronic/alginate gels in drug eluting stents preparation", Proceedings of *CHISA2010/ECCE 7*, Praha, Czech Republic, 28 August - 1 September, 2010.
5. Barba A.A.; d'Amore M.; Rabbia L.; **Cascone S**.; Lamberti G.; Titomanlio G.; Grassi M.; Grassi G.; "Gelification of polymer blends for coating of eluting stents", Proceedings of *7th World Meeting on Pharmaceutics, Biopharmaceutics and Pharmaceutical Technology*, La Valletta (Malta), 8-11 March, 2010.
6. Barba A.A.; d'Amore M.; **Cascone S**.; Rabbia L.; Lamberti G.; Titomanlio G.; "Novel microencapsulation technique of active molecules in pharmaceutical and nutraceutical preparations", Proceedings of *7th World Meeting on Pharmaceutics, Biopharmaceutics and Pharmaceutical Technology*, La Valletta (Malta), 8-11 March, 2010.
7. Barba A.A, d'Amore M, **Cascone S**, Lamberti G, Titomanlio G. Microencapsulation of nutraceuticals and pharmaceuticals by ultrasonic atomization. Proceedings of *Effost 2009*. Budapest, Hunghery, 11-13 November, p. 1-4, 2009.
8. Barba A.A, **Cascone S**, Di Muria M, Lamberti G. Micro-particles by ultrasonic atomization: new strategy towards novel drug carrier. Proceedings of *CRS36*. Copenhagen, Denmark, 18-22 July, 2009.
9. Barba A.A, d'Amore M, **Cascone S**, Lamberti G, Titomanlio G. Intensification of pharmaceuticals atomization by ultrasonic: experiments and correlations testing. Proceedings of *GPE-EPIC*. Venice, Italy, 14-17 June 2009.
10. **Cascone S**, Chirico S, Lamberti G., Titomanlio G. Water and theopylline transport phenomena within HPMC based tablets. Proceedings of *Innovation in Drug Delivery*. Naples, 30 September - 3 October 2007.

…Siamo arrivati al momento dei ringraziamenti …

Vorrei dire grazie a diverse persone:

Grazie al prof. Giuseppe Titomanlio, per avermi sapientemente guidato in questi anni, e ricordargli che abbiamo ancora una partita a tennis in sospeso …

Grazie a Gaetano per aver reso questo lavoro e questi anni davvero … ehm … vabbè, grazie di tutto …

Grazie a Anna Angela per tutti i consigli che mi ha dato e, soprattutto, per tutte le volte che mi ha liberato …

Grazie ad Annalisi per avermi accompagnato in questo percorso, compagna di vacanze … ehm … convegni e di GRICU, ma soprattutto per l'angolo del gossip al mattino …

Grazie a tutti i ragazzi del laboratorio che hanno contribuito tutti all'allegria delle giornate passate insieme, siete la parte migliore di tutto il mio lavoro …

Grazie a mio fratello per il suo supporto, ed anche, perché no, per il trasferimento di scienza anche se non so quanto fosse consentito …

Grazie a mia madre per i 'proverbi per ogni occasione', solo recentemente ho capito che erano inventati; e grazie a mia sorella che continua a tenermi aggiornata …

Grazie a Mordicchio, davvero l'unico ad avermi accompagnato sempre per tutto il percorso … Woof!

Grazie ad Elena per l'ora del tè e per avermi costantemente ed instancabilmente chiamato scema durante questi anni…

Grazie a tutti coloro che hanno contribuito alla mia crescita umana e professionale, avrei preferito anche una crescita in altezza, ma grazie lo stesso, apprezzo comunque l'impegno …

Amore mio, a te non posso che rivolgere un unico ringraziamento: Grazie per la gru …